EARLY NEOPROTEROZOIC MARINE REDOX CONDITIONS RECORDED IN BLACK SHALE FROM THE LITTLE DAL GROUP, NORTHWEST TERRITORIES, CANADA

by

Sean Patrick O'Hare

A thesis submitted in partial fulfilment
of the requirements for the degree of
Master of Science (M.Sc.) in Geology

The School of Graduate Studies
Laurentian University
Sudbury, Ontario, Canada

THESIS DEFENCE COMMITTEE/COMITÉ DE SOUTENANCE DE THÈSE

Laurentian Université/Université Laurentienne
School of Graduate Studies/École des études supérieures

Title of Thesis Titre de la thèse	EARLY NEOPROTEROZOIC MARINE REDOX CONDITIONS RECORDED IN BLACK SHALE FROM THE LITTLE DAL GROUP, NORTHWEST TERRITORIES, CANADA
Name of Candidate Nom du candidat	O'Hare, Sean P.
Degree Diplôme	Master of Science
Department/Program Département/Programme	Geology
Date of Defence Date de la soutenance	June 12, 2014

APPROVED/APPROUVÉ

Thesis Examiners/Examinateurs de thèse:

Dr. Elizabeth Turner
(Supervisor/Directeur(trice) de thèse)

Dr. Balz Kamber
(Committee member/Membre du comité)

Dr. Darrel G. F. Long
(Committee member/Membre du comité)

Dr. Peir K. Pufahl
(External Examiner/Examinateur externe)

Approved for the School of Graduate Studies
Approuvé pour l'École des études supérieures

Dr. David Lesbarrères
M. David Lesbarrères
Director, School of Graduate Studies
Directeur, École des études supérieures

ACCESSIBILITY CLAUSE AND PERMISSION TO USE

This page is left intentionally blank

Abstract

Black shale in the Little Dal Group (ca. <817 Ma), Mackenzie Mountains Supergroup (<1005 Ma; >779 Ma), was deposited during the early Neoproterozoic, and is one of the few known black shale deposits from this crucial time in Earth's evolutionary history. Relative iron enrichment (Fe_T/Al) and conventional iron speciation (DOP), along with enrichment in molybdenum, total sulphur, and total organic carbon, were studied. Iron systematics (Fe_T/Al >0.5 and DOP <0.80) indicate ferruginous, anoxic, and possibly oxic bottom-water conditions over the time of deposition of the entire black shale unit. The enrichment factors of several of the authigenic redox-sensitive trace elements (U, Mo, V) are strongly correlated, and appear to be related to both the Fe_T and the organic carbon content of the black shale. Molybdenum enrichment (<10 ppm) is limited, which is in very good agreement with data from Mesoproterozoic black shales, but is much lower than Mo enrichments in Paleozoic black shales (typically >100 ppm). Several black muddy siltstones yielded similar results, but authigenic iron was greatly overwhelmed by siliciclastic sedimentation. These new data support the theory that ocean bottom-waters returned from sulphidic to ferruginous prior to development of oxygenated conditions in the Ediacaran open ocean. This study documents a predominantly open-marine basin that was characterised by ferruginous conditions, similar to Archean and early Paleoproterozoic conditions, with brief intervals when oxic conditions developed.

Co-Authorship statement

Although I am named as sole author of this dissertation, the paper that will arise from Chapter 2 will be submitted for publication under the authorship of O'Hare, Turner, Babechuk and Kamber, to better reflect the contributions of my supervisors and colleagues to the project. Elizabeth Turner conceived the project theme, provided guidance, and reviewed the draft manuscript. Balz Kamber provided guidance and training in geochemistry, advice on interpretation of data, and a critical review of the analytical part of the manuscript. Michael Babechuk provided guidance and assistance during laboratory techniques, and a critical review of the manuscript. I determined the direction of the project, managed it, and wrote the manuscript. My supervisors' knowledge, experience, and insights were invaluable, however, they never forced their views on me, they allowed me to draw my own conclusions, and any mistakes are my own.

Acknowledgements

My primary source of support for this project was from NSERC Discovery Grants to Drs. Elizabeth Turner and Balz Kamber. In addition the Northwest Territories Geoscience Office, the Northern Science Training Project (Department of Indian and Northern Affairs), and a student research grant from the Society for Economic Geology Foundation (SEGF) provided support. Funding and field time were provided by Terralogic Exploration Inc. and Aurora Geosciences Ltd. I thank Aaron Higgs and Dave White respectively for their support and guidance during the summer.

I would like to thank my primary supervisor Elizabeth Turner for her patience and guidance from day one through to my final draft. She has been an inspirational motivator and has been amazingly understanding through these years. Balz Kamber, my second supervisor, taught me to think critically and guided me through the geochemistry of black shale. Michael Babechuk and Geoffrey Baldwin were essential in helping with geochemical lab techniques, suggestions, and letting me use them as sounding boards for my ideas. This study would not have been possible without the help of Annette Gladu and Joseph Petrus in preparation and analysis. I also thank Dr. Darrel Long for being unfailingly supportive and encouraging. I would like to offer my immeasurable gratitude to Anne McDonald for her support through the final stages of this project. Encouragement from my colleges, friends, and family were essential in completing this thesis.

Table of contents

List of tables

List of figures

Chapter 1

Chapter 2

CHAPTER 1: Thesis Introduction

1.1 Statement of Problem

It has been amply demonstrated that Earth's surface, including both its atmosphere and ocean, has evolved from a reducing condition to the modern oxic condition through the gradual addition of molecular oxygen produced by photosynthesising organisms. Although the overall shift from reduced to oxidised is not in dispute, the timing and geochemical status of the transitional stages are controversial. One of the early, popular, and commonly used models for Proterozoic ocean chemistry is referred to as the 'Canfield ocean,' (Canfield, 1998; Canfield et al., 2008). This model proposed that the Archean global ocean was dominated by anoxic ferruginous conditions marked by the deposition of banded iron formations (BIF). At some point between 2.3 and 2.0 Ga, after the "Great Oxygenation Event" (GOE), the global ocean began a gradual compositional change from ferruginous to sulphidic, as indicated by a sulphur-isotope excursion (Hayes et al., 1992). According to this model, cessation of BIF deposition, at approximately 1.8 Ga, marked a transition to deep oceans dominated by sulphidic conditions. This model calls on renewed deposition of BIFs at ca. 700 Ma, when the global ocean once again returned to a ferruginous state before becoming fully oxygenated by ca. 580 Ma. The 'Canfield ocean' model is testable using the chemistry of marine shales (fissile, black, organic-rich mudstones) that span the proposed duration of the sulphidic ocean. A complete reconstruction of the evolution Proterozoic ocean chemistry requires the study of rare open-marine sediment deposited throughout this time span. Many recent studies have found significant evidence to suggest that ferruginous conditions may have dominated the deep ancient ocean, contrary to the proposed sulphidic conditions in the

'Canfield ocean' model (Canfield et al., 2008; Feng et al., 2010; Johnston et al., 2010; Li et al., 2010; Och et al., 2013; Planavsky et al., 2011; Xiao et al., 2012). The late Meso- to Neoproterozoic was a time when very little black shale was deposited and, consequently, the ocean chemistry of this time span remains relatively underconstrained. This thesis presents the results of a study on such a shale, deposited during the late Proterozoic.

Black shale is a commonly used source of data about the redox conditions of ocean water at the time of sediment deposition. Some of the widely used proxies for paleoredox conditions include degree of pyritisation, DOP; total iron compared to aluminium, FeT/Al; highly reactive iron, Fe_{HR}; pyrite iron, Fe_{PY}, trace metal enrichments (e.g., Mo_{EF}, U_{EF}, V_{EF}), and total organic carbon (TOC). These proxies, when accompanied by other data such as rare earth element plus yttrium patterns, and sedimentological/stratigraphic data, allow for basin reconstruction and an understanding of the major geochemical components of the sedimentary system.

One basic measure of ancient redox status is Fe_T/Al, which evaluates the proportion of authigenic Fe relative to the volume of siliciclastic sediment to provide a view on the dissolved oxygen concentration of bottom water (Lyons and Severmann, 2006). When applied as a redox proxy, Fe_T/Al is understood to indicate oxic conditions when the ratio is below 0.5, and anoxic conditions above 0.5. Sulphidic conditions commonly have Fe_T/Al values above 0.6, but this is not a definitive measurement because significant siliciclastic input can elevate the boundary for oxic sediments and depress the boundary for sulphidic sediments (Lyons and Severmann, 2006).

A number of recent studies have suggested to supersede the Fe_T/Al proxy in favour of other more sensitive measurements of iron speciation but their validity relies on perfectly preserved apportioning of iron from sediment to sedimentary rock.

Degree of pyritisation (DOP), the ratio of Fe in pyrite to that in pyrite and in phases soluble in HCl ($Fe_{PY}/Fe_{PY}+Fe_{HCl}$), is considered to be a reliable proxy for redox status, although boundary values between redox states vary among studies and between ancient and modern materials (e.g., Raiswell et al., 1988; Lyons and Severmann, 2006). The proxy values used for ancient rocks has an oxic to anoxic/ferruginous boundary at 0.46 and an upper boundary indicating sulphidic depositional conditions at 0.75. DOP is a good proxy for ancient materials because it is unaffected by loss of reactive iron phases during burial alteration, but is commonly replaced by more sensitive proxies originally designed for use on modern sediments (Lyons et al., 2009; Raiswell and Canfield, 1998).

Total organic carbon (TOC) is the organic (reduced) carbon remaining in rock; "high" TOC values are generally taken to indicate that fixation of C from biological sources was not matched by its respiration (decay) such that organic C was buried without being recycled in the biosphere. Organic carbon burial generally takes place under anoxic conditions, where bacterial decay is suppressed by the absence of free oxygen, and so TOC is a fairly simple proxy for redox conditions. The role of TOC in paleoredox studies is important because certain redox-sensitive elements bind preferentially to organic matter and can themselves be used as redox proxies. TOC

values below approximately 2.5 wt.% indicate sediments deposited in a low-oxygen oxic environment, values up to approximately 10 wt.% indicate an anoxic environment, and values exceeding 10 wt.% indicate a complete depletion of benthic O_2 and an accumulation of free H_2S in the water column causing sulphidic conditions (Algeo and Maynard, 2004).

Highly reactive iron (Fe_{HR}) refers to the amount of iron bound in sedimentary sulphides, carbonates, and oxides. The ratio of Fe_{HR} to total iron (Fe_{HR}/Fe_T) is used as a measure of the redox status of the water beneath which a given sediment was deposited. Studies of modern and Phanerozoic basins have shown that sediment deposited under a restricted, anoxic water column has Fe_{HR}/Fe_T ratios $\geq$0.38, whereas sediment deposited under an oxic water column has Fe_{HR}/Fe_T ratios of $\leq$0.22 (Poulton and Canfield, 2011; Poulton and Raiswell, 2002; Raiswell and Canfield, 1998; Wijsman et al., 2001). Under certain circumstances, it is possible that anoxic conditions existed even if measured values of Fe_{HR} are between 0.22 and 0.38, because the Fe_{HR} pool may have become depleted during burial diagenesis or metamorphism, when unsulphidised iron-bearing minerals may be converted to unreactive sheet silicate phases (Poulton and Canfield, 2011). Furthermore, dramatic increases in sedimentation rate can mask water-column Fe enrichments (Canfield, 1998; Poulton et al., 2004). The details of Fe_{HR} enrichment are outlined in the shelf-to-basin shuttle review of Lyons et al. (2009).

The Fe_{PY}/Fe_{HR} ratio indicates the amount of Fe_{HR} that resides in pyrite versus the other biogeochemically available reservoirs (Raiswell and Canfield, 1998), and is an indication of the concentration of dissolved sulphide in the water from which a sediment was deposited. Modern

sulphidic basins such as the Black Sea contain sediment with Fe_{PY}/Fe_{HR} ratios ≥0.80, whereas ferruginous basins have sediment with Fe_{PY}/Fe_{HR} ratios ≤0.80 (Anderson and Raiswell, 2004; Canfield et al., 2008; Poulton et al., 2004). März et al. (2008), working on Phanerozoic sedimentary rocks, found that the upper threshold for a ferruginous water column is approximately 0.7. Although Fe_{HR}/Fe_T and Fe_{PY}/Fe_{HR} were not obtained in the present study, these measures have been used in the redox assessment of other black shale deposits, and are addressed in the discussion below.

Redox-sensitive elements are also used in redox studies of ancient sedimentary rocks. The various metals used have different redox behaviours, and so the use of each one may be subject to specific conditions. For example, although Mo is considered to be a good indicator of oxic/anoxic status, and can be used to identify sulphidic conditions, its relationship with sulphide is not simple. Other redox-sensitive elements that are commonly used include V and U. The relative redox-sensitive trace element concentrations are often reported as 'enrichment factors', which eliminates any possible detrital contribution of the element by normalising relative to a proxy for siliciclastic content. Enrichment factors can then be compared to possible controlling factors such as TOC (for elements that preferentially bind to organic matter) and DOP (for elements that preferentially combine with sulphide).

Most known black shale units were deposited during the Phanerozoic, at a time when complex life was well established. This project, however, summarises the results of field and laboratory investigations of a rare Proterozoic black shale deposit from a previously poorly understood time

in Earth's history. This rare black shale unit belongs to the mid to late Proterozoic Mackenzie Mountains Supergroup (MMSG) of the Northwest Territories and Yukon. The shale analysed is part of the Stone Knife Formation (<817 Ma; >779 Ma; Heaman et al., 1992; Powell and Scheider, 2013).

1.2 Thesis Objectives

- to produce detailed geochemical analyses of the black shale unit, to better understand redox conditions during the Proterozoic;
- to test the 'Canfield ocean' model (Fig. 1A) proposed by Canfield (1998)

Field work was completed in the summers of 2009 and 2010 by E.C. Turner. Laboratory work was completed early in 2012. The results of the Little Dal black shale project were presented in the poster session of GAC-MAC 2011 (O'Hare et al., 2011) and will be submitted to Chemical Geology as a complete manuscript in 2014.

1.3 Regional Geology

The Mackenzie Mountains Supergroup

This information expands on the brief description in Chapter 2 of the geological setting of the project area. For a completed detailed description of all units mentioned, see such works as Turner and Long (2008; 2012), Turner (2011), Turner et al., (2011), Long and Turner (2012) and papers cited therein. The Proterozoic sedimentary strata of northwestern Canada have been divided into three major unconformity-bounded sequences (A, B, and C), approximately corresponding to the Mesoproterozoic, early Neoproterozoic, and late Neoproterozoic (Young et al., 1979; Young et al., 1982). The unconformities separating the sequences are dated at ca. 1000 Ma (A/B) and ca. 750 Ma (B/C). In the Wernecke and Mackenzie Mountains the strata of sequence B that overlie the Pinguicula Group and underlie the Coates Lake Group have been named the Mackenzie Mountains Supergroup (MMSG; Fig.1; Aitken, 1981; Gordey and Roots, 2011; Long et al., 2008; Long and Turner, 2012; Narbonne and Aitken, 1995; Rainbird et al., 1996; Turner, 2011; Turner and Long, 2008; Turner and Long, 2012; Young et al., 1979; Young et al., 1982).

Approximately 4-5 kilometres of strata in the Mackenzie Mountains and >1 kilometre of strata in the Wernecke Mountains make up the MMSG (Fig. 1; Turner, 2011; Turner et al., 2011), which is composed of terrigenous clastic, carbonate and evaporite rocks that were deposited in fluvial to deep-marine settings in an extensional basin. These strata in stratigraphic order are: the

Hematite Creek Group (Wernecke Mtns; >810 m, Mackenzie Mountains; ~2 km), Katherine Group (Wernecke Mtns; unmeasured, Mackenzie Mtns; ~1.5 km), and Little Dal Group (Wernecke Mtns; >250 m, Mackenzie Mtns; ~2 km; Turner, 2011; Turner et al., 2011). The strata of the MMSG collectively record deposition on the Laurentian continent in an extensional basin, at a relatively low paleolatitude (Evans, 2006; Park and Jefferson, 1991), during the early to middle Neoproterozoic (Turner and Long, 2008). In the Northwest Territories, the MMSG extends approximately 500 kilometres along strike. The supergroup occupies a prominent, arched deviation in the structural grain of the Canadian Cordillera that mimics the inferred margin of the Neoproterozoic basin (Aitken, 1981). The Shaler Supergroup of Victoria Island and the adjacent mainland is directly correlative to the MMSG (Aitken and Long, 1978; Long et al., 2008; Rainbird et al., 1996). Other possible correlative units have been proposed in the Tindir and Fifteenmile groups, although definitive evidence remains to be found.

The material in this study is from the Little Dal Group, of which the maximum possible depositional age is 817 Ma (Ar-Ar detrital muscovite; Powell and Schneider, 2013) A minimum age for the top of the supergroup is given by Rb-Sr dates of 770 Ma from diabase sills that cut the Tsezotene Formation and Katherine Group (Armstrong et al., 1982), and by a fault-bounded quartz diorite body dated at 779 Ma (Heaman et al., 1992; Jefferson and Parrish, 1989), all of which are thought to be related to the "Little Dal basalt," which lies between the MMSG and overlying Coates Lake Group.

The top contact of the MMSG is unconformable, and depending on geographic location, is overlain by younger Neoproterozoic units ("Little Dal basalt"; Coates Lake Group; upper Windermere Supergroup), or by Cambro-Ordovician stratigraphic units. The erosional surface between the MMSG and Paleozoic rocks gradually cuts downward eastward from the Plateau fault (Turner et al., 2011). In the area surrounding the Plateau fault, the upper units of the MMSG are overlain by the Coates Lake Group (or, locally, by the "Little Dal basalt"). Jefferson (1983) has shown that there are only minor variations in the stratigraphic level of these contacts, implying that the hiatus between deposition of the upper MMSG and lower Coates Lake Group was brief.

Little Dal Group

The Little Dal Group has been subdivided into seven formal units: Dodo Creek, Stone Knife, Silverberry, Gayna, Ten Stone, Snail Spring, and Ram Head Formations (Turner and Long, 2012). The group unconformably overlies the Katherine Group, is > 3 kilometres thick, and forms an internally conformable succession. The upper unit of the Little Dal Group (Ram Head Formation) is unconformably overlain by the Coates Lake Group and locally by the "Little Dal basalt" (Turner et al., 2011).

Dodo Creek Formation

The Dodo Creek Formation (formerly the Mudcracked formation of Aitken, 1981) is a thin (10-68 m) terrigenous clastic unit that, depending on location, slightly unconformably (Batten et al., 2004) to conformably (Turner et al., 1997) overlies the Katherine Group (Aitken, 1981). Many sections have been measured through this formation by Aitken (1981), Turner (1999), Batten (2002), and Aitken et al. (2011). The formation is dominated by quartz arenite and green, red and grey siltstone, with subordinate carbonate layers. Shallow-marine sedimentary structures are pervasive throughout the formation, and include hummocky cross-stratification, trough cross-bedding, both asymmetrical and symmetrical ripple cross-laminations, tool marks, synaeresis cracks, gutter casts, halite casts, and tempestites with graded shale chips. Many of the bedding surfaces have a black veneer that was probably a microbial mat during the time of deposition (Turner et al., 2011). The upper contact of the Dodo Creek Formation is conformable, and was placed at the base of an orange-weathering oncoid grainstone, that acts as an easily discernible marker unit (Turner and Long, 2012).

Stone Knife Formation

The Stone Knife Formation (formerly Basinal assemblage; Aitken, 1981; Turner et al., 1997; Turner, 1999; Turner and Long, 2008, 2012) is 143 to 622 metres thick, depending on location, and is the deep-water lateral equivalent of, and is contemporaneous with, the Silverberry Formation. The conformable basal contact with the underlying Dodo Creek Formation is placed

at the base of a regional oncoid marker unit. The Stone Knife Formation is composed of four shale-to-carbonate cycles (LD1 to 4; Turner et al., 1997; Turner and Long, 2008) that define informal members, each with laterally variable thickness, between 16 and 400 metres. Recessive, green-grey siltstone and fissile mudstone, overlain by a distinctive, ubiquitous, resistant weathering stromatolite biostrome make up member 1 (16 to >91 m) of the formation. Member 2 is composed of black- to red-weathering fissile mudstone, commonly with intraclast rudstone near the base of the member, which is normally in part interlayered with nodular to medium-bedded, medium-grey-weathering lime mudstone (85 - 200 m), and is overlain by a resistant, medium-bedded lime mudstone with no conspicuous sedimentary structures (12 - 300 m). Member 3 generally consists of recessive, argillaceous lime mudstone, or medium-grey siltstone and mudstone (15 - 115 m) that is overlain by silty, argillaceous lime mudstone (20 - 110 m). Rarely, the carbonate rocks of member 3 contain stromatolites, molar-tooth structure, and/or desiccation cracks. Member 4 consists of grey to black fissile mudrocks (0 - 60 m) overlain by molar-tooth bearing lime mudstone (25 - 100 m). Among carbonate rocks of member 4, 15 metres of magnetite-facies iron-formation have been reported (Hewton, 1982), but this observation has not been validated.

The Stone Knife Formation was deposited in a deep-water environment that experienced cyclic changes in sea-level and sea-water composition, that affected water-column chemistry (Turner et al., 2011). Relative rises in sea level are recorded as the shale-dominated lower parts of the four members, whereas highstands and falls are recorded as the carbonate mudstone dominated upper

sections of the members (Turner et al., 1997). Each of these shallowing-upwards cycles records a distinct bathymetric succession of lithofacies (Turner and Long, 2008). During the time of deposition, the basin floor was below the photic zone, and normally below storm wave-base, except during the deposition of the shallowest parts of the carbonate units (Turner et al., 1997). The fault-influenced paleotopography of the basin floor (Turner and Long, 2008) controlled the redistribution of pelagic lime mudstone, originally precipitated from the water column (Turner et al., 1997), and hemipelagic terrigenous fines, as thin, poorly defined turbidites. The upper contact with the Gayna Formation is placed where molar-tooth bearing lime mudstone passes gradationally upward to dolomitic ooid-intraclast grainstone. See Turner (1999; appendix) and Aitken et al., (2011) for detailed sections.

Silverberry Formation

The Silverberry Formation (previously the Platformal assemblage; Aitken, 1981; Batten et al., 2004; Turner and Long, 2008; Turner and Long, 2012) is up to 812 metres thick, and is laterally equivalent to, and contemporaneous with, the Stone Knife Formation. The basal contact of the formation is conformable and placed below the oncoid marker unit at the top of the Dodo Creek Formation. The formation is dominated by stromatolitic, oolitic, intraclastic, and molar-tooth bearing carbonate rocks. Similar to the Stone Knife Formation, it contains four transgressive-regressive cycles (Batten et al., 2004). The first cycle is capped with a thick stromatolitic unit that forms a basin-wide stratigraphic marker. The rest of the cycles consist of transgressive intraclastic units which are overlain, with some lateral variation by lime mudstone, shallowing

into molar-tooth bearing dolomudstone, ooid grainstone and stromatolitic boundstone (Turner and Long, 2008). The Silverberry Formation records repeated shallowing of a carbonate ramp system from near to or below storm wave-base up to sea-level (Turner et al., 2011). The upper contact with the Gayna Formation is gradational and conformable, marked with desiccation-cracked dolomudstone.

Gayna Formation

The Gayna Formation (previously the Grainstone formation; Aitken, 1981; Batten, 2002; Batten et al., 2004; Hewton, 1982) is up to 390 m thick, and conformably overlies the laterally equivalent Stone Knife and Silverberry Formations. The formation is dominated by yellow-buff-weathering, thin-bedded, quartz-silty, buff-orange-weathering oolitic and intraclastic dolo-grainstone, desiccation-cracked dolomudstone, and local molar-tooth, stromatolitic, and cherty units. The sedimentary structures in the dolograinstones include ripple cross-lamination, trough cross-stratification, hummocky cross-stratification, and grading. Fine quartz sand and silt are also present in the upper dolostones (Turner et al., 2011). The Gayna Formation erases the pronounced paleotopographic differential between the formerly deep- and shallow-water areas of the Stone Knife and Silverberry Formations, marking the return to a comparatively uniform bathymetric environment throughout the Little Dal Group's depositional area (Turner et al., 2011). The upper contact of the Gayna Formation is not gradational, and no transitional facies is present. This suggests that the then exposed desiccation-cracked, thin-bedded, quartz-silty and

shaly dolostones of the supratidal flat were abruptly placed in a considerably deeper-water setting, probably by a basin-wide tectonic adjustment (Turner, 2009).

1.4 Precambrian oceanic paleoredox conditions

The reconstruction of paleo-ocean redox conditions is crucial for understanding connections between ocean chemistry and the evolution of the atmosphere and biosphere. There is widespread, but not total, support for the hypothesis that continued oxygenation of the deep ocean did not take place during the first rise in global oxygen (the Great Oxidation Event; GOE, Holland, 1984) at approximately 2.4 Ga, but instead took place over a lengthy time-span following the GOE and/or during the Neoproterozoic oxygenation event (NOE; ~850 Ma; Shields-Zhou and Och, 2011). Protracted anoxia would have constrained eukaryote evolution and limited primary productivity, which would have limited organic carbon burial and, in turn, oxygen accumulation (Anbar and Knoll, 2002). According to some workers, at 580 Ma there was a final rise in oxygen levels that ventilated the deep ocean and allowed for the subsequent and rapid evolution of the first large, multicellular plants and animals (Canfield et al., 2008; Canfield et al., 2007). On the other end of the spectrum, times of ocean anoxia in the Paleozoic have been used to explain prominent episodes of mass extinction (Meyer and Kump, 2008), whereas anoxic events (OAEs) during the Mesozoic have been linked to rapid radiation and turnover in marine plankton (Leckie et al., 2002).

Detailed knowledge of the exact nature of ocean oxidation-reduction (redox) conditions relies on interpretation of the links between evolution of the biosphere and the ocean chemistry in which organisms lived for the first 85-90% of life's history. Previous reconstructions of ocean redox conditions have tended to focus on extreme cases of anoxia (i.e., sulphidic or euxinic conditions), primarily as a result of the available geochemical analytical techniques. However, the redox state of the ocean, and of individual basins, can vary widely, both spatially and temporally, from various levels of oxygenation, to oxygen depletion, into ferruginous (anoxic, Fe^{2+} -rich, but non-sulphidic conditions) to fully sulphidic (with free H_2S). It is in the intermediate state between oxic and euxinic end-members that ferruginous conditions develop and that the environmental behaviour of iron plays a central role in redox reactions. Iron can be mobilised as ferrous iron [Fe(II)], which will result in the development of ferruginous water-column conditions (Poulton and Canfield, 2011). As an anti-thesis to the "Canfield ocean" model, ferruginous conditions may have been the dominating feature of anoxic oceanic intervals throughout much of early Earth's history, and so understanding the mechanisms driving these conditions and the broader effects of such conditions is currently an area of major interest and debate.

Understanding the processes that lead to ferruginous water-column conditions can be assisted by studies of the modern global iron cycle, and considerable effort has been spent in quantifying the operation of the global iron cycle. Major advances have resulted from studying biogeochemically reactive iron minerals in surface and near-surface environments (Poulton and Raiswell, 2002; Raiswell and Canfield, 1998; Raiswell et al., 2006). In the modern ocean, under oxic conditions,

most of the Fe(II) generated by deep-sea hydrothermal vents is either oxidised to ferric (oxyhydr) oxide minerals or reacts rapidly with dissolved sulphide and is deposited close to the vents as pyrite (FeS_2). Iron(II) generated by reductive dissolution of reactive ferric (oxyhydr) oxide minerals, during diagenesis may also be released to the overlying water column. As with hydrothermal iron, some of the Fe(II) is quickly reoxidised and deposited. Both sources may have some Fe(II) escape precipitation, and this iron would contribute to the oceanic dissolved-iron inventory (Raiswell, 2006; Tagliabue et al., 2010).

The role of diagenetic and hydrothermal dissolved-Fe(II) sources becomes much more significant under anoxic conditions. Reduced iron released from these sources is virtually stable until transported to an environment where precipitation and deposition can occur (Poulton and Canfield, 2011). Under a sulphidic environment, Fe(II) is quickly titrated when it encounters water-column sulphide, which results in enrichment of pyrite in the deposited sediment (Raiswell and Canfield, 1998). It has been suggested that enrichments in sediment iron following water-column precipitation in anoxic environments is a unique feature of sulphidic depositional conditions (Lyons and Severmann, 2006). However, recent work on ancient sediments (Canfield et al., 2008; Canfield et al., 2007; Feng et al., 2010; Johnston et al., 2010; Li et al., 2010; Marz et al., 2008; Planavsky et al., 2011; Poulton et al., 2004; Poulton et al., 2010; Xiao et al., 2012) has found that enrichments in sediment iron content may also develop during ferruginous depositional conditions. Under ferruginous conditions the additional iron flux is the result of water-column formation of unsulphidised minerals, such as ferrous carbonates (e.g., siderite)

and/or ferric (oxyhydr)-oxides (e.g. ferrihydrite). These minerals may readily react with dissolved sulphide, and are commonly partially sulphidised during diagenesis. In general the tendency is for sulphidic iron enrichments to be dominated by pyrite, whereas ferruginous conditions tend to keep a significant proportion of the authigenic iron minerals unsulphidised (Canfield et al., 2008; Poulton et al., 2004).

1.5 Structure of thesis

This thesis is written as two chapters: an introduction, which summarises the problem investigated, provides a detailed regional geology, outlines the geochemical concepts involved, and provides a description of the thesis structure. This is followed by a draft of a scientific journal article intended for submission to Chemical Geology. The text, figures and reference styles are in compliance with the format of Chemical Geology. All geochemical data are presented in Appendix A.

1.6 Statement of responsibilities

The thesis as presented includes one journal paper with co-authors. The candidate performed all of the analytical research, prepared all of the samples for analysis, performed all laboratory work up to submission for analysis, and wrote the first draft of the thesis. Drs. E.C. Turner and B.S. Kamber designed the project, provided supervision, guidance, and advice during the research,

and edited the penultimate versions of the papers and thesis. Sample collection was undertaken by E.C. Turner, and solution analysis was performed by B.S. Kamber and the Ontario Geoscience Laboratories (GeoLabs).

1.7 Figures

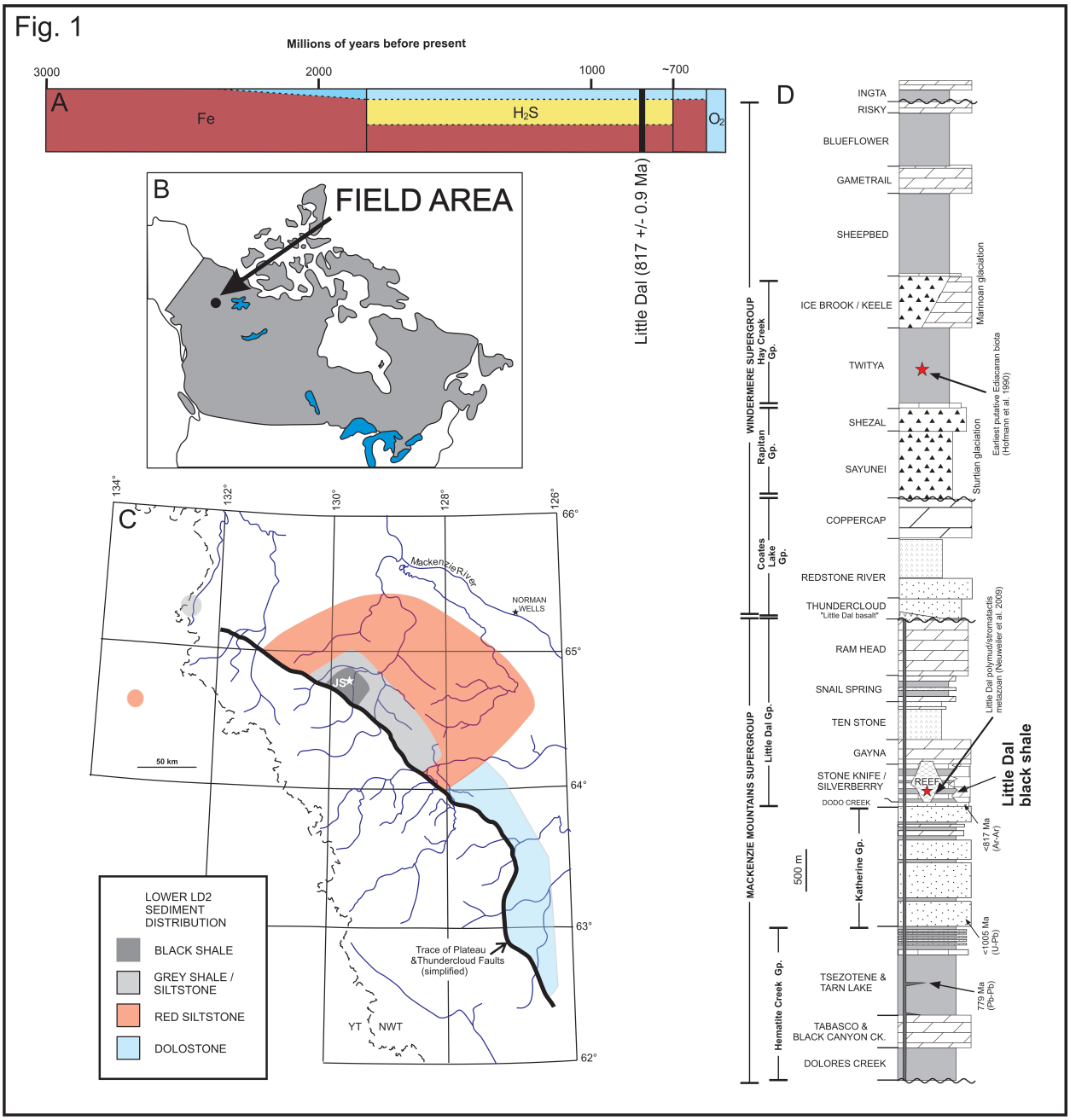
Fig. 1
Millions of years before present
3000
2000
1000
~700
A
Fe
H2S
O2
Little Dal (817 +/- 0.9 Ma)
B
FIELD AREA
C
134°
132°
130°
128°
126°
66°
65°
64°
63°
62°
Mackenzie River
NORMAN WELLS
JS
50 km
Trace of Plateau &Thundercloud Faults (simplified)
YT
NWT
LOWER LD2 SEDIMENT DISTRIBUTION
BLACK SHALE
GREY SHALE / SILTSTONE
RED SILTSTONE
DOLOSTONE
D
INGTA
RISKY
BLUEFLOWER
GAMETRAIL
SHEEPBED
ICE BROOK / KEELE
Marinoan glaciation
TWITYA
Earliest putative Ediacaran biota (Hofmann et al. 1990)
SHEZAL
SAYUNEI
Sturtian glaciation
COPPERCAP
REDSTONE RIVER
THUNDERCLOUD
"Little Dal basalt"
RAM HEAD
SNAIL SPRING
Little Dal polymud/stromatactis metazoan (Neuweiler et al. 2009)
TEN STONE
GAYNA
STONE KNIFE / SILVERBERRY
REEF
DODO CREEK
Little Dal black shale
<817 Ma (Ar-Ar)
500 m
TSEZOTENE & TARN LAKE
<1005 Ma (U-Pb)
779 Ma (Pb-Pb)
TABASCO & BLACK CANYON CK.
DOLORES CREEK
WINDERMERE SUPERGROUP
Hay Creek Gp.
Rapitan Gp.
Coates Lake Gp.
MACKENZIE MOUNTAINS SUPERGROUP
Little Dal Gp.
Katherine Gp.
Hematite Creek Gp.

Figure 1. Geological context of the Little Dal black shale. (A) The "Canfield ocean" timeline (Canfield, 1998; Canfield et al., 2008) proposed that widespread anoxia in the lower part of the global water column persisted to at least 540 Ma. At 1800 Ma the deep ocean became dominated by H_2S rather than Fe, ending the deposition of banded iron formation (BIF). At ~700 Ma the deep oceans are suggested to have returned to a ferruginous state, allowing once again deposition of BIFs, before reaching present day deep-ocean oxygenation. (B) Location map of the study area in Northwest Territories, Canada. (C) Distribution of shallow- and deep-water environments of the Silverberry and laterally equivalent Stone Knife Formations during deposition of black shale, Little Dal Group, based on Aitken et al. (2011). Isolated pink circle is Stone Knife Formation inlier in Yukon (Turner, 2011). (D) Stratigraphic section through the Mackenzie Mountains Supergroup and overlying Windermere Supergroup. Formal names for the formation-scale units of the Little Dal Group (above the section) are from Turner and Long (2012). Radiometric dates are from Heaman et al. (1992), Leslie (2009), and Powell and Scheider (Powell and Scheider, 2013).

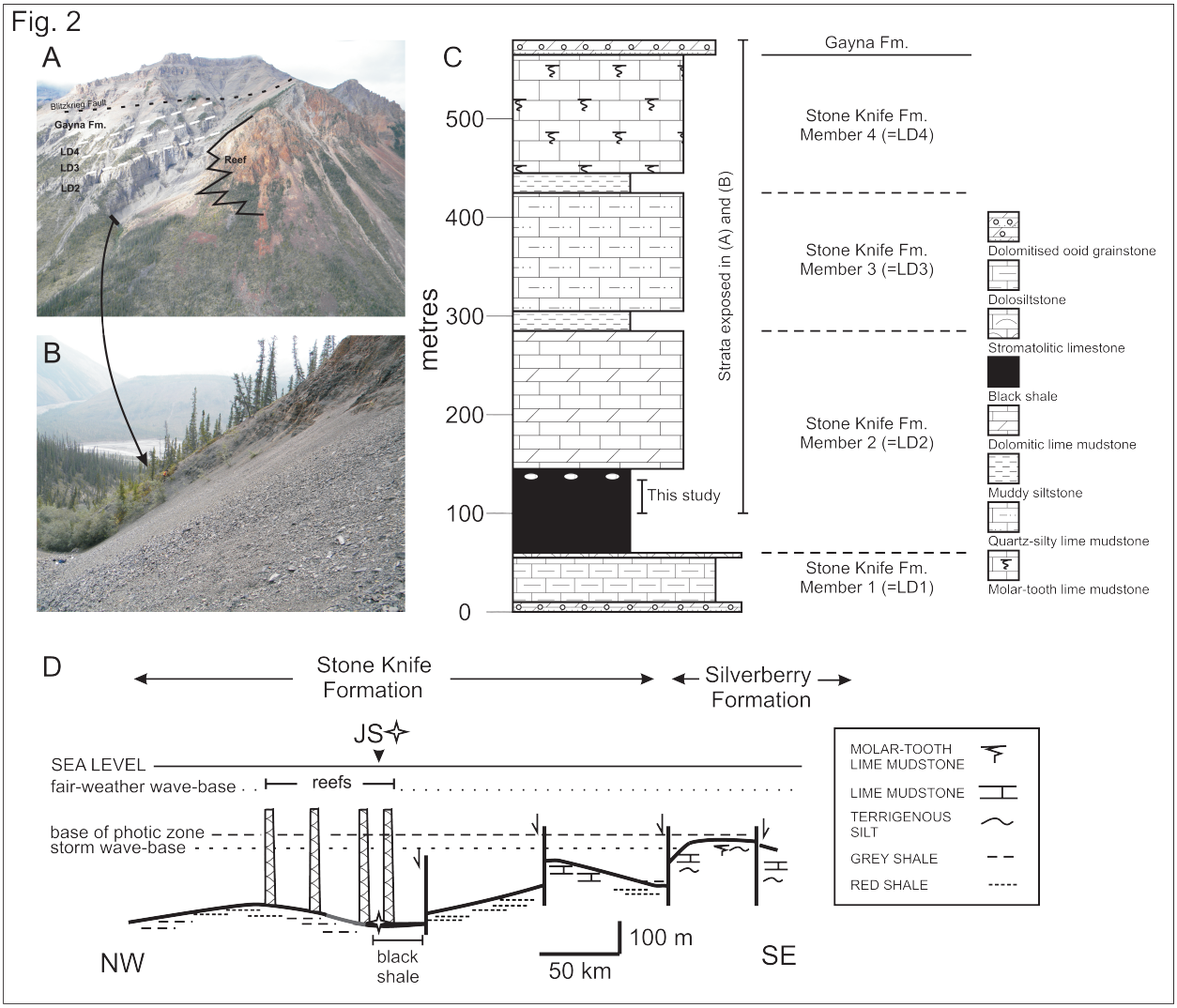

Figure 2. Exposure and stratigraphic context of black shale in the Stone Knife Formation, Little Dal Group. (A) and (B) Exposure of Stone Knife Formation layered strata and associated deep-water reef near Stone Knife River. Subdivisions (LD2-4) of the Stone Knife Formation correspond to transgressive-regressive packages (Turner and Long, 2008). The black shale interval (upper part of lower LD2) analysed in this paper is highlighted in (B) and (C). The lower

part of the Stone Knife Formation is not exposed at this location. (C) Strata exposed in (A) and (B) form part of composite section 92-SKR (Turner and Long, 2008). (D) Paleogeographic reconstruction of the transgressive phase of Stone Knife Formation member 2, showing sea-floor lithofacies, relative disposition of water-column interfaces, faults that were active during deposition of LD2 transgressive phase, limited distribution of black shale and reefs, and location of studied section JS. Diagram is modified after Turner and Long (2008).

CHAPTER 2: Early Neoproterozoic marine redox conditions recorded in black shale from the Little Dal Group, Northwest Territories, Canada

Sean P. O'Hare [a]*, Elizabeth C. Turner [a], Michael G. Babechuk[a.b], Balz S. Kamber [a,b]

[a] Department of Earth Sciences, Laurentian University, 935 Ramsey Lake Road, Sudbury, ON., Canada P3E 2C6
[b] Department of Geology, School of Natural Sciences, Museum Building, Trinity College Dublin, Dublin 2, Ireland

* Corresponding author at: Department of Earth Sciences, Laurentian University, 935 Ramsey Lake Road, Sudbury, ON, Canada P3E 2C6
Phone: 705-675-1151 ext. 2267
E-mail address: sp_ohare@laurentian.ca

2.1 Abstract

Black shale in the Little Dal Group (ca. <817 Ma), Mackenzie Mountains Supergroup (<1005 Ma; >779 Ma), was deposited during the early Neoproterozoic, and is one of the few known black shale deposits from this crucial time in Earth's evolutionary history. Relative iron enrichment (Fe_T/Al) and conventional iron speciation (DOP), along with enrichment in molybdenum, total sulphur, and total organic carbon, were studied. Iron systematics (Fe_T/Al >0.5 and DOP <0.80) indicate ferruginous, anoxic, and possibly oxic bottom-water conditions over the time of deposition of the entire black shale unit. The enrichment factors of several of the authigenic redox-sensitive trace elements (U, Mo, V) are strongly correlated, and appear to be related to both the Fe_T and the organic carbon content of the black shale. Molybdenum enrichment (<10 ppm) is limited, which is in very good agreement with data from Mesoproterozoic black shales, but is much lower than Mo enrichments in Paleozoic black shales (typically >100 ppm). Several black muddy siltstones yielded similar results, but authigenic iron was greatly overwhelmed by siliciclastic sedimentation. These new data support the theory that ocean bottom-waters returned from sulphidic to ferruginous prior to development of oxygenated conditions in the Ediacaran open ocean. This study documents a predominantly open-marine basin that was characterised by ferruginous conditions, similar to Archean and early Paleoproterozoic conditions, with brief intervals when oxic conditions developed.

2.2 Keywords:
Paleo-redox conditions
Neoproterozoic
Iron speciation
Molybdenum
Ocean chemistry
Black shale

2.3 Introduction

Paleoredox conditions of the ancient ocean are a vital component in understanding ocean chemistry and the evolution of early life. During the Neoproterozoic (1000-541 Ma), the Earth underwent dramatic climatic changes, which included multiple glaciations (Hoffman et al., 1998) and a proposed change from sulphidic, to ferruginous, and eventually to fully ventilated and oxygenated ocean conditions (Canfield, 1998; Canfield et al., 2008). These climatic changes would have had dramatic effects on evolution: iron geochemistry, along with sulphur isotope data from Australia, Canada, China, and Oman, suggest a stepwise oxygenation of the Ediacaran ocean that would have promoted the evolution of early aerobic life (Canfield et al., 2007; Fike et al., 2006; Komiya et al., 2008; Maruyama and Santosh, 2008; Poulton and Canfield, 2011; Scott et al., 2008).

One of the early models for Protoerozoic redox evolution, the 'Canfield ocean' proposed that global open-ocean anoxia persisted to at least 540 Ma (Fig. 1A; Canfield, 1998; Canfield et al., 2008). According to this model, after the Great Oxidation Event at approximately 2,400 Ma, the ocean underwent a gradual compositional shift from a ferruginous to a sulphidic state. Fully sulphidic conditions dominated by approximately 1,800 Ma, bringing to an end the deposition of banded iron formation (BIF; Canfield, 1998). The deep ocean then apparently returned to a ferruginous state around 700 Ma, allowing for renewed deposition of BIFs. Eventually, the ocean became fully oxygenated, without reverting to a sulphidic or ferruginous state (ca. 540 Ma; Canfield, 1998; Canfield et al., 2008). More recent work suggests a more complex evolution than the "Canfield ocean" hypothesis (e.g., Planavsky et al., 2011), requiring models accommodating

both ferruginous and sulphidic oceans. Specifically, a number of studies (e.g., Baldwin et al., 2012; Canfield et al., 2008; Johnston et al., 2010; Li et al., 2010; Poulton and Canfield, 2011; Poulton et al., 2010) have identified extensive evidence for widespread, ferruginous deep-ocean conditions and only sporadic evidence for sulphidic conditions, prior to ~0.58 Ga, when widespread deep-ocean oxygenation took place (Canfield et al., 2007). These studies suggest a deep ocean dominantly in a ferruginous state, but with oxygenated near-surface waters, and a wedge-shaped, persistent or transient, sulphidic zone. This new model serves as a useful discussion point for ancient redox studies.

Proterozoic black shale (fissile, black, sulphide-bearing, organic-rich mudstone) units are of particular interest in reconstructing paleoredox evolution because they are capable of recording critical events in ocean geochemistry. Currently there is a limited amount of black shale data from the early to middle Neoproterozoic, which severely limits the understanding of this critical time. The reason for the paucity in data is that very limited black shale from this time interval is preserved, meaning that the rare black shale successions that are known from this time are especially critical to understanding early to middle Neoproterozoic ocean composition. The Stone Knife Formation of the Little Dal Group (Mackenzie Mountains Supergroup; <1005 Ma; >779 Ma; Aitken, 1981; Heaman et al., 1992; Leslie, 2009; Turner and Long, 2012) contains one of the few known black shale deposits of early Neoproterozoic age (Fig. 2). The geochemistry of this black shale thus helps to fill a knowledge gap during a crucial part of the middle Neoproterozoic.

The redox status of ancient ocean bottom waters can be addressed via several proxies derived from black shale. The proxies do not yield exactly the same information (e.g. some address anoxia, others euxinia), and conflicting conclusions have been drawn from different redox proxy data. The proxies used in any given study depend on subject material, preservation status of the sedimentary rocks, analytical capacity, and the ability to compare results of different studies can be complicated by the differences among the proxies. In cases where different proxies yield conflicting results, it can be difficult to determine whether the proxies truly indicate a meaningful contrast, whether they are fundamentally unreliable, or whether the material analysed was inappropriate (i.e., not truly black shale). Unfortunately, the published literature on ancient redox conditions also contains many misleading datasets obtained from material not suitable for the analytical techniques employed.

One basic measure of ancient redox status is Fe_T/Al, which evaluates the proportion of authigenic Fe relative to the volume of siliciclastic sediment, and provides a measure for dissolved oxygen concentration of bottom water (Lyons and Severmann, 2006). When applied as a redox proxy, Fe_T/Al is understood to indicate oxic conditions when the ratio is below 0.5, and anoxic conditions above 0.5. Sulphidic conditions commonly have Fe_T/Al values above 0.6, but this is not a conclusive measurement as a significant siliciclastic sedimentation rate can increase the threshold for oxic sediments and decrease the limit for sulphidic sediments (Lyons and Severmann, 2006). A number of recent studies have suggested to supersede the Fe_T/Al proxy in favour of other more sensitive measurements of iron speciation but their validity relies on perfectly preserved apportioning of iron from sediment to sedimentary rock.

Degree of pyritisation (DOP), the ratio of Fe in pyrite to that in pyrite and in phases soluble in HCl ($Fe_{PY}/Fe_{PY}+Fe_{HCl}$), is considered to be a reliable proxy for redox status, although boundary values between redox states vary among studies and between ancient and modern materials (e.g., Raiswell et al., 1988; Lyons and Severmann, 2006). The proxy values used for ancient rocks has an oxic to anoxic/ferruginous boundary at 0.46 and an upper boundary indicating sulphidic depositional conditions at 0.75. DOP is a good proxy for ancient materials because it is unaffected by loss of reactive iron phases during burial alteration, but is commonly replaced by more sensitive proxies originally designed for use on modern sediments (Lyons et al., 2009; Raiswell and Canfield, 1998).

Total organic carbon (TOC) is the organic (reduced) carbon remaining in rock; "high" TOC values are generally taken to indicate that fixation of C from biological sources was not matched by its respiration (decay) such that organic C was buried without being recycled in the biosphere. Organic carbon burial generally takes place under anoxic conditions, where bacterial decay is suppressed by the absence of free oxygen, and so TOC is a fairly simple proxy for redox conditions. The role of TOC in paleoredox studies is important because certain redox-sensitive elements bind preferentially to organic matter and can themselves be used as redox proxies. TOC values below approximately 2.5 wt.% indicate sediments deposited in a low-oxygen oxic environment, values up to approximately 10 wt.% indicate an anoxic environment, and values exceeding 10 wt.% indicate a complete depletion of benthic O_2 and an accumulation of free H_2S in the water column causing sulphidic conditions (Algeo and Maynard, 2004).

Highly reactive iron (Fe_{HR}) refers to the amount of iron bound in sedimentary sulphides, carbonates, and oxides. The ratio of Fe_{HR} to total iron (Fe_{HR}/Fe_T) is used as a measure of the redox status of the water beneath which a given sediment was deposited. Studies of modern and Phanerozoic basins have shown that sediment deposited under a restricted, anoxic water column has Fe_{HR}/Fe_T ratios $\geq$0.38, whereas sediment deposited under an oxic water column has Fe_{HR}/Fe_T ratios of $\leq$0.22 (Poulton and Canfield, 2011; Poulton and Raiswell, 2002; Raiswell and Canfield, 1998; Wijsman et al., 2001). Under certain circumstances, it is possible that anoxic conditions existed even if measured values of Fe_{HR} are between 0.22 and 0.38, because the Fe_{HR} pool may have become depleted during burial diagenesis or metamorphism, when unsulphidised iron-bearing minerals may be converted to unreactive sheet silicate phases (Poulton and Canfield, 2011). Furthermore, dramatic increases in sedimentation rate can mask water-column Fe enrichments (Canfield, 1998; Poulton et al., 2004). The details of Fe_{HR} enrichment are outlined in the shelf-to-basin shuttle review of Lyons et al. (2009).

The Fe_{PY}/Fe_{HR} ratio indicates the amount of Fe_{HR} that resides in pyrite versus the other biogeochemically available reservoirs (Raiswell and Canfield, 1998), and is an indication of the concentration of dissolved sulphide in the water from which a sediment was deposited. Modern sulphidic basins such as the Black Sea contain sediment with Fe_{PY}/Fe_{HR} ratios $\geq$0.80, whereas ferruginous basins have sediment with Fe_{PY}/Fe_{HR} ratios $\leq$0.80 (Anderson and Raiswell, 2004; Canfield et al., 2008; Poulton et al., 2004). März et al. (2008), working on Phanerozoic sedimentary rocks, found that the upper threshold for a ferruginous water column is approximately 0.7. Although Fe_{HR}/Fe_T and Fe_{PY}/Fe_{HR} were not obtained in the present study,

these measures have been used in the redox assessment of other black shale deposits, and are addressed in the discussion below.

Redox-sensitive elements are also used in redox studies of ancient sedimentary rocks. The various metals used have different redox behaviours, and so the use of each one may be subject to specific conditions. For example, although Mo is considered to be a good indicator of oxic/anoxic status, and can be used to identify sulphidic conditions, its relationship with sulphide is not simple. Other redox-sensitive elements that are commonly used include V and U. The relative redox-sensitive trace element concentrations are often reported as 'enrichment factors', which eliminates any possible detrital contribution of the element by normalising relative to a proxy for siliciclastic content. Enrichment factors can then be compared to possible controlling factors such as TOC (for elements that preferentially bind to organic matter) and DOP (for elements that preferentially combine with sulphide).

Several studies (Canfield, 2004; Canfield et al., 2008; Scott et al., 2008) have suggested that sulphidic conditions were not the dominant state of the deep ocean in the mid-Proterozoic, but instead that the deep ocean was ferruginous. Canfield (2004) proposed that this chemical condition was due to the subduction of sedimentary sulphides, which would have lowered the mass of the Earth-surface sulphur pool. Scott et al. (2008) suggested that a nutrient-limiting feedback associated with molybdenum made sulphidic conditions unsustainable, and therefore an improbable condition for the dominant redox state of the deep ocean. A significant amount of data presented by Canfield et al. (2008) showed that the late Neoproterozoic deep ocean was

predominantly ferruginous, with a few instances of possibly localised sulphidic conditions. Feng et al. (2010) concluded that Neoproterozoic Datangpo Formation black shale was deposited under predominantly ferruginous conditions, with brief sulphidic and possibly oxic excursions. Johnston et al. (2010) also found that ferruginous conditions dominated late Neoproterozoic deep ocean sediment preserved in the Chuar Group of the Grand Canyon. Coupled with the data presented by Canfield et al. (2008), Johnston et al. (2010) proposed a model dominated by ferruginous conditions, but with variable to long-lived mid-depth sulphidic conditions that were similar to the 'sulphidic wedge' model proposed by Poulton et al. (2010) for the 1.8 Ga Rove Formation (Thunder Bay, Ontario). Li et al. (2010) developed a similar 'sulphidic wedge' model, but upon closer inspection of geochemical signatures from the Doushantuo Formation samples (Fig. 3), it is obvious that the majority of the samples analysed by these authors were not truly black shale. When such samples are excluded from the dataset, the evidence and data trends for the proposed model disappear. Xiao et al. (2012), working on similar sections in the South China Block, found that the lower Doushantuo Formation sediment was deposited in a non-sulphidic water column, but state that more data are required before a sulphidic wedge model can be confirmed. Working on different sections in the South China Block (Shiyantou and Yuanshan Formations), Och et al. (2013), proposed a stratified ocean model in which rising sea level led to an increase in the Mo budget and subsequent upwelling of sulphidic waters onto the predominantly ferruginous Yangtze Platform. Based on these disparate models, further work is required to resolve the evolving picture of the basin chemistry of the South China Block. The South China Block, along with other preserved Neoproterozoic basins, is an essential asset in determining the ancient ocean redox state and the implications for life at this time. Planavsky et

al. (2011) studied several black shale deposits, including the 1.64 Ga Barney Creek formation in the McArthur basin, the 1.64 Ga Lady Loretta formation in the Mount Isa basin, the 1.7 Ga Chuanlinggou Formation in northern China, the 1.45 Ga Belt Supergroup in the north-central USA, and the 1.1 Ga Borden basin in Arctic Canada. The majority of samples from these basins yielded a ferruginous signature, with only minor episodes in which sulphidic conditions were reached. A more recent, detailed study of the Arctic Bay Formation, in the Borden Basin (Turner and Kamber, 2012), found that that basin was in fact deposited under primarily sulphidic conditions.

In summary, it is evident that the various proxies applied to the relatively few "black shale" occurrences have in some cases yielded conflicting information about the redox state of the Neoproterozoic ocean. This conundrum may be because of variable redox states, because information from black shale is not always totally reliable, because the deduced redox conditions only apply to a relatively isolated basin and not the open ocean, or because some studies were not performed on true black shales but instead on dark siltstone or calcareous shale. For example, close inspection of major element geochemistry from the Doushantuo Formation (Li et al., 2010) reveals that most of the samples were carbonates that had very low amounts of iron and aluminium, which in turn resulted in extremes in the iron speciation data. In contrast, the Stone Knife Formation, studied here, contains true black shale from a particularly crucial time in the Neoproterozoic.

This paper presents a detailed geochemical study of the black shale from the Little Dal Group, and compares it with other black shale deposits of Precambrian and Phanerozoic age. The study is based on major and ultra-trace element analysis, complemented by an analysis of the iron to aluminium ratio, and conventional iron speciation. Iron speciation and redox-sensitive trace metals (e.g., Mo) are used as proxies for ancient basin redox conditions.

2.4 Geologic Setting

Neoproterozoic strata of the Mackenzie Mountains, northwestern Canada, include the epicratonic Mackenzie Mountains Supergroup (Aitken, 1981; Long and Turner, 2012; Turner and Long, 2012) and the rift to passive margin succession of the Windermere Supergroup (Fig. 1; Long et al., 2008; Narbonne and Aitken, 1995). The Little Dal Group is dominated by carbonate, evaporite, and fine clastic rocks, and forms the upper part of the Mackenzie Mountains Supergroup (Fig. 1; Aitken, 1981). The Little Dal Group is conformably underlain by the fluvio-deltaic Katherine Group (Aitken et al., 1978; Long, 1977; Long and Turner, 2012) and is unconformably overlain by the Coates Lake Group (basal Windermere Supergroup; Aitken, 1981; Rainbird et al., 1996; Young et al., 1982). The Little Dal Group has been subdivided into seven units (Fig. 1; Turner and Long, 2012) and outcrops throughout the Mackenzie Mountains with an average thickness of 2 km.

The lowest formation-scale unit in the Little Dal Group is the Dodo Creek Formation, which is composed primarily of siltstone and sandstone that were deposited on a shallow-water shelf. It is conformably overlain by the Stone Knife and Silverberry Formations (Aitken, 1981; Batten et

al., 2004; Turner et al., 1997; Turner and Long, 2008; Turner and Long, 2012), which are the units most relevant to this study. The shallow-water Silverberry Formation in the southeast is composed primarily of dolomitic ooid and intraclast grainstone and stromatolites (Aitken, 1981; Batten et al., 2004). This lithofacies assemblage passes northwestward, crossing a boundary at a high angle to the paleo-basin margin, into the Stone Knife Formation (Aitken, 1981; Turner and Long, 2008). The deep-water Stone Knife Formation, the unit investigated in this paper (Figs. 2 & 4), is composed primarily of thin-bedded lime mudstone, shale and siltstone (black, grey and red), and large microbial build-ups (Turner et al., 1997). Black shale in the Stone Knife Formation was deposited in the deepest zone of a tilted subaqueous half-graben, which formed between two transfer faults in a zone of crustal extension (Turner and Long, 2008) that limits its geographic distribution. Based on all available data, the small area identified herein appears to be the only one that contains true black shale (Aitken et al., 2011; Turner and Long, 2008). Conformably overlying both the Silverberry and Stone Knife Formations are shallow-water ooid dolograinstone and dolomudstone of the Gayna Formation. The remainder of the Little Dal Group is not relevant to the present study; only the Stone Knife Formation is known to contain black shale.

The maximum possible depositional age of the Little Dal Group is provided by a detrital muscovite 40Ar/39Ar age of 817.8±0.9 Ma from the basal Dodo Creek Formation (Powell and Scheider, 2013), and by a youngest detrital zircon age of 1005 Ma from quartz arenite of the Katherine Group (U-Pb; Leslie, 2009). The minimum possible depositional age of the Little Dal Group is provided by a Pb-Pb age of 779 Ma on baddeleyite from a regionally continuous sill in

the Tsezotene Formation (Fig. 1), which has been interpreted as being coeval with dykes that cross-cut the Little Dal Group and with the "Little Dal basalt" (Heaman et al., 1992), a volcanic unit that locally overlies the Little Dal Group. The Stone Knife Formation has not been directly dated. In more general stratigraphic terms, it is important to note that the Stone Knife Formation underlies the ~720 Ma Rapitan Group banded iron formation by at least 2 km of strata belonging to the Little Dal and Coates Lake groups. By comparison with other Neoproterozoic black shales recently studied, the Stone Knife Formation is clearly older.

2.5 Materials and Methods

2.5.1 Samples

2.5.1.1 Terrigenous Clastic Sediment

Black shale and black muddy siltstone samples were collected for this study from the JS section of the Stone Knife Formation west of the Stone Knife River (equivalent to part of composite section 92-SKR of Turner and Long, 2008, and "Flank Gully" section of Aitken et al., 2011; Fig. 1C; NTS 106A, 64°47' N, 129°40' W). Samples were collected from a steep slope underlain by very gently dipping black shale and black siltstone near the base of Member 2 of the Stone Knife Formation (Turner et al., 1997; Turner and Long, 2008). The base of the shale interval is not exposed at this location but other work indicates that the black shale interval may be as much as 85 m thick in a poorly exposed drift-covered section nearby (Turner, 1999). The possibility of post depositional alteration was addressed and there is no significant evidence to suggest that this is a matter of concern at present. Deglaciation of the Mackenzie Mountains took place between

~18 and ~12 ka (Dyke, 2004), and so it should be understood that the material sampled has probably experienced a small degree of modern weathering. To minimize the influence of modern weathering, a shallow pit was excavated (~30 – 50 cm) for each sample and a large amount (ca. 1 kg) of material from a thin stratigraphic interval (1 – 3 cm) was removed using a pocket knife or rock pick. The freshest possible chips of shale were isolated for high-precision ultra-trace element and highly reactive iron analysis at Laurentian University. Elements that are typically mobile under modern weathering conditions (e.g., U) show no significant loss, indicating that the data in this study are robust. In addition, three strongly weathered yellow shale layers were also included in the sample set to assess the effects of weathering.

2.5.1.2 Sample Preparation

Thirty-five samples (~1.0 kg) were crushed using a hardened steel mallet, and from this a small sample, devoid of visible weathering, was hand-picked. The non-weathered material was pulverised to a +6 phi size and homogenised in a hardened steel percussion mill, which was cleaned thoroughly between samples to prevent cross-contamination.

2.5.2 Trace Element Analysis

The digestion and solution preparation procedures are similar to those described in Babechuk et al. (2010). All samples were digested using a low-pressure, closed beaker attack. Aliquots of the sample and rock standards weighing 100 mg were digested in Teflon beakers on hotplates at 130°C. Procedural blanks were prepared for each batch of samples. All acids used for the digestion were purified through a sub-boiling distillation process to minimize blank contribution.

Samples were attacked with 2.5 mL of concentrated HF acid and 1.0 ml of concentrated HNO_3 for 60 hours and then dried down. Upon dry-down, 1 mL of concentrated HCl was added to each beaker to further attack the remaining carbonaceous material. The HCl was then dried down and residues converted using concentrated HNO_3. The samples were evaporated to dryness once more and dissolved into a final 3N HNO_3 stock solution. Solutions were transferred to transparent polystyrene tubes, and inspected for residual fluorides and undissolved refractory minerals. Other than a residual carbonaceous flocculate suspended in some sample solutions, no refractory minerals or fluorides were noted. In preparation for ultra-trace analysis, the solutions were transferred to pre-cleaned polypropylene test tubes, an internal standard was added, and the samples were diluted with Milli-Q water to yield a 2% HNO_3 solution with dilution factors of 3,000. Samples were analysed at Laurentian University on a Thermo XSeriesII inductively coupled plasma mass spectrometer (ICP-MS) using the analytical procedures described in Eggins et al. (1997) and the modifications outlined in Kamber et al. (2005) and Kamber (2009). A full suite of trace elements for 32 Little Dal black shale samples was analysed as part of two separate experiments. For each batch of samples the calibration standards were 2,500x dilutions of two separate digestions of W-2 analysed at the start of each experiment run. The preferred calibration concentrations for W-2 have been published previously (e.g., Babechuk et al., 2010; Kamber et al., 2003; Marx and Kamber, 2010), and can be found in the Supplementary Information. The full trace element data for each sample are also presented in the Supplementary Information. An abbreviated version, with the most relevant data is reported in Table 1.

In addition to the black shales, each experiment batch included a digest of the USGS Cody Shale standard (SCo-1) to establish the accuracy and precision of the sample preparation and analysis. Siliciclastic sedimentary rocks may contain refractory heavy minerals such as zircon, which are resistant to the low-pressure chemical digestion procedure outlined above. From analyses of SCo-1 in previous studies, in the laboratory, it was apparent that the beaker digestion does not liberate all of the Zr, Hf, HREE, Ti, and Cr, as compared to a high-pressure bomb digest (Marx and Kamber, 2010). The analyses of all other lithophile elements and metals, however, compared well between the two digestion procedures. In the supplementary information, the data from the SCo-1 digest that accompanied each experiment batch are reported in addition to the average of the beaker and bomb digests obtained by the lab previously. In the case of the Little Dal black shale, the lack of visible residual minerals suggests that the low-pressure digest was successful at dissolving all of the mineral phases, and that the underestimation of Zr, Hf, and the REE has not significantly influenced the reported data. This conclusion is further supported by constant ratios of Zr/Hf in the black shale (Table 1). To demonstrate the reproducibility of the low-abundance lithophile elements using the low-pressure digest, the long-term average for the depleted basalt standard BIR-1 is also reported in the Supplementary Information.

2.5.3 Major Element Analysis

The major elements other than silicon were determined by ICP-MS using a more diluted (18,000x) aliquot of the original stock solution, which allows direct comparison for the Fe speciation data. The internal standards and operating procedures were the same as those described in section 3.2 for the trace element analyses. The data were calibrated using the

average of two digests of W-2 at the same dilution factor as the samples, to matrix-match the solutions; the certified USGS values were used for the calibration. Dilutions of SCo-1 and the more widely analysed USGS standards BCR-2 and BHVO-2 were also run as part of the major element experiment for the purpose of quality control (see Supplementary Table 1). The major element oxide determinations for BCR-2 and BHVO-2 are within 3% of the certified USGS values, with the exception of P_2O_5, and deviate by less for most of the elements. The accuracy of the major element determinations for SCo-1 relative to the certified USGS values is lower, but still within acceptable limits: the major element oxide values were within 20% or less of the certified USGS values for the first experiment batch and between 4 and 12% for the second experiment. The lower reproducibility of the SCo-1 standard almost certainly reflects a weigh-in mistake during preparation of the dilution. One consequence of analysing the major elements on the ICP-MS from an HF-HNO_3 digest is the inability to determine the Si concentration due to its volatility as a fluoride during the digestion procedure. For this reason, the major elements reported in Table 1 for the Little Dal black shale do not include SiO_2.

Carbon and sulphur contents were measured at the Ontario Geoscience Laboratories (GeoLabs). The elements were measured via infrared absorption as carbon and sulphur oxides generated during combustion in an oxygen-rich environment. Determination of the carbonate content and calcite/dolomite ratio was also performed at the GeoLabs using a Chittick apparatus. The total C was used in combination with the percentage of calcite and dolomite in the sample to determine the total organic carbon composition (TOC) of the black shale samples. All of the aforementioned values are reported in Table 1.

2.5.4 Degree of Pyritisation and Associated Trace Metal Analysis

Most studies of modern sediment and unweathered, well-preserved black shale employ a sequential extraction for iron speciation. Here, the traditional, non-sequential 12 N HCl boil degree of pyritisation (DOP) extraction technique for ancient sedimentary deposits (Roychoudhury et al., 2003), described in Raiswell et al. (1988; 1994) and Poulton and Canfield (2005) was used for the liberation of Fe_{HCl} for two reasons. First, because the paleomagnetic signature of the Little Dal black shale contains secondary components (Park, 1981) that must affect iron speciation, since the shale does not preserve its original mineralogy. Second, because an additional objective of this study was to attempt a determination of redox-sensitive trace metals in the HCl-digested fraction. The sequential extraction (Poulton and Canfield, 2005) uses a large number of chemicals and apparatus that cannot be easily cleaned to the level of purity required for ultra-trace element analysis. The desire to analyse the trace metals in the HCl extract necessitated a few small modifications to the conventional DOP method. Most importantly, triple-distilled acid and Teflon beakers were used instead of standard glass test tubes because elements can be leached from the glass and add significant contaminants. A precisely weighed 100 mg aliquot of sample was transferred into a Teflon beaker. A batch of concentrated, triple-distilled HCl was brought to a boil and added as a 1 mL aliquot to each beaker, which was subsequently sealed and placed on a hotplate for a full one-minute acid attack. The samples were then quenched by placing the sealed beakers in dry ice to avoid digestion of any of the unreactive silicate phases. The supernatant was centrifuged to separate the unreacted silicate phases from the HCl solution and transferred to pre-cleaned polypropylene test tubes. This solution was weighed and transferred back into a Teflon beaker to be dried down and converted using HNO_3,

in the same manner described in the trace element analysis section. A final 2% HNO_3 stock solution was diluted by 250x for elemental analysis by ICP-MS following the same procedure as for the whole rocks. The Fe_2O_3 from this HCl extraction was used in combination with the $Fe_2O_{3(T)}$ and S data to calculate the various species of Fe (reported in Table 1).

2.6 Results and Discussion

2.6.1 Major element geochemistry

The Little Dal black shale samples plot in a tight cluster on an Al_2O_3, MgO, CaO ternary plot, indicating that there is very little variation in the major element composition of the black shale (Fig. 3A). Three black shale standards, United States Geological Survey (USGS) SDO-1, and Vinogradov Institute of Geochemistry (VIG) SCHS-1 and SLg-1, along with USGS marine shale SCo-1 and carbonate-rich shale SGR-1, were compared to the Little Dal black shale (Fig. 3A). The Little Dal black shale samples plot close to the black shale standards but have a somewhat greater proportion of Al_2O_3, indicating that the sediment supplied to the basin had experienced a greater degree of weathering than the standards, or that the shale standards contain a greater proportion of CaO. The Little Dal black shale is locally interbedded with rare carbonate rocks, and so calcite and dolomite were also plotted (Fig. 3A) to verify that the samples were not contaminated with calcareous material, or that black carbonates had not been sampled inadvertently.

2.6.2 Characteristics of sediment sources for Little Dal Group

Prior to detailed discussion of redox-sensitive trace metals, it is important to examine rare earth element + yttrium (REE+Y) patterns, Nb/Ta, Zr/Hf, and Y/Ho ratios, to determine the sediment source of the black shale, and to establish that the source remained constant throughout deposition. Consistency of the sediment source is an important factor when considering trace metal enrichments, because change in apparent enrichment may be related to variations in sediment supply. Normalised REE+Y patterns and elemental ratios such as Nb/Ta, Zr/Hf, and Y/Ho can be used to distinguish sedimentary sources; significant changes in these ratios likely reflect a change in sediment source. The shale-normalised REE+Y pattern for the Little Dal black shale (Fig. S1) is relatively flat, which is expected of sediment derived from weathering of upper continental crust (UCC). There is a negative Eu anomaly, which is consistent with extensive weathering of the precursor material via loss of plagioclase (e.g., Marx and Kamber, 2010). The high field strength element ratios are very constant through the profile. The Nb/Ta ratio averages 12.81±0.46, the Zr/Hf ratio yields an average of 34.76±0.53, and the Y/Ho average is 25.69±1.09. All of these values are within the range of typical upper-crustal averages. The flat REE+Y pattern and the small spread of the conservative element ratios suggest not only that the sediment source remained stable throughout deposition, even though there is a minor grain-size distribution change over the depositional interval, but also that variations in trace metal concentrations cannot be attributed to a change in sediment source.

The only notable difference between shale and siltstone samples is the level of total organic carbon (TOC). The shale samples have an average TOC of 4.79 wt% (maximum value 8.05

wt%), whereas the muddy siltstone samples have an average TOC of 1.91 wt% (maximum value 5.22 wt%) (Fig. 5A). Both sediment types are organic-rich as compared to material in other black shale studies (Canfield et al., 2008; Feng et al., 2010; Johnston et al., 2010); approximately half of the samples are in the low-oxygen oxic range and half are in the anoxic range. Most of the shale samples are above the 2.5 wt.% threshold for anoxia, and most of the siltstones fall below this threshold into oxic conditions. However, the minimum TOC criterion may not apply to the siltstone samples due to the increased sedimentation rate.

2.6.3 Iron speciation

Iron concentrations are relatively constant throughout the stratigraphic interval studied, with a total iron (Fe_T) average of 4.26±0.93 wt.% (maximum value 6.44 wt.%). These values compare well with those from other black shales (Canfield et al., 2008; Feng et al., 2010; Johnston et al., 2010). The Fe_T consists of two components: unreactive iron (Fe_U), contributing on average 40% of the Fe, and Fe_{HCl}, contributing the remaining 60% of the Fe on average. The Fe_{HCl} pool was also determined to be, on average, 25% held in pyrite (Fe_{PY}), and 75% in the oxide and carbonate phases. The Fe_{PY} concentration ranges from 0.01 wt.% to 1.65 wt.% throughout the studied interval, with the highest enrichments in the lowest 15 m and the least enriched samples in the 15-30 m interval.

Ratios of iron species, for example Fe_T/Al, Fe_{HR}/Fe_T, Fe_{PY}/Fe_{HR} and DOP, give valuable information on the redox state of ocean systems. At the present time it is unclear whether the more classic measures of Fe speciation (Fe_T/Al and DOP) yield more valid conclusions than the

more sophisticated sequential extraction technique (Fe_{HR}/Fe_T and Fe_{PY}/Fe_{HR}), because the latter was developed for unconsolidated sediment, whereas the former has been successfully applied only to rocks. The one very obvious requirement for being able to analyse Fe_{HR} is that the sedimentary rock carries a purely primary magnetisation, which ensures that all Fe is still in near-original state. The Little Dal Group is known to carry both a primary and secondary magnetisation (Park, 1981), and so this criterion is not met by the studied samples.

The most cautious approach for the Little Dal black shale is to interrogate the section initially with Fe_T/Al and DOP. Trace metal concentrations in black shale have varied through time, a phenomenon that has been attributed to the oxygenation of the atmosphere and increased continental weathering through time (Scott et al., 2008). The trace metal concentrations in shale, particularly those that are redox-sensitive, are strongly affected by the oxidation state of the paleo-atmosphere, the composition of the sedimentary rocks being deposited and the redox status of the overlying water column.

In the Black Sea, a modern sulphidic basin, the Fe_T/Al ratio ranges from 0.6 to 1.2. Ancient sulphidic basins generally have Fe_T/Al ratios >1, and can have values as high as 13, whereas ancient black shales deposited under oxic conditions have Fe_T/Al ratios up to 0.5 (Feng et al., 2010; Lyons and Severmann, 2006; Raiswell et al., 2008; Raiswell et al., 2011; Reinhard et al., 2009). The Little Dal black shale and siltstone samples have Fe_T/Al values from 0.29 to 0.85, with an average of 0.51 (Fig. 5B). This range is very similar to the average Fe_T/Al for Mud of Queensland (MUQ), an UCC proxy derived from C-rich modern alluvial sediment (Kamber et

al., 2005). The Little Dal black shale samples have Fe_T/Al values from 0.36 to 0.85 (average 0.58); the majority of samples are above the oxic threshold, indicating that they were deposited beneath an anoxic water column (Fig. 5B). The black muddy siltstone samples have lower Fe_T/Al values, ranging from 0.29 to 0.68 (average 0.47; Fig. 5B). The majority of the black siltstone samples fall into the range indicating oxic conditions, but several are in the anoxic field. The Little Dal Group has been largely unaffected by modern weathering and is unmetamorphosed, indicating that there has not been a significant gain or loss of Al. Low Fe_T/Al can develop under ferruginous conditions when authigenic Fe is volumetrically overwhelmed by a comparatively high siliciclastic supply (Lyons and Severmann, 2006). This may be the origin of the lower Fe_T/Al values in the coarser-grained (silty) samples. If a comparatively high sedimentation rate overwhelmed the authigenic Fe produced under anoxic, ferruginous conditions, material that had been deposited under anoxic conditions could yield misleading oxic results. This problem highlights the importance of ensuring that shale samples used in redox studies are truly black shale rather than silty shale or siltstone. Even though many of the Little Dal samples yielded anoxic Fe_T/Al signatures, the relatively low Fe_T/Al suggests that the sediment was not deposited under a predominantly sulphidic water column, as would be predicted by the Canfield (1998) and Canfield et al. (2008) ocean model.

This study places special emphasis on degree of pyritisation (DOP; Raiswell et al. (1988) the ratio of $Fe_{PY}/ (Fe_{PY} + Fe_{HCl})$. Sediment deposited beneath a sulphidic water column yields DOP >0.8. When the pyrite formed by the shuttle-enrichment of iron (Lyons and Severmann, 2006) is overwhelmed by significant siliciclastic sedimentation, the DOP value can fall below the 0.8

threshold, yielding misleading data. The samples from the Stone Knife Formation have DOP values ranging from 0.002 to 0.458, with an average ratio of 0.188 (Fig 5F). Both black shale and black muddy siltstone fall well below the sulphidic threshold, but it should be noted that, as indicated by Lyons and Severmann (2006), coarser material (deposited under conditions of increased siliciclastic sedimentation) has a lower average DOP than does pure black shale. The black shale samples have an average ratio of 0.21, and the black muddy siltstones have an average ratio of 0.17 (Fig 5F). The unexpectedly low DOP values may suggest that sulphide production by sulphate reduction in the Little Dal sediments was slow, and that pyrite formation was limited by the availability of reactive iron (Canfield et al., 1992). This would suggest that all the iron oxyhydroxides and oxides were not consumed in pyrite formation and that free H_2S was not in the water column. The low DOP ratio, suggesting a non-sulphidic basin, is in agreement with the Fe_T/Al values.

Based on the speciation of Fe, elevated Fe_T/Al, and low DOP, the depositional environment of the Little Dal black shale was predominantly ferruginous with oxic episodes, rather than sulphidic (Lyons et al., 2009). This implies that the Little Dal black shale was deposited in either a shallow-marine setting that at times was ferruginous, or a deep ferruginous basin with oxic episodes. The sedimentology and stratigraphy of the Stone Knife Formation strongly support a comparatively deep basin (below photic zone and storm wave-base; Turner et al., 1997; Turner and Long, 2008). Deposition of the Stone Knife Formation took place under comparatively normal, open-marine conditions, with no significant restriction of water circulation; the succession contains no evidence of evaporite minerals, indicating that no physical barrier limited

circulation of marine water into the basin, that fetch would not have been limited, and that storm wave-base was not constrained by basin configuration. The four members of the Stone Knife Formation were deposited as four transgressive – regressive cycles that are shale- or siltstone-dominated in their lower, transgressive parts and lime-mudstone-dominated in their upper, regressive parts (Turner et al., 1997; Turner and Long, 2008). The transgressive interval of Stone Knife Formation Member 2 contains the deepest-water lithofacies of the entire Little Dal Group, represented by the black shale that is the focus of this study (Figs. 1, 2D). The Stone Knife Formation above the top of Member 1 was deposited entirely below the photic zone and almost entirely below storm wave-base: level-bottom strata of Stone Knife Formation Members 2 and 3 in the black shale location contain no microbialites and regionally contain only local, rare hummocky cross-stratification (HCS), in the shallowest parts of regressive cycle tops (Turner, 1999; Turner et al., 1997), suggesting a hypothetical minimum water depth of approximately 50-70 m for a sea-floor under a comparatively clear water column. The black shale location is spatially associated with large, deep-water reefs (Fig. 2). Geometric relations between the reefs and surrounding layered strata of the Stone Knife Formation (Turner et al., 1997) suggest that the basin floor was at some times >100 m below the reef growth surface, which was in the middle of the photic zone during most stages of reef growth, based on stromatolite morphology, associated sediment composition and sedimentary structures in the reefs (Turner et al., 2000). Reef talus blocks that fell from reefs during shale deposition of Member 2 are up to several tens of metres in diameter, providing another assessment of minimum basin depth. This collective evidence indicates paleo-water-depth of at least 100 m during deposition of Stone Knife Formation Member 2 black shale.

The ferruginous state of deep water during deposition of this part of the Little Dal Group indicates that the mid-Neoproterozoic ocean, by the time of Little Dal shale deposition, may not have been sulphidic, as was proposed by Canfield (1998) and Canfield et al. (2008). These findings from the Little Dal black shale are consistent with recent work published by Feng et al. (2010), Johnston et al. (2010), Planavsky et al. (2011), and Sperling (2013). The Datangpo black shale of the South China Block, deposited between 663 and 654.5 Ma (Zhang et al., 2008; Zhou et al., 2004), shows fairly constant ferruginous paleoredox conditions, with the exception of several oxic excursions that generated Fe_{HR}/Fe_T ratios of <0.38. The interpretation of the Datangpo black shale is in good agreement with that of the Little Dal black shale: predominantly ferruginous conditions with the exception of several brief intervals during which sulphidic conditions developed (Feng et al., 2010). By comparison, black shale in the Chuar Group, U.S.A., deposited at approximately 742 Ma (Karlstrom et al., 2000), shows slightly more complex ocean paleoredox conditions than does the Little Dal black shale. Data published by Johnston et al. (2010), which contains Chuar Group black shale data previously published by Canfield et al. (2008), shows a basin that had significant depositional intervals of both anoxia and oxia. The significant thickness of Chuar Group black shale with Fe_{HR}/Fe_T values <0.38 may record cyclic incursions of oxygenated water into an anoxic basin, or significant thicknesses of black shale deposited in an oxygenated, shallow-shelf setting. The remaining samples, with Fe_{HR}/Fe_T values >0.38, would have been deposited in a deeper zone, below an anoxic water column. The Fe_{PY}/Fe_{HR} data of Johnston et al. (2010) showed that all of the samples studied had been deposited under ferruginous conditions (Fe_{PY}/Fe_{HR} ratios <0.80). The data from Canfield et al. (2008) contain several samples high in the studied stratigraphic interval that were deposited

under sulphidic conditions (Fe_{PY}/Fe_{HR} >0.80). The combined Chuar Group data suggest that that basin experienced both oxic and ferruginous conditions, and also that there was an interval late in basin development during which sulphidic conditions were reached. Additionally, the 800 Ma black shale of the Fifteenmile Group, Ogilvie Mountains, Canada, show similar paleoredox conditions as the Little Dal and Datangpo sediments. The Fifteenmile black shale indicates an oxygenated surface layer, down to storm wave base, overlying a generally anoxic deep basin. The deep basin had several fluctuations between mainly ferruginous and sporadic sulphidic conditions (Sperling et al., 2013).

Other ferruginous basins appear to have experienced redox fluctuations. Black mudstones from the 1.64 Ga Barney Creek and Lady Loretta formations in the McArthur and Mount Isa basins, 1.7 Ga Chuanlinggou Formation in northern China, and the 1.45 Ga Belt Supergroup in the north-central USA were found to have had prolonged intervals of a deep ferruginous water column with brief episodes approximating sulphidic conditions (Planavsky et al., 2011). The Mt Isa superbasin and the Belt Supergroup had several samples with significant iron enrichments and Fe_{PY}/Fe_{HR} ratios above the 0.7-0.8 sulphidic threshold, indicating that sulphidic conditions may have been episodic. The interpretation for these mid-Proterozoic black mudstones is also in good agreement with the Little Dal black shale. In summary, the four older mid-Proterozoic and the two younger Neoproterozoic basins had paleoredox conditions that resemble those of the Little Dal black shale, although their geochemical histories, in certain instances, were more complex. The South China Block, Chuar Group, Mt Isa, and Belt basins experienced a wide range of redox conditions that included both brief sulphidic episodes and extended intervals of

oxia, which could be the result of changing basin architecture, or the effect of changing sea level that moved a 'sulphidic wedge' through the water column (Li et al., 2010). The Stone Knife Formation basin appears to have been ferruginous with oxic, rather than sulphidic, excursions.

2.6.4 Trace elements and metal enrichment factors

Calculation of enrichment factors (EF) allows for detailed analysis of metal enrichments throughout a given black shale succession, and relationships among different metals can be identified. With a stable sediment source, variations in trace metal concentration can be attributed to organic scavenging of metals, scavenging by sedimentary particles, or interactions with pore water (Lyons et al., 2009). To determine trace metal enrichments in the Little Dal black shale, EFs were calculated (Fig. 5C-E) by normalising the trace metal concentrations to Al and comparing them to the upper crust average MUQ: $EF_X = (X/Al)/(X_{MUQ}/Al_{MUQ})$, where X represents the metal in question. Traditionally, EFs have been calculated by comparing Al-normalised trace metals to the average shale values of Wedepohl (1971; 1991) (e.g., Feng et al., 2010; Tribovillard et al., 2004), but in this study, MUQ was used because it removes from consideration both authigenic enrichment during deposition and supergene weathering. The Fe_T/Al ratio of MUQ is approximately 0.5, which is consistent with other averages of the UCC (Taylor and McLennan, 1985), and justifies the use of MUQ in calculating EFs for the materials used in this study. An EF >1 for the trace metal indicates enrichment relative to MUQ, whereas a value <1 indicates depletion.

Molybdenum is of particular interest because it tends to have low background values and is a sensitive redox proxy for both local and global paleoredox. In the modern ocean, Mo is the most overly enriched transition metal. It occurs as the molybdate anion (MoO_4^{2-}), which converts to thiomolybdate ($MoO_{4-x}S_x^{2-}$) or oxythiomolybdate ions ($MoO_xS_{4-x}^{2-}$) in environments with free hydrogen sulphide. These ions may then have interactions with organic matter or sulphide minerals and become incorporated into the minerals and accumulate in sediment (Erickson and Helz, 2000; Helz et al., 1996; Lyons et al., 2009; Tribovillard et al., 2004; Zheng et al., 2000). Marine molybdenum concentrations were relatively low during the Precambrian, modestly enriched during the Paleoproterozoic, and significantly higher from the Cambrian to the present (Fig. 6). According to the sulphidic ocean model, Mo enrichment in Proterozoic black shale was limited owing to constant burial of Mo and organic carbon, which decreased the oceanic Mo reservoir (Scott et al., 2008). Considering that the Little Dal black shale was deposited under ferruginous conditions during the early Neoproterozoic, and in keeping with other Proterozoic black shale, its Mo concentrations (Figs. 5C & 6) are significantly lower than those of Phanerozoic examples. This is in agreement with previously published values for Mo concentration, and indicates that the oceanic Mo pool at the time was limited (Alberdi-Genolet and Tocco, 1999; Caplan and Bustin, 1998; Cruse and Lyons, 2004; Dahl et al., 2011; Feng et al., 2010; Hatch and Leventhal, 1992; Hatch and Leventhal, 1997; Hirner and Xu, 1991; Leventhal, 1991; Mongenot et al., 1996; Och et al., 2013; Sageman et al., 2003; Scott et al., 2008; Sperling et al., 2013; Werne et al., 2002; Yamaguchi, 2002). This condition is most readily explained by semi-continuous transfer of Mo into S-rich sediment that was accumulating in parts of the ocean. Molybdenum concentrations increased markedly at around 663 Ma (Scott et al.,

2008), which may indicate a rise in the global ocean molybdate reservoir caused by oxidative weathering and a shift away from sulphidic shallow-water conditions.

The markedly low Mo concentrations (maximum 7 ppm) in the Little Dal black shale do not mean that Mo is not enriched, because there is a strong correlation with many other trace metal enrichment factors (Fig. 5D-E). Iron speciation, trace metal enrichments, and TOC are proxies for the redox state of seawater (Fig. 5). In the present dataset, enrichment of Mo, U, and V covary. These trace metal enrichments coincide with elevated Fe_T/Al, and with increased TOC values (Fig. 5). The enrichment of these trace metals varies under certain conditions; Mo reacts to euxinic conditions, becoming enriched, whereas U and V do not. The enrichment of Mo, elevated Fe_T/Al, and TOC at the top of the succession also corresponds with elevated DOP values, suggesting that the water column may have been approaching sulphidic conditions during this interval. Confirming sulphidic conditions would require a full sequential extraction, but given that the Stone Knife Formation material is not completely unweathered, and does not have iron in its original species, as shown by its complex paleomagnetic signature, the necessary conditions for sequential extraction are not met.

From the existing dataset, it can be gathered that generally, the samples with the highest DOP also have strong enrichments in the trace metals, including enrichment in Mo that deviates from U and V. These relationships suggest either that persistent oxic weathering took place on land, increasing the global availability of these trace metals, or that scavenging of these trace metals by organic carbon controlled metal enrichments in the black shale. Based on the model of Algeo

and Tribovillard (2009) the enrichment factors of Mo and U in the Little Dal black shale indicate that the sediment was deposited in an anoxic open-marine setting similar to the Eastern Tropical Pacific, with minor sill-restriction that was similar to that of the Cariaco basin, but not nearly as extreme (Fig. 7).

The Fe_{EF} in the Little Dal sediment yields surprising results suggesting that there was an overall deficit in Fe compared to average UCC (Fig 8A). The Fe in the material studied is predominantly in the highly reactive phases, and although its concentration is highest in black shale and its depletion relative to UCC the least pronounced, the Fe concentration in the other two rock types is not significantly different. This indicates that the Little Dal sediments were not strongly anoxic and that there may have been episodes of deposition under an oxic water column. A possible cause for the unexpected depletion of Fe is the weathering status of the original source material. MUQ is weathered from an Fe-rich mafic source, whereas the Little Dal sediments would have been sourced from older exposed strata and cratonic granites from the present-day east.

A novel aspect of this study is that several trace elements were also analysed in the highly reactive iron phase. Of those Mo, U, and V were of particular interest due to levels of enrichment and correlations with redox proxies in the whole rocks (Fig. 8). Results from the highly reactive iron phase analysis show that Mo has an association with pyrite, with a large proportion being held in the highly reactive phases liberated during the HCl extraction (Fig 9A,C, & 8B), and is the most enriched relative to MUQ (Fig. 8A). Although Mo is known to be shuttled to the sea-floor with sulphur under sulphidic conditions, in the Stone Knife sediments it is more strongly

associated with TOC than with pyrite (Fig. 9B & D). Both Fe_T and DOP are low in Stone Knife sediments, and although sulphur was involved with the shuttle to the sea-floor, apparently sulphide was not involved with long-term sequestration in the sediment, due possibly to depleted levels of Fe. This outcome seems to strongly support the conclusions of Chappaz et al. (2013) that Mo is not held in highly reactive pyrite phases. Given that the multiple redox proxies do not indicate sulphidic water-column conditions, it is unclear why Mo enrichment occurred in the Stone Knife sediment. One possibility is that Mo may not require sulphidic conditions in order to be exported to the seafloor, and that instead low oxygen or ferruginous conditions may be sufficient for Mo removal. Thus, the redox behaviour of Mo may be more complicated than originally proposed (see also Scholz et al., 2013 & Chappaz et al., 2013) and may be explained by the strong association with TOC rather than with pyrite formed under euxinic conditions.

It is clear that U and V enrichments are not associated with pyrite in the Stone Knife material, and only a small proportion is held in the highly reactive phases (Fig. 9E, G, I, K, & 8B), suggesting that the majority of U and V are held in silicate minerals. Relative to MUQ, both U and V are enriched (Fig. 8A), but they are most strongly enriched in the black shale, which may reflect a minor hydrogenous contribution relative to the clastic component. There is a weak correlation between U and TOC that is not present with V, suggesting a difference in redox behaviour whereby U was scavenged by organic matter but V was not. Both U and V covary with Mo (Fig. 5) but do not show the same levels of enrichment, or the strong association with TOC, suggesting that a different redox mechanism controlled their enrichment. This relationship requires further study.

2.6.5 Implications for paleoredox conditions

Recent work on Proterozoic to early Paleozoic black shale formations has revealed a general trend of primarily ferruginous conditions, with isolated sulphidic areas, throughout this interval (Canfield et al., 2008; Feng et al., 2010; Johnston et al., 2010; Li et al., 2010; Och et al., 2013; Planavsky et al., 2011; Poulton et al., 2010; Sperling et al., 2013; Turner and Kamber, 2012; Xiao et al., 2012). A compilation of Proterozoic to early Paleozoic black shale Fe_{PY}/Fe_{HR} helps to clarify the evolving perception of ocean chemistry at this time. Very few Neoproterozoic black shale units have Fe_{PY}/Fe_{HR} >0.7 or DOP >0.8, and so most were not deposited under sulphidic conditions. Most black shale successions deposited during the Neoproterozoic were deposited under ferruginous conditions, and even though the early Cambrian does record an increase in sulphidic conditions, the majority of these shale units were deposited under a non-sulphidic water column.

2.7 Conclusions

The material collected from the Little Dal Group is true black shale, with high TOC, moderate enrichment in redox-sensitive metals, and limited geographic extent. Black muddy siltstone samples are geochemically very similar to black shale samples, with the only major (and expected) distinctions being lower TOC and lower authigenic iron in the siltstone. This relationship highlights the importance of using only true black shale in redox studies, because misleading variability in paleoredox results can be produced by even subtle increases in siliciclastic sediment supply. Iron speciation ratios and Mo concentrations from the Little Dal samples indicate that early to mid Neoproterozoic (<817 Ma; >780 Ma) deep-ocean water conditions were ferruginous with episodic transitions to oxia. One stratigraphic interval yielded iron species ratios and trace element enrichment that may indicate a brief episode during which the lower water column was strongly anoxic; this may represent a short-lived excursion, or perhaps the migration of a sulphidic wedge relative to sea level or sulphate production in mid-depth waters. These findings alone are not definitive regarding the sulphidic wedge model for ocean chemistry, but when combined with other studies (e.g., Baldwin et al., 2012; Canfield et al., 2008; Feng et al., 2010; Johnston et al., 2010; Poulton and Canfield, 2011; Poulton et al., 2010) the evidence for a mid-depth sulphidic wedge is compelling. The geochemistry of the Little Dal black shale shows that the predominant redox structure of the early Neoproterozoic deep ocean was ferruginous with oxic episodes, and the findings of Poulton and Canfield (2011) stating that the late Neoproterozoic deep-water conditions were ferruginous rather than sulphidic, can be extended back into the early Neoproterozoic.

2.8 Acknowledgements

This work would not have been possible without Geoffrey J. Baldwin and Annette Gladu, who helped with stimulating discussions, laboratory assistance, and sample collection. Darrel G.F. Long is thanked for his advice and suggestions throughout the writing of this paper. The assistance and suggestions on black shale formation of Peir K. Pufahl were greatly appreciated. Fieldwork was supported by the Northwest Territories Geoscience Office, the Northern Science Training Project (Department of Indian and Northern Affairs), a student research grant from the Society for Economic Geology Foundation (SEGF), and NSERC Discovery Grants to both ECT and BSK. Special thanks to Chao Li for providing the unpublished data from the Doushantou Formation. This is Northwest Territories Geoscience Office contribution number 0058.

2.9 Figures

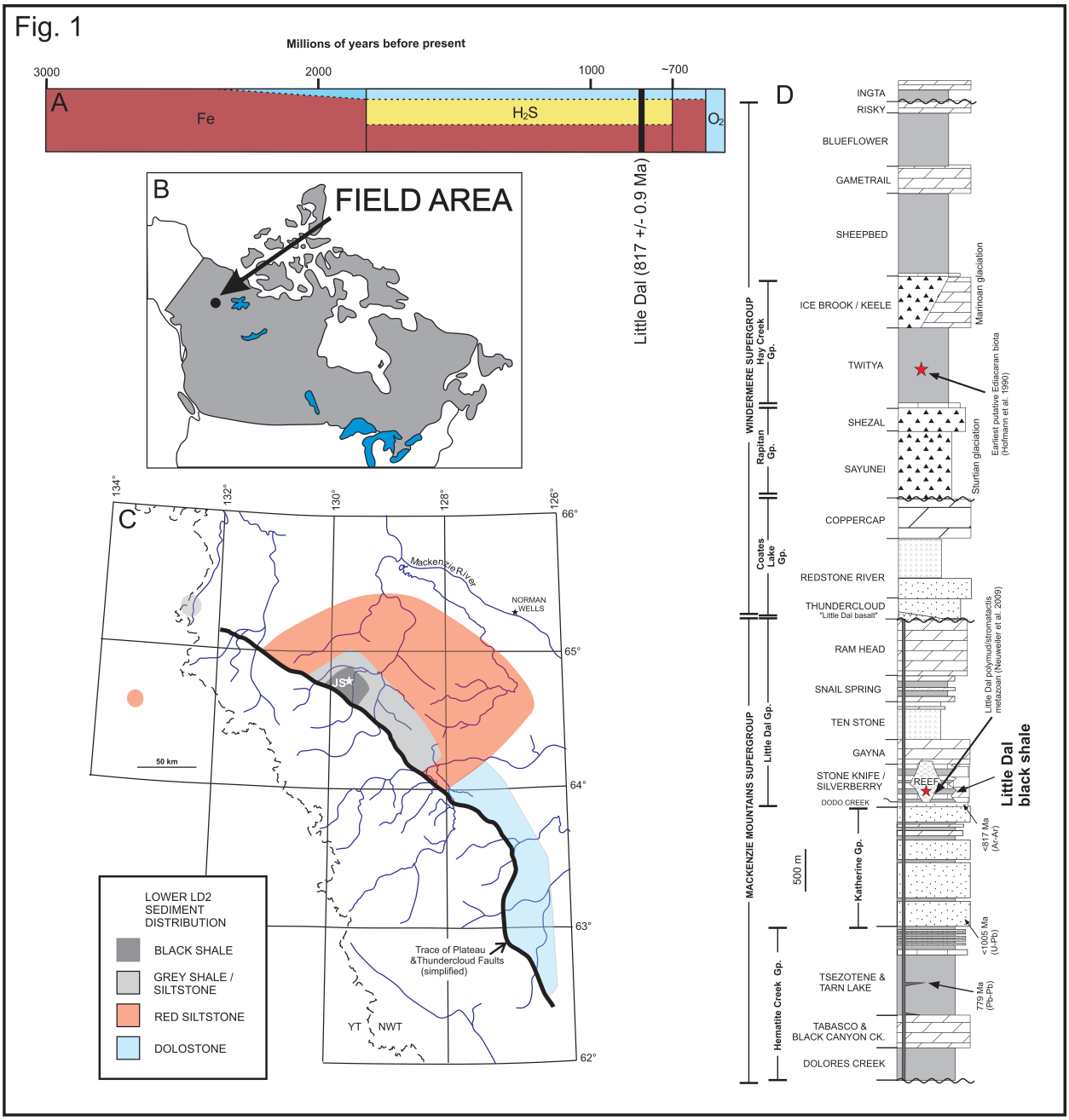

Figure 1. Geological context of the Little Dal black shale. (A) The "Canfield ocean" timeline (Canfield, 1998; Canfield et al., 2008) proposed that widespread anoxia persisted to at least 540 Ma. At 1800 Ma the deep ocean became dominated by H_2S rather than Fe, ending the deposition

of banded iron formations (BIFs). At ~700 Ma the deep oceans are suggested to have returned to a ferruginous state allowing, once again, for deposition of BIFs before reaching present-day deep-ocean oxygenation. (B) Location map of the study area in Northwest Territories, Canada. (C) Distribution of shallow- and deep-water environments of the Silverberry (blue) and laterally equivalent Stone Knife formations (red, grey, and black) during deposition of black shale, Little Dal Group, based on Aitken et al. (2011). Isolated pink circle is Stone Knife Formation inlier in Yukon (Turner, 2011). (D) Stratigraphic section through the Mackenzie Mountains Supergroup and overlying Windermere Supergroup. Radiometric dates are from Heaman et al. (1992) and Leslie (2009).

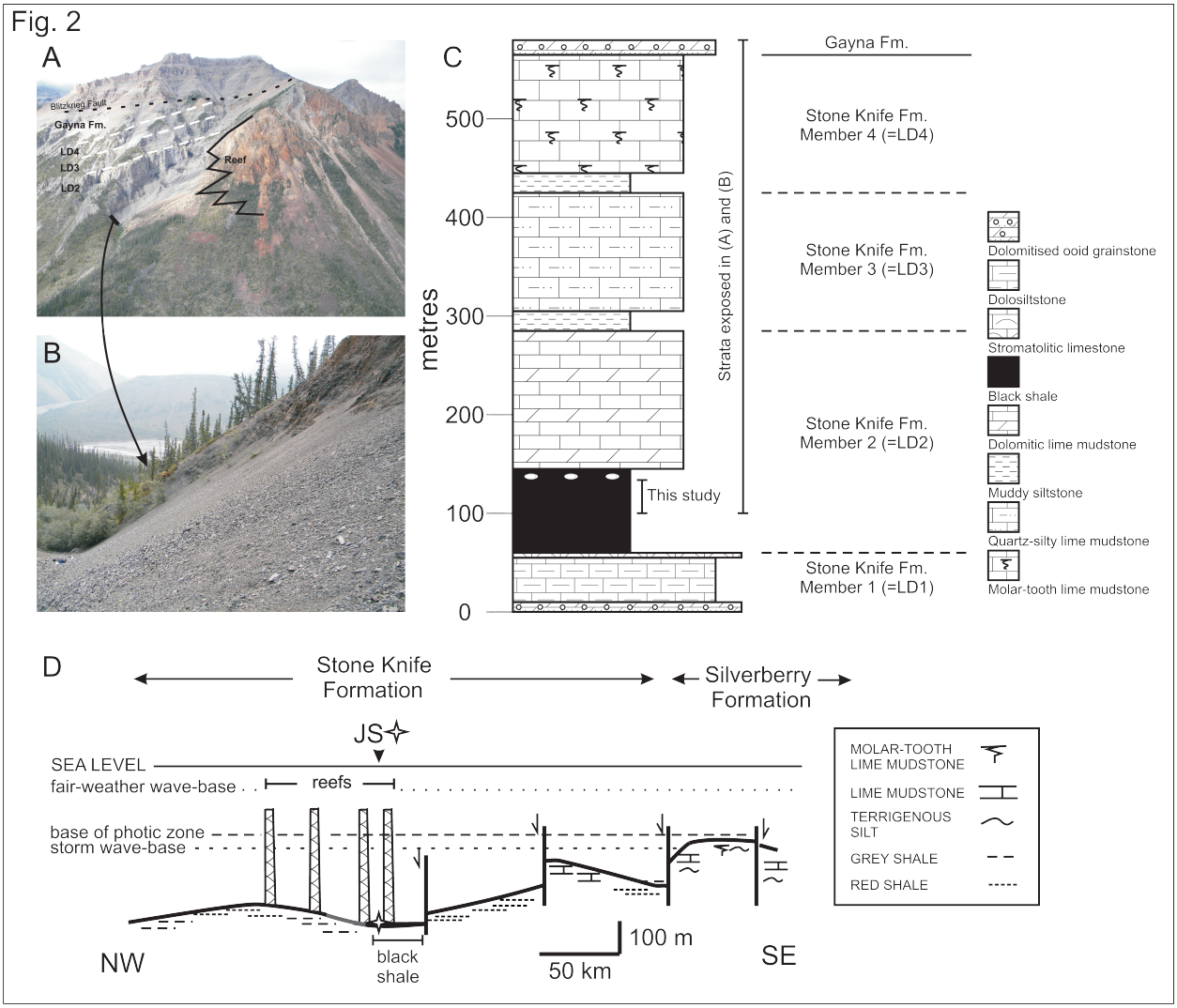

Figure 2. Exposure and stratigraphic context of black shale in the Stone Knife Formation, Little Dal Group. (A) and (B) Exposure of Stone Knife Formation layered strata and associated deep-water reef near Stone Knife River. Subdivisions (LD2-4) of the Stone Knife Formation correspond to transgressive-regressive packages (Turner and Long, 2008). The black shale interval (upper part of lower LD2) analysed in this paper is highlighted in (B) and (C). The lower part of the Stone Knife Formation is not exposed at this location. (C) Strata exposed in (A) and (B) form part of composite section 92-SKR (Turner and Long, 2008). (D) Paleogeographic

reconstruction of the transgressive phase of Stone Knife Formation member 2, showing sea-floor lithofacies, relative disposition of water-column interfaces, faults that were active during deposition of LD2 transgressive phase, limited distribution of black shale and reefs, and location of section JS. Diagram is modified after Turner and Long (2008).

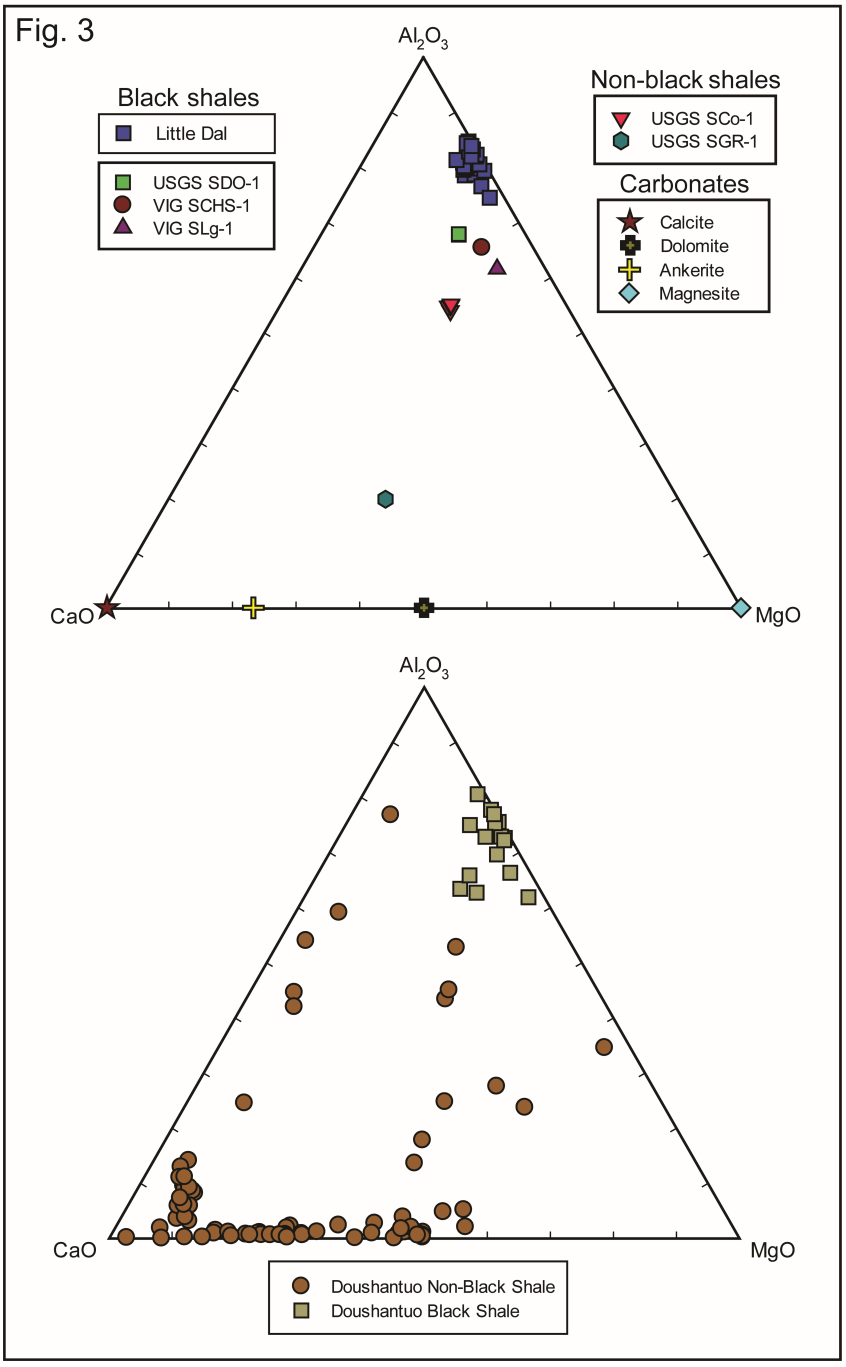

Figure 3. Major element geochemistry of the Little Dal black shale. (A) Al_2O_3, MgO, CaO ternary plot for Little Dal black shale, as well as black shale standards SDO-1, SCHS-1, and SLg-1, including non-black marine shale SCo-1, carbonate-rich shale SGR-1, and elemental

concentrations of calcite, dolomite, ankerite, and magnesite. Due to very consistent trace element geochemistry, the Little Dal black shale samples plot in a tight cluster at >70% Al_2O_3, approx. 15-20% MgO, and <10% CaO. Comparison of the shale standards and carbonate rocks with the Little Dal samples shows that the latter was not contaminated by calcareous material. The Little Dal black shale samples and the black shale standards do not overlap perfectly, perhaps owing to original compositional variations or to weathering. (B) Al_2O_3, MgO, CaO ternary plot for material from the Doushantuo Formation (unpublished data from Li et al., 2010). Comparison of Doushantuo Formation material with shale standards and carbonate rocks (A) shows that most samples do not plot near black shale or other shale standards, but that the majority of the samples overlap with calcite, ankerite, and dolomite. When this is taken into account the trends and evidence for the 'sulphidic wedge' model proposed by Li et al. (2010) are no longer evident.

Fig. 4

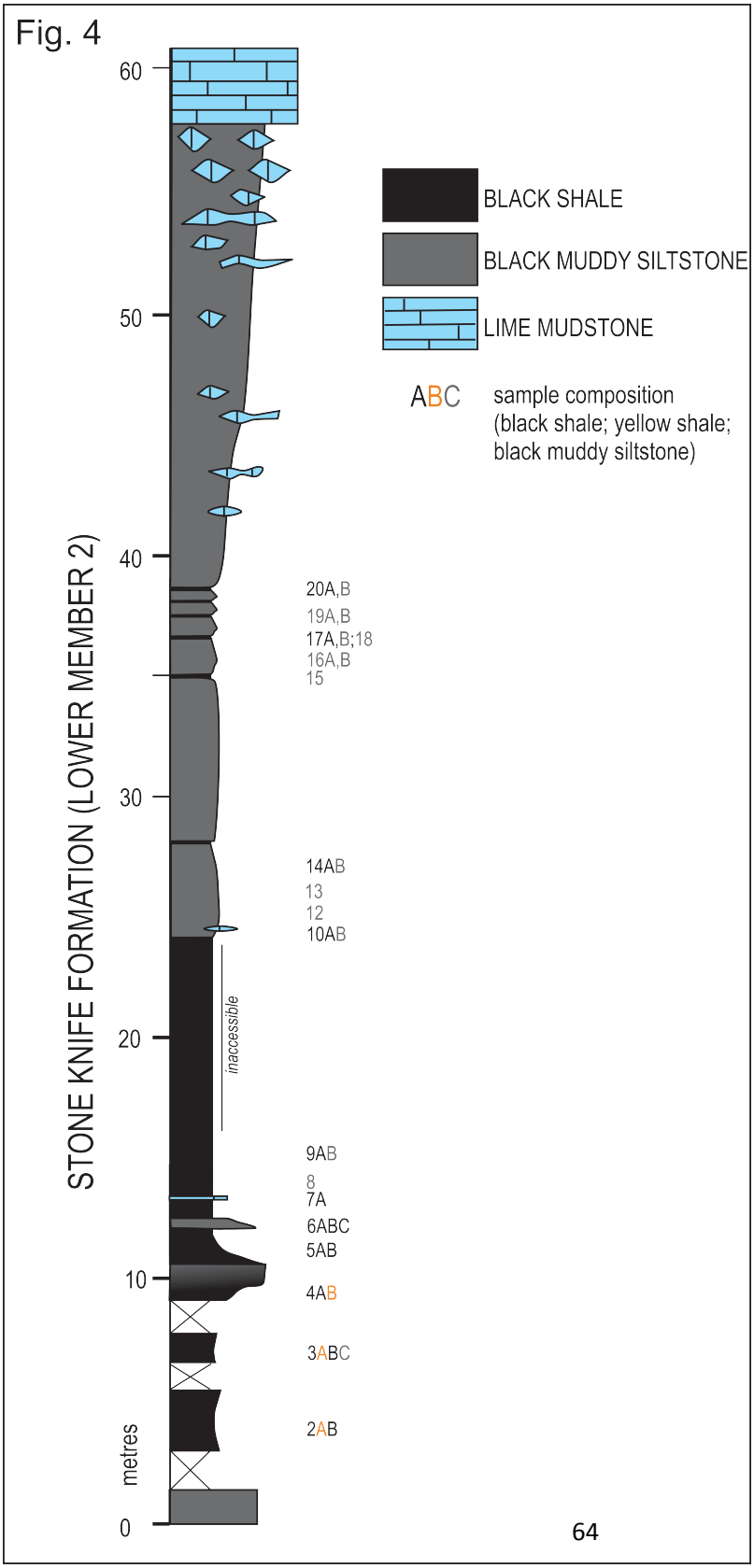
STONE KNIFE FORMATION (LOWER MEMBER 2)
metres
0
10
20
30
40
50
60
BLACK SHALE
BLACK MUDDY SILTSTONE
LIME MUDSTONE
ABC
sample composition
(black shale; yellow shale;
black muddy siltstone)
20A,B
19A,B
17A,B;18
16A,B
15
14AB
13
12
10AB
inaccessible
9AB
8
7A
6ABC
5AB
4AB
3ABC
2AB

Figure 4. Detailed stratigraphic section showing the Stone Knife Formation (LD lower member 2). The deep-water Stone Knife Formation is composed primarily of thin-bedded lime mudstone, shale and siltstone (black, grey and red), and large microbial build-ups (Turner et al., 1997). The shallow-water area is composed primarily of transgressive intraclastic carbonate and deep-water lime mudstone that is overlain by a shallowing succession of stromatolites, oolite, and molar-tooth bearing carbonates (Turner and Long, 2008). Black shale in the Stone Knife Formation was deposited in the deepest zone of a tilted half-graben, which formed between two transfer faults in a zone of crustal extension (Turner and Long, 2008). Numbers correspond to samples and letter colour corresponds to sample type.

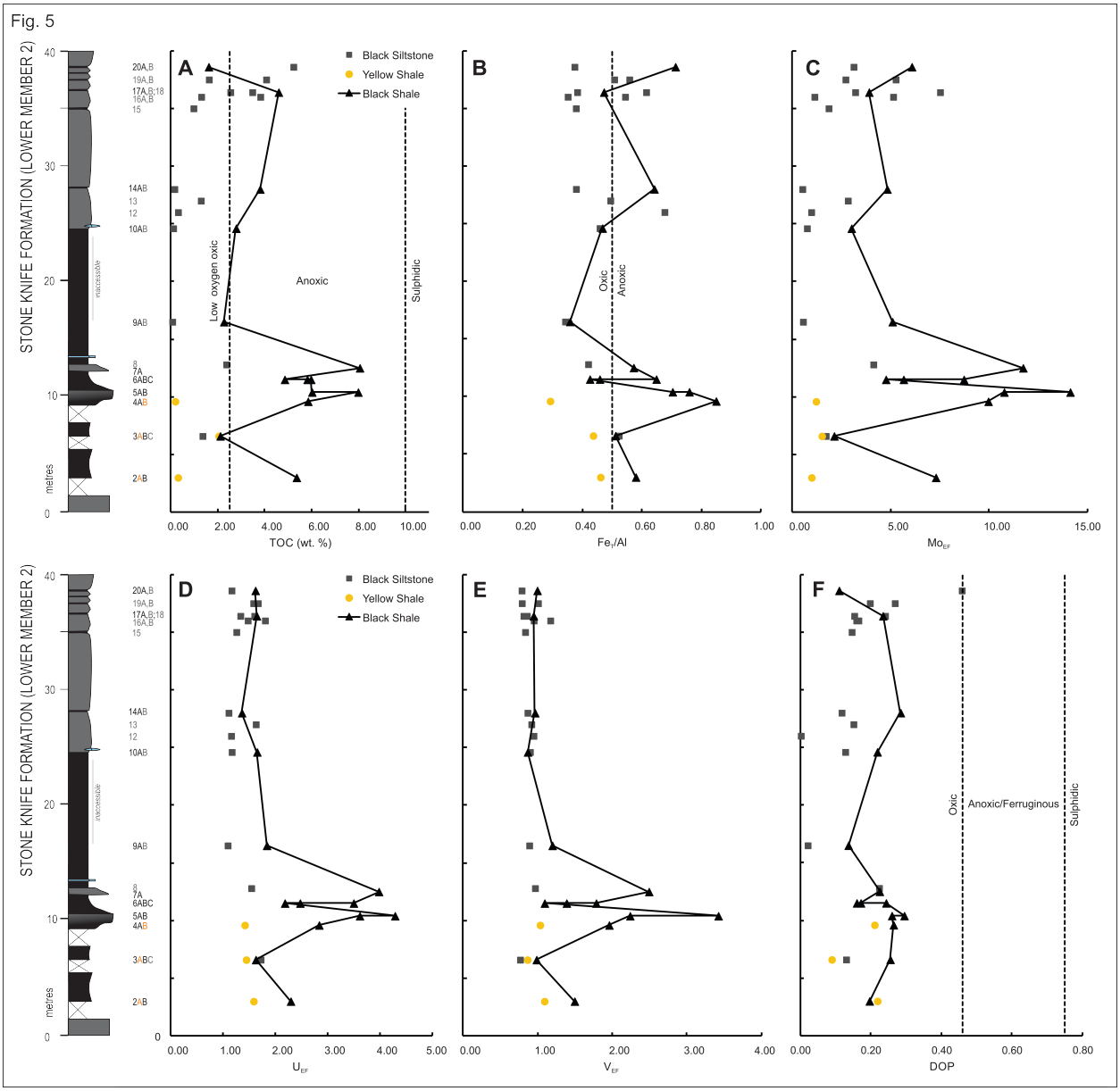

Figure 5. Stratigraphic variation in TOC (wt. %), iron relations (Fe_T/Al and DOP), and trace metal enrichment factors, that reflect aspects of water column chemistry and the paleo-redox state of the Little Dal basinal seawater. (A) TOC is elevated in all black shale samples and many of the black muddy siltstones as well, have peaks at similar stratigraphic positions as those in the trace metal enrichments, suggesting that the redox-sensitive metal content is a function of

organic carbon. Dashed line indicates change in water column redox state: values <2.5 wt. % indicate low oxygen oxic, values between 2.5-10 wt. % indicate anoxic, and values >10 wt. % indicate sulphidic conditions (Algeo and Maynard, 2004). (B) Stratigraphic variation in Fe_T/Al, that reflects aspects of water column chemistry and the paleo-redox state of the Little Dal basinal seawater. The Fe_T/Al ratio is a proxy for oxygenation state, with values ≤0.5 indicating oxic conditions, whereas values ≥0.5 indicating anoxic conditions (dashed line). (C) Molybdenum enrichment factors (Mo_{EF}). Because background concentrations of Mo are so low, Mo is the most sensitive redox trace metal. (D) U_{EF} and (E) V_{EF} trends resemble the Mo trend, indicating that the parameters causing enrichment in these trace metals are related. (D) DOP measures the amount of Fe^{2+} bound in a sulphide phase, and indicates oxic conditions when values fall below 0.46, anoxic conditions when values are between 0.46-0.75, whereas sulphidic conditions are reached when values are ≥0.8 (dashed lines). The samples that plot the highest are iron-rich, with Fe_T/Al above 0.5, however, the low DOP values may suggest that sulphide production by sulphate reduction in the Little Dal sediments was slow and that pyrite formation was limited by the availability of reactive iron (Canfield et al., 1992). This would suggest that all the iron oxyhydroxides and oxides were not consumed in pyrite formation and that free H_2S was not in the water column. The low DOP ratio, suggesting a non-sulphidic basin, is in agreement with the Fe_T/Al values.

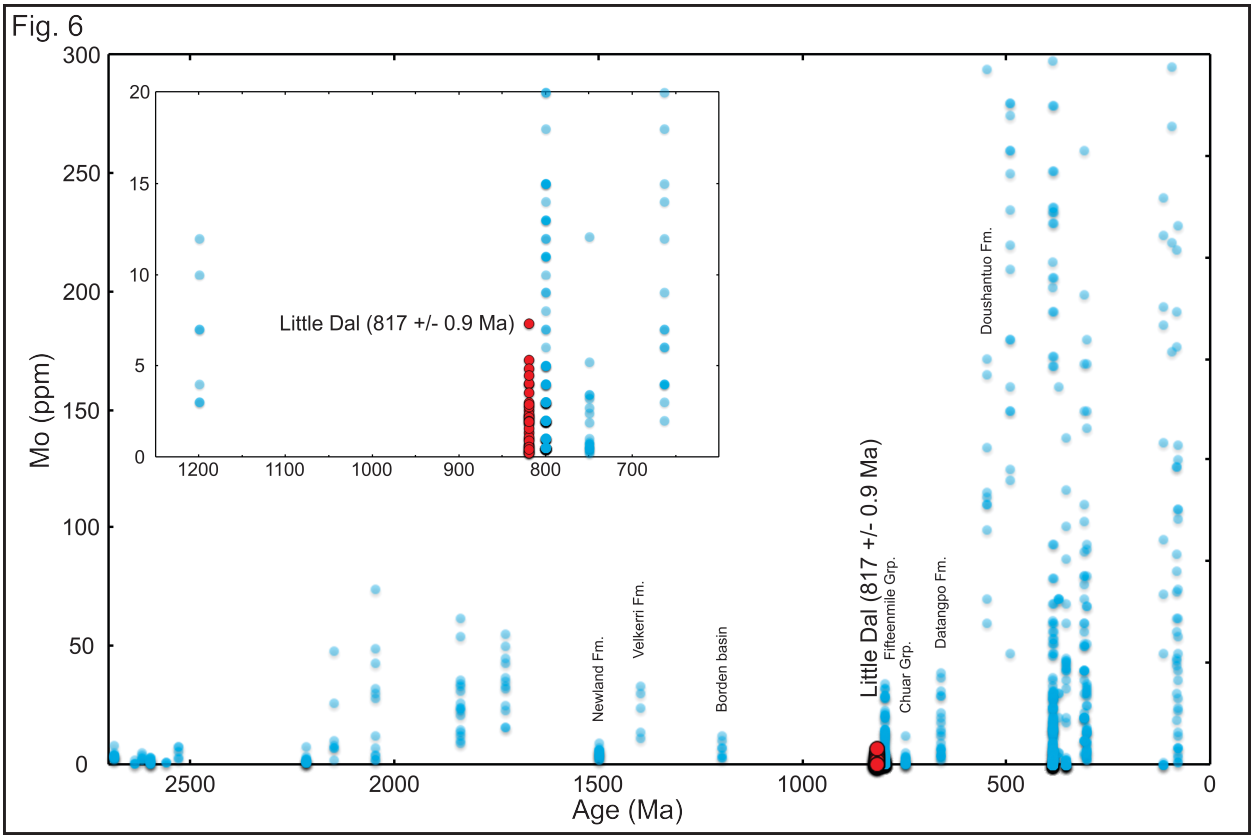

Figure 6. Temporal trends in Mo concentration from black shales deposited between the late Archean and late Mesozoic. Red circles represent samples from this study and blue circles represent data from previous work (Alberdi-Genolet and Tocco, 1999; Caplan and Bustin, 1998; Cruse and Lyons, 2004; Dahl et al., 2011; Feng et al., 2010; Hatch and Leventhal, 1992; Hatch and Leventhal, 1997; Hirner and Xu, 1991; Leventhal, 1991; Mongenot et al., 1996; Och et al., 2013; Sageman et al., 2003; Scott et al., 2008; Sperling et al., 2013; Werne et al., 2002; Yamaguchi, 2002). The concentration of Mo, which is scavenged from seawater under sulphidic conditions, increased markedly around 663 Ma. This change in Mo concentrations may indicate a rise in the global ocean molybdate reservoir caused by oxidative weathering and a shift away from a sulphidic ocean. This would indicate that the deep oceans prior to the mid-Neoproterozoic

were anoxic. Inset shows the same data from 1250 Ma to 600 Ma, and from 0 ppm to 20 ppm. The Little Dal black shale Mo concentrations are spread between <1 ppm and approximately 7 ppm.

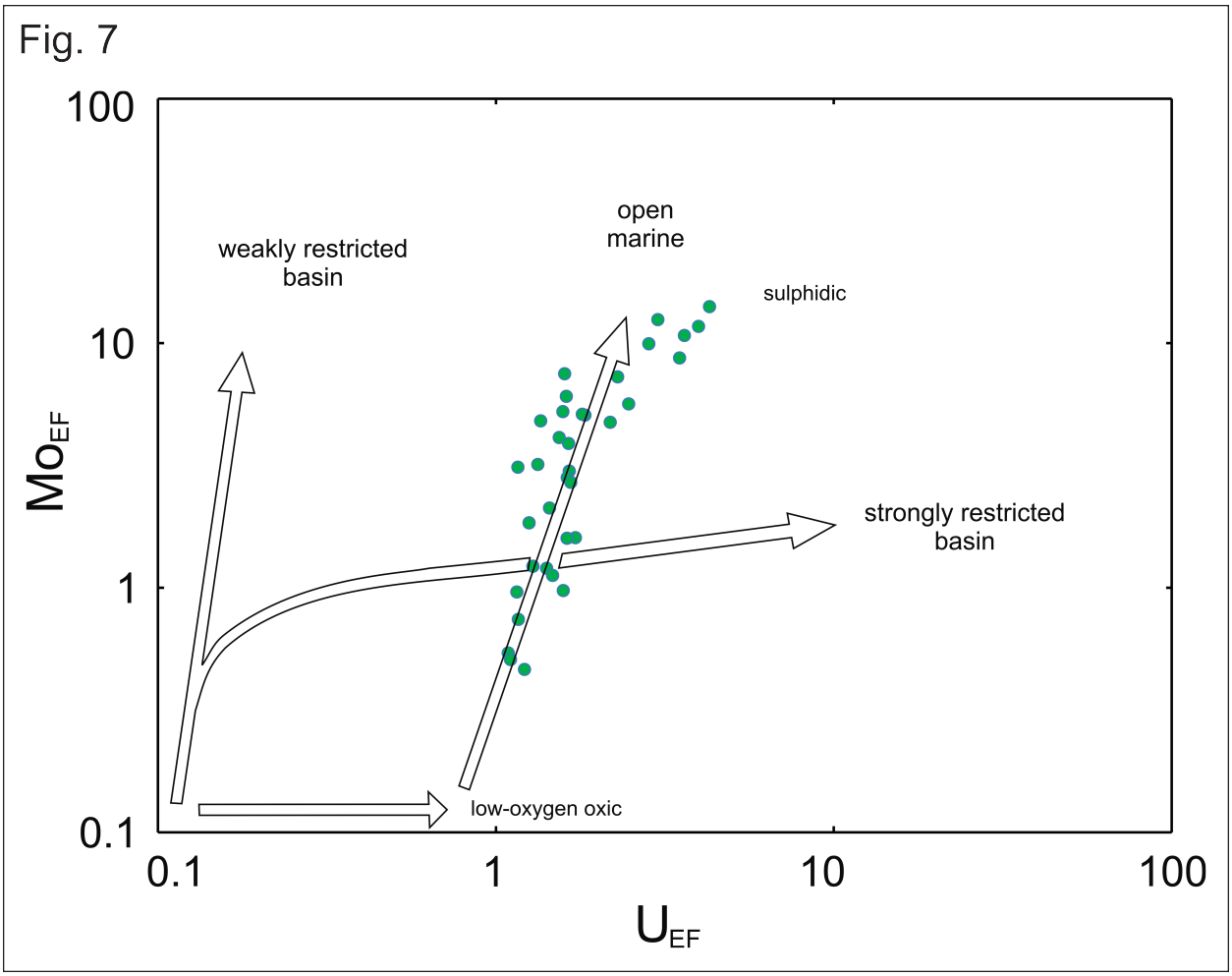

Figure 7. Mo_{EF} and U_{EF} scatter plot for Little Dal black shale superimposed on the paleoceanographic model of Algeo and Tribovillard (2009), in which covariation of Mo_{EF} and U_{EF} in sediment are used to define different redox-sensitive basin types. When sulphidic conditions are reached in weakly restricted (silled) basins (upper left), Mo is strongly fixed as

long as it is continually refreshed, whereas U fixation, which is not controlled by H_2S, continues to be fixed at a steady background rate. When sulphidic conditions are reached in strongly restricted basins, Mo rapidly becomes supply-limited, but because the rate of U fixation is so low, the limited recharge is adequate for U fixation to occur at approximately the same background rate (right). Under open-marine conditions, two trends can develop. In a low-oxygen oxic continental margin upwelling system, very minor amounts of Mo are fixed and U fixation continues at a constant background rate (bottom). In an evolving, unrestricted, sulphidic open-marine system there is an abundant supply of Mo and U, with sufficient recharge for both to maintain a steady enrichment (centre). The Little Dal black shale data follow a trend that resembles the path proposed for open-marine circulation; at higher metal concentrations, however, Mo_{EF} starts to level out while U_{EF} continues to increase, indicating that minor basin-restriction may have occurred.

Fig. 8

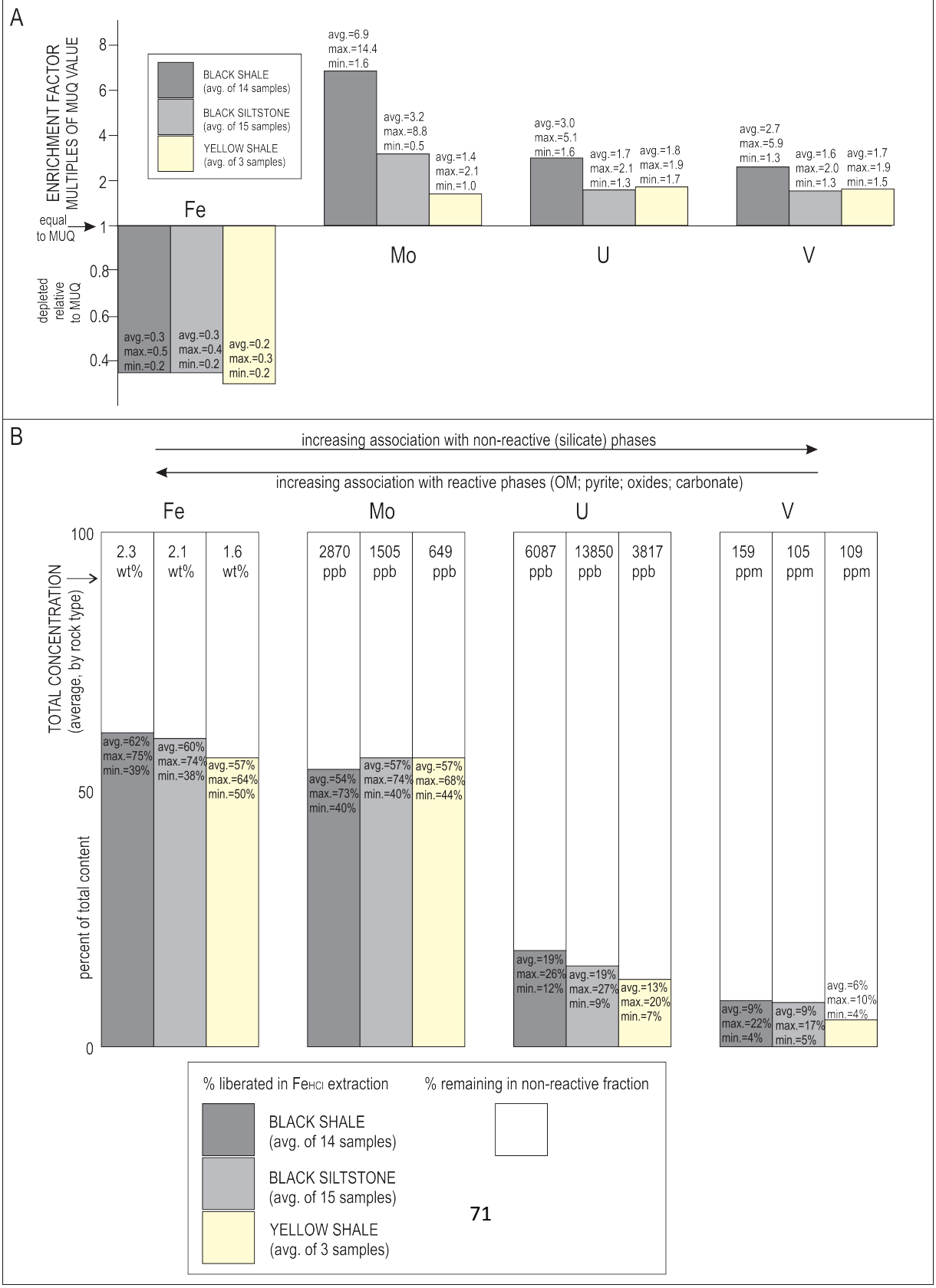
A
ENRICHMENT FACTOR
MULTIPLES OF MUQ VALUE
BLACK SHALE
(avg. of 14 samples)
BLACK SILTSTONE
(avg. of 15 samples)
YELLOW SHALE
(avg. of 3 samples)
equal to MUQ
depleted relative to MUQ
Fe
Mo
U
V
avg.=0.3 max.=0.5 min.=0.2
avg.=0.3 max.=0.4 min.=0.2
avg.=0.2 max.=0.3 min.=0.2
avg.=6.9 max.=14.4 min.=1.6
avg.=3.2 max.=8.8 min.=0.5
avg.=1.4 max.=2.1 min.=1.0
avg.=3.0 max.=5.1 min.=1.6
avg.=1.7 max.=2.1 min.=1.3
avg.=1.8 max.=1.9 min.=1.7
avg.=2.7 max.=5.9 min.=1.3
avg.=1.6 max.=2.0 min.=1.3
avg.=1.7 max.=1.9 min.=1.5
B
increasing association with non-reactive (silicate) phases
increasing association with reactive phases (OM; pyrite; oxides; carbonate)
TOTAL CONCENTRATION
(average, by rock type)
percent of total content
2.3 wt%
2.1 wt%
1.6 wt%
2870 ppb
1505 ppb
649 ppb
6087 ppb
13850 ppb
3817 ppb
159 ppm
105 ppm
109 ppm
avg.=62% max.=75% min.=39%
avg.=60% max.=74% min.=38%
avg.=57% max.=64% min.=50%
avg.=54% max.=73% min.=40%
avg.=57% max.=74% min.=40%
avg.=57% max.=68% min.=44%
avg.=19% max.=26% min.=12%
avg.=19% max.=27% min.=9%
avg.=13% max.=20% min.=7%
avg.=9% max.=22% min.=4%
avg.=9% max.=17% min.=5%
avg.=6% max.=10% min.=4%
% liberated in FeHCl extraction
% remaining in non-reactive fraction
BLACK SHALE
(avg. of 14 samples)
BLACK SILTSTONE
(avg. of 15 samples)
YELLOW SHALE
(avg. of 3 samples)

Figure 8. Fe, Mo, U, and V enrichment factors and absolute abundances for Little Dal black shale, black muddy siltstone, and yellow shale samples. Fe is fairly similar in all three rock types; depleted compared to MUQ and ~60% is bound in the reactive phases liberated during the HCl digestion. The depletion of Fe may be caused by differences in the original source material. MUQ is weathered from an Fe-rich mafic source whereas the Little Dal sediments would have weathered from older exposed sediments and cratonic granites. Mo was most highly enriched in the black shale and the majority was bound in the reactive phases liberated during the HCl digestion. Some Mo would be shuttled to the sea-floor along with sulphur, but the majority would be transported alongside the organic carbon, which is highest in the black shale and lower in the other sedimentary types. Both U and V are enriched relative to MUQ with the black shales having the highest levels of enrichment reflecting a minor hydrogenous contribution relative to the clastic component. The majority of the U and V are bound in silicate phases and this is represented by the minor amounts liberated during the HCl digestion.

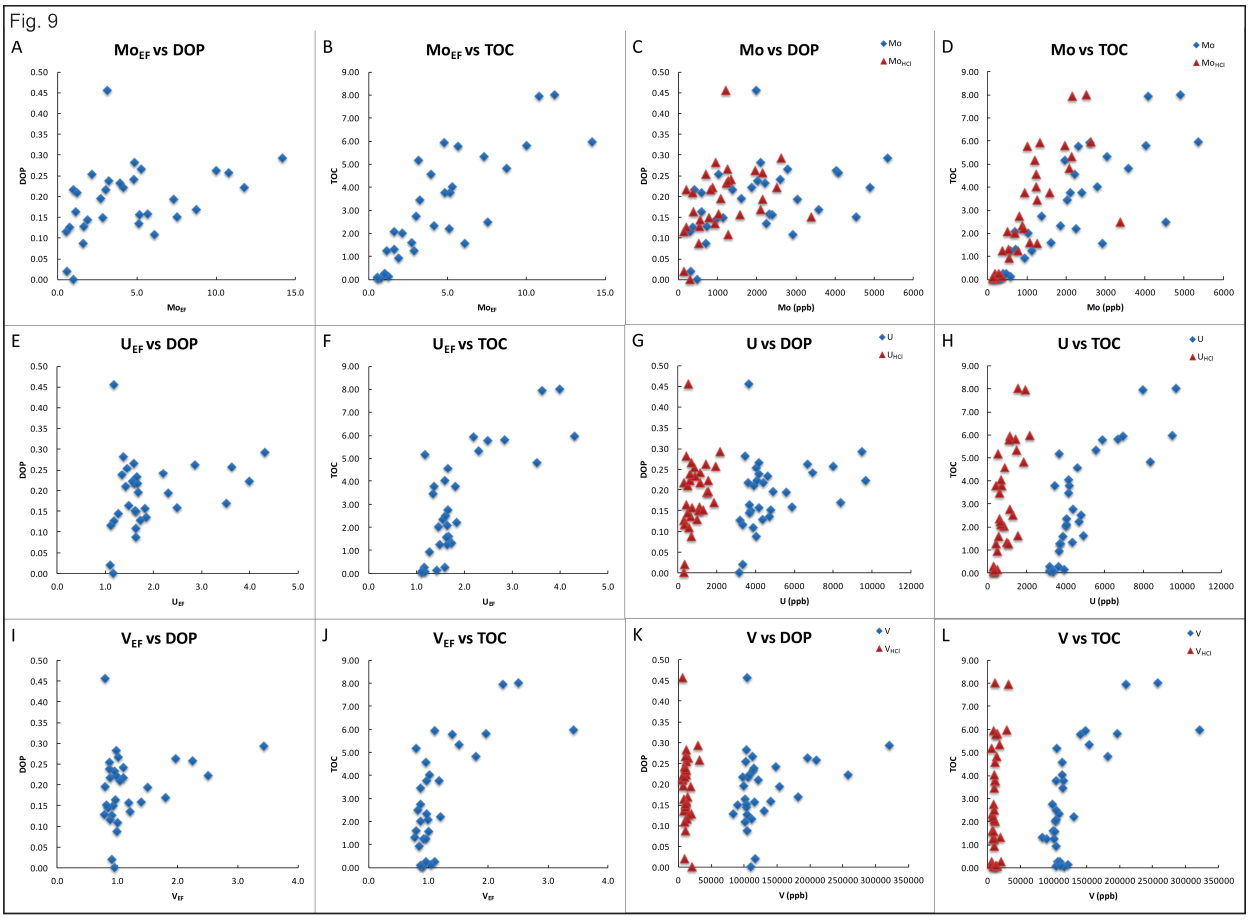

Figure 9. Enrichment factors and absolute abundances of Mo, U, and V compared to DOP and TOC. (A-D) A significant portion of the Mo is held in the highly reactive phases liberated during the HCl extraction but there is not a significant correlation between Mo enrichment and pyrite formation, or DOP. Mo enrichment and the Mo liberated during the HCl extraction are, however, strongly correlated to TOC, suggesting that elevated Mo in black shale deposits is not caused entirely by euxinic conditions, but by elevated levels of TOC. (E-L) U and V are primarily bound within the silicate minerals and not pyrite as a very little fraction was liberated during the HCl extraction. U does show a weak correlation with TOC similar to Mo suggesting that U may also, under the correct redox conditions, be scavenged by organic matter, whereas V is not. U and V

do covary with Mo, but do not show the same levels of enrichment, or the strong association with TOC. This would suggest that there is a different redox mechanism controlling their enrichment which requires further study.

2.10 Tables

Table 1: Whole-rock major element (wt. %) and trace element (ppb) data for Little Dal Group sediments

	09-JS-2A	09-JS-2B	09-JS-3A	09-JS-3B	09-JS-3C	09-JS-4A	09-JS-4B	09-JS-5A	09-JS-5B	09-JS-6A	09-JS-6B	09-JS-6C	09-JS-7A	09-JS-8	09-JS-9A	09-JS-9B
Strat (m)	3	3	6.6	6.6	6.6	9.6	9.6	10.4	10.4	11.5	11.5	11.5	12.5	12.8	16.5	16.5
TiO_2	0.80	0.85	0.94	0.90	0.87	0.89	0.89	0.85	0.87	1.13	0.88	0.85	0.88	0.95	0.94	0.94
Al_2O_3	13.85	14.75	16.89	15.34	15.04	14.34	16.82	13.45	13.47	19.37	14.47	14.57	14.84	15.97	15.57	18.66
$Fe_2O_{3(T)}$	4.83	6.47	5.58	6.07	5.82	9.21	3.72	7.72	7.16	6.23	5.02	7.15	6.42	5.07	4.22	4.84
MnO	0.00	0.00	0.01	0.01	0.00	0.00	0.00	0.00	0.00	0.01	0.00	0.00	0.02	0.01	0.01	0.01
MgO	1.17	1.28	1.58	1.65	1.34	1.18	1.39	1.12	1.12	1.57	1.12	1.19	1.15	1.18	1.15	1.85
CaO	0.18	0.43	0.31	0.29	0.23	0.39	0.16	0.25	0.30	0.48	0.33	0.33	0.25	0.09	0.08	0.10
K_2O	4.47	4.76	5.25	4.48	4.85	4.83	5.35	4.80	4.73	6.28	4.76	4.75	4.83	5.05	4.95	5.35
Na_2O	0.30	0.47	0.46	0.81	0.48	0.70	0.30	0.60	0.65	0.88	0.56	0.64	0.51	0.49	0.46	0.24
P_2O_5	0.06	0.08	0.12	0.10	0.10	0.14	0.07	0.14	0.14	0.12	0.07	0.12	0.13	0.09	0.07	0.12
S	0.70	0.90	0.88	0.54	0.34	1.89	0.40	1.62	1.74	0.62	0.48	0.76	0.97	0.68	0.28	0.04
CO_2	1.80	20.00	8.25	5.48	8.62	21.90	1.52	30.10	22.60	22.70	21.70	18.20	29.80	9.36	8.65	1.08
$C_{(T)}$	0.49	5.45	2.25	1.49	2.35	5.97	0.41	8.21	6.16	6.19	5.92	4.96	8.13	2.55	2.36	0.29
% Calcite	0.65	0.58	0.51	0.68	0.87	0.69	0.49	0.87	0.93	0.88	0.70	0.69	0.33	0.65	0.71	0.75
$C_{calcite}$	0.08	0.07	0.06	0.08	0.10	0.08	0.06	0.10	0.11	0.11	0.08	0.08	0.04	0.08	0.09	0.09
% Dolomite	1.60	0.46	2.17	0.91	2.05	0.68	2.50	1.82	0.57	1.71	0.34	0.46	0.57	1.60	0.23	2.06
$C_{dolomite}$	0.11	0.03	0.15	0.06	0.14	0.05	0.17	0.13	0.04	0.12	0.02	0.03	0.04	0.11	0.02	0.14
TOC	0.30	5.35	2.04	1.35	2.10	5.84	0.18	7.98	6.01	5.97	5.81	4.85	8.05	2.36	2.26	0.06
Fe_T/Al	0.46	0.58	0.44	0.52	0.51	0.85	0.29	0.76	0.70	0.43	0.46	0.65	0.57	0.42	0.36	0.34
DOP	0.22	0.20	0.25	0.13	0.09	0.26	0.21	0.26	0.29	0.24	0.16	0.17	0.22	0.22	0.14	0.02
Y	36087	29042	37609	28158	31711	25778	38732	26628	24497	31437	25350	27698	24131	34269	36027	46132
Nb	14349	13816	14480	14659	14604	13729	15923	14360	13643	15219	15398	14284	14646	15272	17390	16743
Mo	378	3014	1003	690	672	4002	567	4057	5329	2580	2292	3559	4875	1843	2218	283
La	52191	39758	49704	27027	47549	32383	63425	36105	35418	41548	40748	39635	31923	47534	47220	61186
Ce	114086	85422	109672	67659	105116	77741	134936	82985	84652	97046	83029	88260	69668	103290	100504	135459
Pr	13259	9352	11979	8209	11469	9401	14806	9898	9685	11464	8563	9951	7625	11216	9906	16148
Nd	45318	35081	46040	34782	43315	38448	49408	39527	38789	45630	30066	37900	28091	41438	39587	57712
Sm	7721	7084	9410	8291	8531	8534	7780	8977	8348	9109	5639	7489	5470	7685	7183	10498
Eu	1415	1224	1724	1473	1498	1312	1401	1600	1405	1426	1030	1234	886	1390	1298	1815
Gd	6415	5777	7807	6546	6673	6184	6112	7609	6833	6638	4953	5925	4756	6457	6227	8584
Tb	1039	924	1178	982	1015	899	1030	1049	971	1005	793	912	750	1036	1038	1385
Dy	6297	5527	6834	5675	5919	5163	6379	5698	5346	6107	4854	5478	4538	6280	6518	8325
Ho	1319	1149	1407	1157	1219	1052	1375	1115	1044	1288	1031	1149	954	1331	1379	1710
Er	3696	3246	3933	3314	3472	2968	3931	3091	2891	3655	3010	3276	2745	3812	3971	4791
Tm	563	502	605	521	541	462	606	477	441	564	479	510	430	587	618	725
Yb	3602	3247	3873	3363	3462	2950	3842	3069	2815	3659	3129	3299	2783	3778	3990	4591
Lu	531	480	576	503	516	436	572	453	410	539	464	486	417	562	588	681
Hf	4296	3486	4120	3689	3726	3565	3882	4083	3688	4272	4048	3724	4277	4322	4838	4326
Ta	1039	1116	1118	1187	1144	1125	1193	1173	1136	1211	1210	1168	1170	1182	1292	1245
Th	12849	14688	14128	15028	14821	15082	13946	18368	14868	15256	14958	15616	14452	14286	15760	15865
U	3584	5530	3960	4313	3993	6649	3886	7946	9440	6904	5849	8332	9651	4019	4670	3318
Th/U	3.59	2.66	3.55	3.48	3.71	2.27	3.59	2.31	1.57	2.21	2.56	1.87	1.50	3.55	3.38	4.78
Y/Ho	27.35	25.27	26.73	24.33	26.02	24.50	28.17	23.87	23.46	24.41	24.59	24.10	25.30	25.75	26.12	26.98
Zr/Hf	34.60	34.90	34.91	33.81	34.56	35.10	33.78	35.14	35.26	35.04	35.26	34.51	34.97	34.89	34.70	34.43
Nb/Ta	13.80	12.38	12.95	12.35	12.76	12.21	13.35	12.24	12.01	12.57	12.72	12.23	12.52	12.93	13.46	13.45
Mo_{HCl}	168	2119	683	505	483	1945	331	2134	2599	1310	993	2066	2491	854	895	114
U_{HCl}	266	1441	800	952	656	1386	453	1898	2127	1094	1065	1808	1503	568	619	287
V_{HCl}	4489	17015	10157	17510	9347	13723	4724	29816	27548	7469	10688	12160	9769	5924	6222	8171

Table 1 Continued

	09-JS-10A	09-JS-10B	09-JS-12	09-JS-13	09-JS-14A	09-JS-14B	09-JS-15	09-JS-16A	09-JS-16B	09-JS-17A	09-JS-17B	09-JS-18	09-JS-19A	09-JS-19B	09-JS-20B	09-JS-20A
Strat (m)	24.6	24.6	26	27	28	28	35	36	36	36.4	36.4	36.4	37.5	37.5	38.6	38.6
TiO_2	1.02	0.91	0.83	0.82	1.00	0.96	0.93	0.75	0.72	0.95	1.02	1.00	0.87	0.87	0.91	0.93
Al_2O_3	16.12	16.49	16.59	13.95	15.33	18.26	17.69	15.17	14.09	17.07	19.00	18.22	15.97	17.86	14.53	19.02
$Fe_2O_{3(T)}$	5.70	5.72	8.48	5.22	7.44	5.24	5.07	4.03	5.79	6.10	5.51	8.47	6.74	6.85	7.83	5.38
MnO	0.01	0.01	0.03	0.01	0.00	0.01	0.01	0.01	0.00	0.00	0.01	0.01	0.00	0.01	0.00	0.01
MgO	1.31	1.50	2.04	1.12	1.08	1.51	1.47	1.25	1.08	1.23	1.43	1.25	1.10	1.42	1.00	1.40
CaO	0.11	0.10	0.28	0.33	0.43	0.08	0.09	0.05	0.05	0.09	0.17	0.12	0.06	0.18	0.09	0.06
K_2O	5.10	4.81	4.20	4.23	5.17	5.48	5.33	4.67	4.43	5.69	6.19	5.88	5.47	5.37	4.92	6.04
Na_2O	0.46	0.36	0.19	0.33	0.49	0.53	0.51	0.45	0.52	0.76	0.78	0.71	0.56	0.67	0.64	0.65
P_2O_5	0.10	0.10	0.23	0.13	0.08	0.09	0.09	0.07	0.07	0.07	0.07	0.07	0.03	0.09	0.07	0.07
S	0.75	0.49	0.01	0.50	1.55	0.29	0.39	0.41	0.63	0.88	0.69	0.62	1.14	0.51	0.51	1.49
CO_2	10.50	1.22	1.44	5.65	14.70	0.90	3.75	5.31	14.30	17.20	13.20	10.30	15.40	6.45	6.93	19.70
$C_{(T)}$	2.86	0.33	0.39	1.54	4.01	0.25	1.02	1.45	3.90	4.69	3.60	2.81	4.20	1.76	1.89	5.37
% Calcite	0.46	0.88	0.46	1.12	0.63	0.58	0.22	0.29	0.46	0.45	0.68	1.10	0.55	0.55	1.10	0.93
$C_{calcite}$	0.06	0.11	0.06	0.13	0.08	0.07	0.03	0.03	0.06	0.05	0.08	0.13	0.07	0.07	0.13	0.11
% Dolomite	0.46	1.83	0.46	1.83	1.94	0.34	0.46	1.71	0.46	0.69	0.68	2.04	1.02	1.03	2.15	0.56
$C_{dolomite}$	0.03	0.13	0.03	0.13	0.14	0.02	0.03	0.12	0.03	0.05	0.05	0.14	0.07	0.07	0.15	0.04
TOC	2.78	0.10	0.31	1.28	3.80	0.15	0.96	1.29	3.81	4.59	3.47	2.54	4.06	1.62	1.61	5.22
Fe_T/Al	0.47	0.46	0.68	0.49	0.64	0.38	0.38	0.35	0.54	0.47	0.38	0.61	0.56	0.51	0.71	0.37
DOP	0.22	0.13	0.00	0.15	0.28	0.12	0.15	0.17	0.16	0.23	0.24	0.15	0.27	0.20	0.11	0.46
Y	38623	36756	57800	37195	23349	29561	37698	35247	36088	37618	34158	37032	27183	40386	27245	30490
Nb	16223	16408	15314	14240	15127	16555	16534	17010	16154	16590	16939	15991	15546	16589	16006	16780
Mo	1356	343	447	1104	2069	260	914	561	2378	2190	2000	4507	2763	1588	2905	1951
La	46374	50795	59746	47968	38164	50796	51964	48441	42228	40479	41663	40568	44113	38137	34031	45369
Ce	103908	109905	136766	114294	81206	107091	113293	100118	89741	87438	86841	85500	92447	79073	70800	95249
Pr	11555	11560	17318	12456	8998	11457	12369	12160	11103	11135	10567	10380	10881	9334	8361	11255
Nd	43423	41716	67141	54180	33504	41762	46067	45101	42382	44422	39995	39213	39329	34856	30388	40633
Sm	8250	7134	16463	11940	6029	7003	7999	8055	8504	9529	7736	7936	6408	7088	5472	6783
Eu	1443	1249	2976	2142	961	1250	1325	1328	1353	1430	1233	1391	1013	1329	909	1101
Gd	6800	5850	14460	9372	4333	5336	6218	6129	6523	6955	5981	7090	4723	7028	4409	5115
Tb	1107	993	2091	1334	678	862	1030	1015	1056	1103	994	1146	793	1176	756	867
Dy	6876	6308	11559	7447	4208	5358	6444	6382	6662	6797	6143	6949	4997	7188	4798	5456
Ho	1448	1350	2217	1482	901	1147	1375	1374	1419	1448	1321	1457	1082	1533	1068	1186
Er	4179	3904	5889	4103	2647	3339	3960	3981	4099	4167	3820	4162	3166	4369	3195	3471
Tm	648	608	867	627	421	527	611	615	630	647	596	639	501	672	514	542
Yb	4201	3885	5435	4019	2790	3371	3918	4009	4095	4195	3865	4136	3271	4339	3394	3527
Lu	629	578	794	597	417	504	581	592	603	612	569	609	484	644	503	522
Hf	4955	4376	4154	4487	4251	4000	4101	4616	4854	4985	4554	4496	4311	4722	4683	4355
Ta	1266	1236	1142	1075	1199	1237	1257	1301	1268	1326	1347	1255	1234	1279	1327	1298
Th	16280	15243	14889	13984	14727	15535	15826	15818	16076	16363	16069	16504	15029	15910	16409	15926
U	4345	3141	3128	3710	3401	3299	3627	3651	4150	4581	4133	4759	4121	4863	3839	3613
Th/U	3.75	4.85	4.76	3.77	4.33	4.71	4.36	4.33	3.87	3.57	3.89	3.47	3.65	3.27	4.27	4.41
Y/Ho	26.67	27.23	26.07	25.10	25.92	25.77	27.42	25.66	25.44	25.99	25.87	25.42	25.12	26.35	25.51	25.70
Zr/Hf	35.90	33.72	34.95	34.74	35.27	33.97	34.50	34.44	34.45	34.86	34.27	35.05	34.70	35.06	36.01	34.42
Nb/Ta	12.82	13.27	13.41	13.25	12.62	13.38	13.15	13.07	12.74	12.51	12.58	12.74	12.60	12.97	12.06	12.93
Mo_{HCl}	784	174	261	750	914	108	533	354	1549	1213	1241	3357	1217	1053	1245	1181
U_{HCl}	1112	275	274	1012	396	313	458	387	678	822	556	1243	653	1517	526	489
V_{HCl}	8235	13136	18792	9219	9585	11432	8942	7075	10496	10046	8728	9507	8464	5321	7770	4867

Chapter 3: References

Aitken, J.D., 1981. Stratigraphy and sedimentology of the upper Proterozoic Little Dal Group, Mackenzie Mountains, Northwest Territories. In: Campbell, F.H.A. (Ed.), Proterozoic basins of Canada, Geological Survey of Canada. Geological Survey of Canada, Ottawa, ON, Canada, pp. 47-71.

Aitken, J.D., Long, D.G.F., 1978. Mackenzie tectonic arc-Reflection of early basin configuration? Geology, 6(10): 626-629.

Aitken, J.D., Long, D.G.F., Semikhatov, M.A., 1978. Progress in Helikian stratigraphy, Mackenzie Mountains. Current Research, Part A; Geological Survey of Canada, Paper 78-1A: 481 - 484.

Aitken, J.D., Turner, E.C., MacNaughton, R.B., 2011. Thirty-six archival stratigraphic sections in the Katherine, Little Dal, Coates Lake, and Rapitan groups (Neoproterozoic), Mackenzie Mountains, Northwest Territories. Geological Survey of Canada, Open File 6391: 9 pages.

Alberdi-Genolet, M., Tocco, R., 1999. Trace metals and organic geochemistry of the Machiques Member (Aptian-Albian) and La Luna Formation (Cenomanian-Campanian), Venezuela. Chemical Geology, 160(1-2): 19-38.

Algeo, T.J., Maynard, J.B., 2004. Trace-element behavior and redox facies in core shales of Upper Pennsylvanian Kansas-type cyclothems. Chemical Geology, 206: 289-318.

Algeo, T.J., Tribovillard, N., 2009. Environmental analysis of paleoceanographic systems based on molybdenum-uranium covariation. Chemical Geology, 268(3-4): 211-225.

Anbar, A.D., Knoll, A.H., 2002. Proterozoic ocean chemistry and evolution: A bioinorganic bridge? Science, 297(5584): 1137-1142.

Anderson, T.F., Raiswell, R., 2004. Sources and mechanisms for the enrichment of highly reactive iron in euxinic Black Sea sediments. American Journal of Science, 304(3): 203-233.

Armstrong, R.L., Eisbacher, G.H., Evans, P.D., 1982. Age and stratigraphic-tectonic significance of Proterozoic diabase sheets, Mackenzie Mountains, northwestern Canada. Canadian Journal of Earth Sciences, 19: 316-323.

Babechuk, M.G., Kamber, B.S., Greig, A., Canil, D., Kodolanyi, J., 2010. The behaviour of tungsten during mantle melting revisited with implications for planetary differentiation time scales. Geochimica et Cosmochimica Acta, 74(4): 1448-1470.

Baldwin, G.J., Turner, E.C., Kamber, B.S., 2012. A new depositional model for glaciogenic Neoproterozoic iron formation: insights from the chemostratigraphy and basin configuration of the Rapitan iron formation. Canadian Journal of Earth Sciences, 49(2): 455-476.

Batten, K.L., 2002. Early Neoproterozoic ramp carbonates and microbialites, Little Dal Group, mackenzie Mountains, N.W.T., Queen's University, Kingston, Ontario.

Batten, K.L., Narbonne, G.M., James, N.P., 2004. Paleoenvironments and growth of early Neoproterozoic calcimicrobial reefs: platformal Little Dal Group, northwestern Canada. Precambrian Research, 133(3-4): 249-269.

Canfield, D.E., 1998. A new model for Proterozoic ocean chemistry. Nature, 396(6710): 450-453.

Canfield, D.E., 2004. The evolution of the Earth surface sulfur reservoir. American Journal of Science, 304(10): 839-861.

Canfield, D.E. et al., 2008. Ferruginous conditions dominated later Neoproterozoic deep-water chemistry. Science, 321(5891): 949-952.

Canfield, D.E., Poulton, S.W., Narbonne, G.M., 2007. Late-Neoproterozoic deep-ocean oxygenation and the rise of animal life. Science, 315(5808): 92-95.

Canfield, D.E., Raiswell, R., Bottrell, S., 1992. The reactivity of sedimentary iron minerals toward sulfide. American Journal of Science, 292(9): 659-683.

Caplan, M.L., Bustin, R.M., 1998. Palaeoceanographic controls on geochemical characteristics of organic-rich Exshaw mudrocks: role of enhanced primary production. Organic Geochemistry, 30: 161 - 188.

Chappaz, A. et al., 2013. Does pyrite act as an important host for molybdenum in modern and ancient euxinic sediments? Geochimica et Cosmochimica Acta.

Cruse, A.M., Lyons, T.W., 2004. Trace metal records of regional paleoenvironmental variability in Pennsylvanian (Upper Carboniferous) black shales. Chemical Geology, 206(3-4): 319-345.

Dahl, T.W. et al., 2011. Molybdenum evidence for expansive sulfidic water masses in ~750 Ma oceans. Earth and Planetary Science Letters, 311(3-4): 264-274.

Dyke, A.S., 2004. Quaternary glaciations - extent and chronology, part II. North America. In: Ehlers, J., Gibbard, P.L. (Eds.), Developments in Quaternary Science 2, pp. 373-424.

Eggins, S.M. et al., 1997. A simple method for the precise determination of ≥40 trace elements in geological samples by ICPMS using enriched isotope internal standardisation Chemical Geology, 134(4): 311-326.

Erickson, B.E., Helz, G.R., 2000. Molybdenum(VI) speciation in sulfidic waters: Stability and lability of thiomolybdates. Geochimica et Cosmochimica Acta, 64(7): 1149-1158.

Evans, D.A.D., 2006. Proterozoic low orbital obliquity and axial-dipolar geomagnetic field from evaporite paleolatitudes. Nature, 444: 51-55.

Feng, L.J., Chu, X.L., Huang, J., Zhang, Q.R., Chang, H.J., 2010. Reconstruction of paleo-redox conditions and early sulfur cycling during deposition of the Cryogenian Datangpo Formation in South China. Gondwana Research, 18(4): 632-637.

Fike, D.A., Grotzinger, J.P., Pratt, L.M., Summons, R.E., 2006. Oxidation of the Ediacaran Ocean. Nature, 444(7120): 744-747.

Gordey, S.P., Roots, C.F., 2011. Chapter 2. Regional Setting. In: Martel, E., Turner, E.C., Fischer, B.J. (Eds.), Geology of the central Mackenzie Mountains of the northern Canadian Cordillera, Sekwi Mountain (105P), Mount Eduni (106A), and northwestern Wrigley Lake (95M) map-areas, Northwest Territories, NWT Special Volume 1, NWT Geoscience Office, pp. 18-30.

Hatch, J.R., Leventhal, J.S., 1992. Relationship between inferred redox potential of the depositional environment and geochemistry of the upper Pennsylvanian (Missourian) Stark Shale Member of the Dennis Limestone, Wabaunsee Country, Kansas, USA. Chemical Geology, 99(1-3): 65-82.

Hatch, J.R., Leventhal, J.S., 1997. Early diagenetic partial oxidation of organic matter and sulfides in the Middle Pennsylvanian (Desmoinesian) Excello Shale Member of the Fort Scott Limestone and equivalents, northern Midcontinent region, USA. Chemical Geology, 134(4): 215-235.

Hayes, J.M., Lambert, I.B., Strauss, H., 1992. The Proterozoic Biosphere: A Multidisciplinary Study. In: Schoff, J.W., Klein, C. (Eds.). Cambridge University Press, pp. 129 -134.

Heaman, L.M., Lecheminant, A.N., Rainbird, R.H., 1992. Nature and timing of Franklin igneous events, Canada - implications for a late Proterozoic mantle plume and the break-up of Laurentia. Earth and Planetary Science Letters, 109(1-2): 117-131.

Helz, G.R. et al., 1996. Mechanism of molybdenum removal from the sea and its concentration in black shales: EXAFS evidence. Geochimica et Cosmochimica Acta, 60(19): 3631-3642.

Hewton, R.S., 1982. Gayna River; a Proterozoic Mississippi Valley-type zinc-lead deposit. In: Hutchinson, R.W., Spence, C.D., Franklin, J.M. (Eds.), Precambrian sulphide deposits. Geological Association of Canada, Specail Paper no. 25, pp. 667-700.

Hirner, A.V., Xu, Z., 1991. Trace-metal speciation in Julia Creek oil-shale. Chemical Geology, 91(2): 115-124.

Hoffman, P.F., Kaufman, A.J., Halverson, G.P., Schrag, D.P., 1998. A Neoproterozoic snowball earth. Science, 281(5381): 1342-1346.

Holland, H.D. (Ed.), 1984. Chemical Evolutions of the Atmosphere and Oceans. Princeton University Press, Princeton, 598 pp.

Jefferson, C.W., Parrish, R.R., 1989. Late Proterozoic stratigraphy, U-Pb zircon ages, and rift tectonics, Mackenzie Mountains, Northwestern Canada. Canadian Journal of Earth Sciences, 26(9): 1784-1801.

Johnston, D.T. et al., 2010. An emerging picture of Neoproterozoic ocean chemistry: Insights from the Chuar Group, Grand Canyon, USA. Earth and Planetary Science Letters, 290(1-2): 64-73.

Kamber, B.S., 2009. Geochemical fingerprinting: 40 years of analytical development and real world applications. Applied Geochemistry, 24(6): 1074-1086.

Kamber, B.S., Greig, A., Collerson, K.D., 2005. A new estimate for the composition of weathered young upper continental crust from alluvial sediments, Queensland, Australia. Geochimica et Cosmochimica Acta, 69(4): 1041-1058.

Kamber, B.S., Greig, A., Schoenberg, R., Collerson, K.D., 2003. A refined solution to Earth's hidden niobium: implications for evolution of continental crust and mode of core formation. Precambrian Research, 126(3-4): 289-308.

Karlstrom, K.E. et al., 2000. Chuar Group of the Grand Canyon: Record of breakup of Rodinia, associated change in the global carbon cycle, and ecosystem expansion by 740 Ma. Geology, 28(7): 619-622.

Komiya, T. et al., 2008. Evolution of the composition of seawater through geologic time, and its influence on the evolution of life. Gondwana Research, 14(1-2): 159-174.

Leckie, R.M., Bralower, T.J., Cashman, R., 2002. Oceanic anoxic events and plankton evolution: Biotic response to tectonic forcing during the mid-Cretaceous. Paleoceanography, 17.

Leslie, C.D., 2009. Detrital zircon, geochronology and rift-related magmatism: central Mackenzie Mountains, Northwest Territories. Unpublished MSc thesis Thesis, The University of British Columbia, Vancouver, 236 pp.

Leventhal, J.S., 1991. Comparison of organic geochemistry and metal enrichment in 2 black shales - Cambrian Alum Shale of Sweden and Devonian Chattanooga Shale of United-States. Mineralium Deposita, 26(2): 104-112.

Li, C. et al., 2010. A stratified redox model for the Ediacaran ocean. Science, 328(5974): 80-83.

Long, D.G.F., 1977. Depositional environments and stratigraphic setting of rocks of the Tsezotene Formation and Katherine Group, Mackenzie Fold Belt, Yukon and Northwest Territories, Canada. In: Reid, R.R., Williams, G.A. (Editors), Society of Economic Geologists' Coeur d'Alene Field Conference. Idaho Bureau of Mines and Geology, Idaho, pp. 119.

Long, D.G.F., Rainbird, R.H., Turner, E.C., MacNaughton, R.B., 2008. Early Neoproterozoic strata (Sequence B) of mainland northern Canada and Victoria and Banks islands: a contribution to the Geological Atlas of the Northern Canadian Mainland Sedimentary Basin. Geological Survey of Canada, Open File 5700: 24.

Long, D.G.F., Turner, E.C., 2012. Formal definition of the Neoproterozoic Mackenzie Mountains Supergroup (Northwest Territories), and formal stratigraphic nomenclature for terrigenous clastic units of the Katherine Group. Geological Survey of Canada, Open File 7113: p. 40.

Lyons, T.W., Anbar, A.D., Severmann, S., Scott, C., Gill, B.C., 2009. Tracking euxinia in the ancient ocean: A multiproxy perspective and Proterozoic case study. Annual Review of Earth and Planetary Sciences, 37: 507-534.

Lyons, T.W., Severmann, S., 2006. A critical look at iron paleoredox proxies: New insights from modern euxinic marine basins. Geochimica et Cosmochimica Acta, 70(23): 5698-5722.

Maruyama, S., Santosh, M., 2008. Models on Snowball Earth and Cambrian explosion: A synopsis. Gondwana Research, 14(1-2): 22-32.

Marx, S.K., Kamber, B.S., 2010. Trace-element systematics of sediments in the Murray-Darling Basin, Australia: Sediment provenance and palaeoclimate implications of fine scale chemical heterogeneity. Applied Geochemistry, 25(8): 1221-1237.

Marz, C. et al., 2008. Redox sensitivity of P cycling during marine black shale formation: Dynamics of sulfidic and anoxic, non-sulfidic bottom waters. Geochimica et Cosmochimica Acta, 72(15): 3703-3717.

Meyer, K.M., Kump, L.R., 2008. Oceanic euxinia in Earth history: Causes and consequences. Annual Review of Earth and Planetary Sciences, 36: 251-288.

Mongenot, T., Tribovillard, N.P., Desprairies, A., LallierVerges, E., LaggounDefarge, F., 1996. Trace elements as palaeoenvironmental markers in strongly mature hydrocarbon source rocks: The Cretaceous La Luna Formation of Venezuela. Sedimentary Geology, 103(1-2): 23-37.

Narbonne, G.M., Aitken, J.D., 1995. Neoproterozoic of the Mackenzie Mountains, Northwestern Canada. Precambrian Research, 73(1-4): 101-121.

O'Hare, S.P., Turner, E.C., Kamber, B.S., 2011. Redox-sensitive metal systematics in black shale of the Basinal assemblage of the Neoproterozoic Little Dal Group, Mackenzie Mountains supergroup, NWT, GAC/AGC - MAC/AMC - SEG - SGA Joint Annual Meeting, Ottawa, Ontario, Canada.

Och, L.M. et al., 2013. Redox changes in Early Cambrian black shales at Xiaotan section, Yunnan Province, South China. Precambrian Research, 225: 166-189.

Park, J.K., 1981. Analysis of the multicomponent magnetization of the Little Dal group, Mackenzie Mountains, Northwest Territories, Canada. Journal of Geophysical Research, 86(NB6): 5134-5146.

Park, J.K., Jefferson, C.W., 1991. Magnetic and tectonic history of the late Proterozoic Upper Little Dal and Coates Lake Groups of northwestern Canada. Precambrian Research, 52: 1-35.

Planavsky, N.J. et al., 2011. Widespread iron-rich conditions in the mid-Proterozoic ocean. Nature, 477(7365): 448-451.

Poulton, S.W., Canfield, D.E., 2005. Development of a sequential extraction procedure for iron: implications for iron partitioning in continentally derived particulates. Chemical Geology, 214(3-4): 209-221.

Poulton, S.W., Canfield, D.E., 2011. Ferruginous conditions: A dominant feature of the ocean through Earth's history. Elements, 7(2): 107-112.

Poulton, S.W., Fralick, P.W., Canfield, D.E., 2004. The transition to a sulphidic ocean similar to 1.84 billion years ago. Nature, 431(7005): 173-177.

Poulton, S.W., Fralick, P.W., Canfield, D.E., 2010. Spatial variability in oceanic redox structure 1.8 billion years ago. Nature Geoscience, 3(7): 486-490.

Poulton, S.W., Raiswell, R., 2002. The low-temperature geochemical cycle of iron: From continental fluxes to marine sediment deposition. American Journal of Science, 302(9): 774-805.

Powell, J., Scheider, D.A., 2013. Preliminary results of detrital muscovite 40Ar/39Ar geochronology from the eastern Mackenzie Mountains and Mackenzie Plain, Northwest Territories. Geological Survey of Canada, Current Research 2013-18: 16 p.

Rainbird, R.H., Jefferson, C.W., Young, G.M., 1996. The early Neoproterozoic sedimentary Succesion B of northwestern Laurentia: correlations and paleogeographic significance. Geological Society of America Bulletin, v. 108: 454-470.

Raiswell, R., 2006. Towards a global highly reactive iron cycle. Journal of Geochemical Exploration, 88(1-3): 436-439.

Raiswell, R., Buckley, F., Berner, R.A., Anderson, T.F., 1988. Degree of pyritization of iron as a paleoenvironmental indicator of bottom-water oxygenation. Journal of Sedimentary Petrology, 58(5): 812-819.

Raiswell, R., Canfield, D.E., 1998. Sources of iron for pyrite formation in marine sediments. American Journal of Science, 298(3): 219-245.

Raiswell, R., Canfield, D.E., Berner, R.A., 1994. A comparison of iron extraction methods for the determination of degree of pyritisation and the recognition of iron-limited pyrite formation. Chemical Geology, 111(1-4): 101-110.

Raiswell, R. et al., 2008. Turbidite depositional influences on the diagenesis of Beecher's Trilobite Bed and the Hunsruck Slate; Sites of soft tissue pyritization. American Journal of Science, 308(2): 105-129.

Raiswell, R. et al., 2011. Formation of syngenetic and early diagenetic iron minerals in the late Archean Mt. McRae Shale, Hamersley Basin, Australia: New insights on the patterns, controls and paleoenvironmental implications of authigenic mineral formation. Geochimica et Cosmochimica Acta, 75(4): 1072-1087.

Raiswell, R. et al., 2006. Contributions from glacially derived sediment to the global iron (oxyhydr) oxide cycle: Implications for iron delivery to the oceans. Geochimica Et Cosmochimica Acta, 70: 2765-2780.

Reinhard, C.T., Raiswell, R., Scott, C., Anbar, A.D., Lyons, T.W., 2009. A Late Archean Sulfidic Sea Stimulated by Early Oxidative Weathering of the Continents. Science, 326(5953): 713-716.

Roychoudhury, A.N., Kostka, J.E., P., V.C., 2003. Pyritization: a palaeoenvironmental and redox proxy reevaluated. Estuarine, Coastal and Shelf Science, 57: 1183-1193.

Sageman, B.B. et al., 2003. A tale of shales: the relative roles of production, decomposition, and dilution in the accumulation of organic-rich strata, Middle-Upper Devonian, Appalachian basin. Chemical Geology, 195(1-4): 229-273.

Scholz, F., McManus, J., Sommer, S., 2013. The manganese and iron shuttle in a modern euxinic basin and implications for molybdenum cycling at euxinic ocean margins. Chemical Geology.

Scott, C. et al., 2008. Tracing the stepwise oxygenation of the Proterozoic ocean. Nature, 452(7186): 456-U5.

Shields-Zhou, G., Och, L., 2011. The case for a Neoproterozoic Oxygenation Event: Geochemical evidence and biological consequences. GSA Today, 21(3): 8.

Sperling, E.A., Halverson, G.P., Knoll, A.H., Macdonald, F.A., Johnston, D.T., 2013. A basin redox transect at the dawn of animal life. Earth and Planetary Science Letters, 371: 143-155.

Tagliabue, A. et al., 2010. Hydrothermal contribution to the oceanic dissolved iron inventory. Nature Geoscience, 3(4): 252-256.

Taylor, S.R., McLennan, S.M., 1985. The Continental Crust: its Composition and Evolution. An Examination of the Geochemical Record Preserved in Sedimentary Rocks. Blackwell Scientific Publications, Oxford, 312 pp.

Tribovillard, N., Riboulleau, A., Lyons, T., Baudin, F.O., 2004. Enhanced trapping of molybdenum by sulfurized marine organic matter of marine origin in Mesozoic limestones and shales. Chemical Geology, 213(4): 385-401.

Turner, E.C., 1999. Grwoth dynamics, framework composition, and microstructure of giant early Neoproterozoic calcimicrobial reeefs, Little Dal Group, Mackenzie Mountains, N.W.T. Ph.D. thesis, Queen's University, Kingston, ON, 276 pp.

Turner, E.C., 2009. Lithostratigraphy and stable isotope values of the early Neoproterozoic Gypsum formation (Little Dal Group, Mackenzie Mountains Supergroup), NWT; Northwest Territories Geoscience Office, NWT Open Report 2009-002, 26 pp.

Turner, E.C., 2011. Stratigraphy of the Mackenzie Mountains supergroup in the Wernecke Mountains, Yukon. In: MacFarlane, K.E., Weston, L.H., Relf, C. (Eds.), Yukon Exploration and Geology. Yukon Geological Survey, pp. 207-231.

Turner, E.C., James, N.P., Narbonne, G.M., 1997. Growth dynamics of Neoproterozoic calcimicrobial reefs, Mackenzie Mountains, northwest Canada. Journal of Sedimentary Research, 67(3): 437-450.

Turner, E.C., James, N.P., Narbonne, G.M., 2000. Taphonomic control on microstructure in early Neoproterozoic reefal stromatolites and thrombolites. Palaios, 15: 87-111.

Turner, E.C., Kamber, B.S., 2012. Arctic Bay Formation, Borden Basin, Nunavut (Canada); basin evolution, black shale, and dissolved metal systematics in the Mesoproterozoic ocean. Precambrian Research, 208-211: 1-18.

Turner, E.C., Long, D.G.F., 2008. Basin architecture and syndepositional fault activity during deposition of the Neoproterozoic Mackenzie Mountains supergroup, Northwest Territories, Canada. Canadian Journal of Earth Sciences, 45(10): 1159-1184.

Turner, E.C., Long, D.G.F., 2012. Formal definition of the Neoproterozic Mackenzie Mountains Supergroup (Northwest Territories), and formal stratigraphic nomenclature for its carbonate and evaporite formations. Geological Survey of Canada, pp. 57 p.

Turner, E.C. et al., 2011. Chapter 3. Stratigraphy. In: Martel, E., Turner, E.C., Fischer, B.J. (Eds.), Geology of the central Mackenzie Mountains of the northern Canadian Cordillera, Sekwi Mountain (105P), Mount Eduni (106A), and northwestern Wrigley Lake (95M) map-areas, Northwest Territories, NWT Special Volume 1, NWT Geoscience Office, pp. 31-192.

Wedepohl, K.H., 1971. Environmental influences on the chemical composition of shales and clays. Physics and Chemistry of the Earth, 8: 305-333.

Wedepohl, K.H., 1991. The Composition of the Upper Earth's Crust and the Natural Cycles of Selected Metals. Metals in Natural Raw Materials. Natural Resources. In: Merian, E. (Ed.), Metals and Their Compounds in the Environment. VCH, New York, pp. 3 - 17.

Werne, J.P., Sageman, B.B., Lyons, T.W., Hollander, D.J., 2002. An integrated assessment of a "type euxinic" deposit: Evidence for multiple controls on black shale deposition in the Middle Devonian Oatka Creek Formation. American Journal of Science, 302(2): 110-143.

Wijsman, J.W.M., Middelburg, J.J., Heip, C.H.R., 2001. Reactive iron in Black Sea sediments: implications for iron cycling. Marine Geology, 172(3-4): 167-180.

Xiao, S. et al., 2012. Integrated chemostratigraphy of the Doushantuo Formation at the northern Xiaofenghe section (Yangtze Gorges, South China) and its implication for Ediacaran stratigraphic correlation and ocean redox models. Precambrian Research, 192-195(0): 125-141.

Yamaguchi, K., 2002. Geochemistry of Archean-Paleoproterozoic black shales: the early evolution of the atmosphere, oceans, and biosphere, Pennsylvania State University, University Park, 485 pp.

Young, G.M., Jefferson, C.W., Delaney, G.D., Yeo, G.M., 1979. Middle and late Proterozoic evolution of the northern Canadian Cordillera and Shield. Geology, 7(3): 125-128.

Young, G.M., Jefferson, C.W., Delaney, G.D., Yeo, G.M., Long, D.G.F., 1982. Upper Proterozoic stratigraphy of northwestern Canada and Precambrian history of the North

American Cordillera. In: Reid, R.R., Williams, G.A. (Eds.), Society of Economic Geologists Coeu d'Alene Field Conference, Idaho - 1977. Idaho Bureau of Mines and Geology, Bulletin V.24, pp. 73-96.

Zhang, S., Jiang, G., Han, Y., 2008. The age of the Nantuo Formation and Nantuo glaciation in South China. Terra Nova, 20(4): 289- 294.

Zheng, Y., Anderson, R.F., van Geen, A., Kuwabara, J., 2000. Authigenic molybdenum formation in marine sediments: A link to pore water sulfide in the Santa Barbara Basin. Geochimica et Cosmochimica Acta, 64(24): 4165-4178.

Zhou, C.M. et al., 2004. New constraints on the ages of Neoproterozoic glaciations in south China. Geology, 32(5): 437-440.

Appendix A

A.1 Supplementary Figures

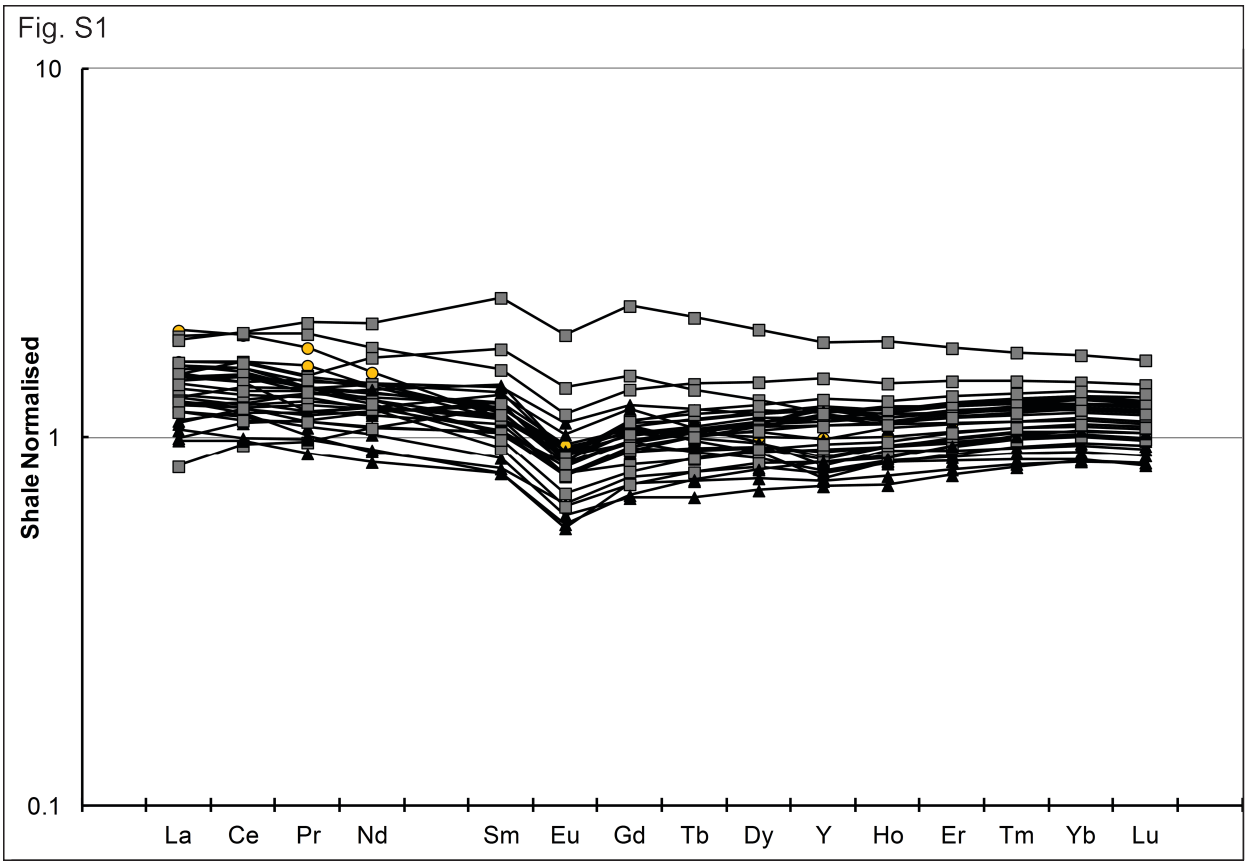

Figure S1. Shale-normalised (Mud of Queensland; Kamber et al., 2005) REE+ Y plot for the Little Dal samples are relatively flat trends, indicating no LREE/HREE enrichment or depletion. Negative Eu anomalies can be attributed to weathering of the sediment source. The consistent shape of REE patterns of the Little Dal black shale indicate a constant and stable sediment supply source for all three sedimentary types.

A.2 Supplementary Tables

Supplementary Table 1: Calibration values and lab standards

	VY-2				SCo-1						BIR-1			BHVO-2				BCR-2		
			This study											This Study				This Study		
	N digestions		1	1										1	1			1	1	
	N analyses		1	1										1	1			1	1	
	calibration values										*certified values*					*certified values*				*certified values*
TiO_2	*1.06*		0.51	0.57							*0.63*			2.75	2.74	*2.73*		2.25	2.29	*2.26*
Al_2O_3	*15.45*		12.2	15.1							*13.7*			13.9	13.8	*13.5*		13.7	13.9	*13.5*
Fe_2O_3m	*10.83*		4.46	5.44							*8.13*			12.5	12.5	*12.3*		13.8	14.2	*13.8*
MgO	*6.37*		2.34	2.87							*2.72*			7.35	7.28	*7.23*		3.59	3.63	*3.59*
MnO	*0.167*		0.05	0.05										0.17	0.17	*0.17*		0.2	0.2	*0.2*
CaO	*10.86*		2.23	2.72							*2.62*			11.4	11.5	*11.4*		7.10	7.22	*7.12*
K_2O	*0.026*		0.38	0.00							*0.07*			0.52	0.52	*0.52*		1.80	1.85	*1.79*
Na_2O	*2.2*		0.09	3.99							*2.77*			2.23	2.33	*2.22*		3.12	3.20	*3.16*
P_2O_5	*0.14*		0.19	0.24							*0.09*			0.31	0.30	*0.27*		0.40	0.40	*0.35*
											0.21									
Li	*9158*		44710	45724	46676	*2.7*	45362	*1.0*				3140	*1.2*							
Be	*617*		1706	1826	1750	*3.4*	1772	*1.0*				93	*3.2*							
Sc	*36074*		11387	11783	10637	*2.6*	10749	*1.8*				44596	*1.3*							
Ti	*6354611*		3288541	3379827	3136773	*2.8*	3343064	*0.7*				5805239	*1.3*							
V	*261597*		122582	128598	114945	*2.5*	123644	*1.2*				323672	*1.4*							
Cr	*92791*		66985	70932	60247	*2.2*	68186	*2.9*				412296	*1.6*							
Co	*44526*		11266	11195	9696	*1.7*	10905	*1.6*				53588	*1.4*							
Ni	*69993*		25229	26259	21903	*1.8*	25498	*1.6*				171488	*1.5*							
Cu	*103000*		26085	26928	24273	*4.0*	27564	*0.7*				120774	*1.9*							
Zn	*77000*		95763	106802	93466	*2.3*	99460	*3.1*				70857	*3.8*							
Ga	*17424*		15927	16560	15810	*1.9*	16507	*1.0*				15516	*1.2*							
As	*833*		7347	8333	7256	*1.5*	8663	*2.1*				95	*32*							
Rb	*19803*		108144	112170	108832	*2.2*	1088974	*0.0*				194	*2.3*							
Sr	*194928*		159316	166612	156202	*1.6*	159412	*0.9*				110090	*1.2*							
Y	*20113*		20860	21551	20946	*1.6*	21946	*1.2*				14728	*1.1*							
Zr	*87966*		114765	120041	118409	*3.1*	172840	*0.4*				14593	*2.6*							
Nb	*7275*		11786	11962	11034	*1.5*	12013	*0.8*				536	*1.4*							
Mo	*423*		1174	1215	1048	*1.5*	1260	*6.2*				40	*39*							
Cd	*77*		127	139	147	*2.8*	148	*2.3*				64	*6.8*							
Sn	*1950*		1956	2820	3262	*2.9*	3778	*0.5*				809	*7.8*							
Sb	*709*		2065	2205	2170	*2.9*	2018	*2.7*				467	*16*							
Cs	*888*		7768	8030	7700	*1.2*	7787	*0.2*				5	*8.5*							
Ba	*699600*		569292	583233	576280	*0.7*	571971	*2.1*				6601	*2.6*							
La	*10521*		28730	29647	28432	*1.1*	27681	*0.6*				608	*1.5*							
Ce	*23216*		56816	58248	56080	*1.6*	55786	*0.9*				1915	*1.6*							
Pr	*3025*		6824	7027	6966	*1.4*	6749	*1.7*				380	*1.2*							
Nd	*12911*		25624	26262	26050	*1.4*	25264	*1.8*				2381	*1.1*							
Sm	*3266*		4942	5104	5079	*1.4*	4828	*1.6*				1102	*0.9*							
Eu	*1094*		1066	1100	1093	*1.3*	1066	*0.9*				525	*0.9*							
Gd	*615*		4268	4447	678	*1.5*	666	*0.2*				966	*0.9*							
Tb	*3708*		656	672	4989	*1.3*	4833	*0.5*				1881	*1.1*							
Dy	*3809*		3928	3921	3963	*1.7*	3984	*0.6*				5563	*1.1*							
Ho	*800*		769	814	827	*1.6*	816	*1.1*				1085	*1.0*							
Er	*2222*		2199	2290	2311	*1.5*	2314	*1.0*				1706	*0.9*							
Tm	*327*		336	346	353	*1.6*	355	*1.3*				253	*0.9*							
Yb	*2058*		2161	2230	2281	*1.4*	2306	*0.8*				1667	*0.8*							
Lu	*301*		325	332	344	*1.6*	345	*1.0*				249	*1.0*							
Hf	*2356*		3293	3412	3591	*2.5*	4655	*0.9*				573	*1.5*							
Ta	*454*		822	835	961	*6.0*	823	*0.1*				37	*1.5*							
W	*240*		1348	1412	1368	*1.3*	1370	*1.6*				6	*9.1*							
Tl	*90*		628	640	630	*1.1*	618	*0.1*				1	*6.9*							
Pb	*7528*		29279	28898	29100	*1.7*	27983	*2.3*				3222	*17*							
Th	*2104*		8863	9064	9110	*1.4*	8488	*0.8*				29	*3.3*							
U	*505*		2983	3061	3040	*2.7*	2763	*2.3*				10	*2.2*							
Y/Ho			26.45	26.47	25.32	*0.7*	26.78	*0.2*				25.17	*0.8*							
Zr/Hf			34.85	35.19	32.68	*0.6*	37.13	*0.4*				25.55	*1.3*							
Nb/Ta			14.33	14.32	12.84	*4.4*	14.59	*0.7*				14.49	*1.1*							
Th/U			3.00	2.96	3.00	*2.3*	3.07	*1.5*				2.87	*4.1*							

Supplementary Table 2: Full whole-rock major element (wt. %), Fe species, and trace element (ppb) data for Little Dal black shale

	09-JS-2A	09-JS-2B	09-JS-3A	09-JS-3B	09-JS-3C	09-JS-4A	09-JS-4B	09-JS-5A	09-JS-5B	09-JS-6A	09-JS-6B	09-JS-6C	09-JS-7A	09-JS-8	09-JS-9A	09-JS-9B
Strat (m)	3	3	6.6	6.6	6.6	9.6	9.6	10.4	10.4	11.5	11.5	11.5	12.5	12.8	16.5	16.5
TiO_2	0.80	0.85	0.94	0.90	0.87	0.89	0.89	0.85	0.87	1.13	0.88	0.85	0.88	0.95	0.94	0.94
Al_2O_3	13.85	14.75	16.89	15.34	15.04	14.34	16.82	13.45	13.47	19.37	14.47	14.57	14.84	15.97	15.57	18.66
$Fe_2O_{3(T)}$	4.83	6.47	5.58	6.07	5.82	9.21	3.72	7.72	7.16	6.23	5.02	7.15	6.42	5.07	4.22	4.84
MnO	0.00	0.00	0.01	0.01	0.00	0.00	0.00	0.00	0.00	0.01	0.00	0.00	0.02	0.01	0.01	0.01
MgO	1.17	1.28	1.58	1.65	1.34	1.18	1.39	1.12	1.12	1.57	1.12	1.19	1.15	1.18	1.15	1.85
CaO	0.18	0.43	0.31	0.29	0.23	0.39	0.16	0.25	0.30	0.48	0.33	0.33	0.25	0.09	0.08	0.10
K_2O	4.47	4.76	5.25	4.48	4.85	4.83	5.35	4.80	4.73	6.28	4.76	4.75	4.83	5.05	4.95	5.35
Na_2O	0.30	0.47	0.46	0.81	0.48	0.70	0.30	0.60	0.65	0.88	0.56	0.64	0.51	0.49	0.46	0.24
P_2O_5	0.06	0.08	0.12	0.10	0.10	0.14	0.07	0.14	0.14	0.12	0.07	0.12	0.13	0.09	0.07	0.12
S	0.70	0.90	0.88	0.54	0.34	1.89	0.40	1.62	1.74	0.62	0.48	0.76	0.97	0.68	0.28	0.04
CO_2	1.80	20.00	8.25	5.48	8.62	21.90	1.52	30.10	22.60	22.70	21.70	18.20	29.80	9.36	8.65	1.08
$C_{(T)}$	0.49	5.45	2.25	1.49	2.35	5.97	0.41	8.21	6.16	6.19	5.92	4.96	8.13	2.55	2.36	0.29
% Calcite	0.65	0.58	0.51	0.68	0.87	0.69	0.49	0.87	0.93	0.88	0.70	0.69	0.33	0.65	0.71	0.75
$C_{calcite}$	0.08	0.07	0.06	0.08	0.10	0.08	0.06	0.10	0.11	0.11	0.08	0.08	0.04	0.08	0.09	0.09
% Dolomite	1.60	0.46	2.17	0.91	2.05	0.68	2.50	1.82	0.57	1.71	0.34	0.46	0.57	1.60	0.23	2.06
$C_{dolomite}$	0.11	0.03	0.15	0.06	0.14	0.05	0.17	0.13	0.04	0.12	0.02	0.03	0.04	0.11	0.02	0.14
TOC	0.30	5.35	2.04	1.35	2.10	5.84	0.18	7.98	6.01	5.97	5.81	4.85	8.05	2.36	2.26	0.06
Fe_T	3.38	4.52	3.90	4.24	4.07	6.44	2.60	5.40	5.01	4.36	3.51	5.00	4.49	3.55	2.95	3.38
Fe_{HR}	2.18	3.21	2.24	3.14	3.02	4.58	1.31	4.03	3.63	1.68	2.19	3.20	2.92	2.06	1.55	1.60
Fe_U	1.20	1.31	1.66	1.10	1.05	1.86	1.29	1.37	1.38	2.68	1.32	1.80	1.58	1.49	1.41	1.78
Fe_{PY}	0.61	0.78	0.77	0.47	0.30	1.65	0.35	1.41	1.52	0.54	0.42	0.66	0.84	0.59	0.24	0.03
Al	7.33	7.81	8.94	8.12	7.96	7.59	8.90	7.12	7.13	10.25	7.66	7.71	7.85	8.45	8.24	9.88
Fe_T/Al	0.46	0.58	0.44	0.52	0.51	0.85	0.29	0.76	0.70	0.43	0.46	0.65	0.57	0.42	0.36	0.34
DOP	0.22	0.20	0.25	0.13	0.09	0.26	0.21	0.26	0.29	0.24	0.16	0.17	0.22	0.22	0.14	0.02

	09-JS-10A	09-JS-10B	09-JS-12	09-JS-13	09-JS-14A	09-JS-14B	09-JS-15	09-JS-16A	09-JS-16B	09-JS-17A	09-JS-17B	09-JS-18	09-JS-19A	09-JS-19B	09-JS-20B	09-JS-20A
Strat (m)	24.6	24.6	26	27	28	28	35	36	36	36.4	36.4	36.4	37.5	37.5	38.6	38.6
TiO_2	1.02	0.91	0.83	0.82	1.00	0.96	0.93	0.75	0.72	0.95	1.02	1.00	0.87	0.87	0.91	0.93
Al_2O_3	16.12	16.49	16.59	13.95	15.33	18.26	17.69	15.17	14.09	17.07	19.00	18.22	15.97	17.86	14.53	19.02
$Fe_2O_{3(T)}$	5.70	5.72	8.48	5.22	7.44	5.24	5.07	4.03	5.79	6.10	5.51	8.47	6.74	6.85	7.83	5.38
MnO	0.01	0.01	0.03	0.01	0.00	0.01	0.01	0.01	0.00	0.00	0.01	0.01	0.00	0.01	0.00	0.01
MgO	1.31	1.50	2.04	1.12	1.08	1.51	1.47	1.25	1.08	1.23	1.43	1.25	1.10	1.42	1.00	1.40
CaO	0.11	0.10	0.28	0.33	0.43	0.08	0.09	0.05	0.05	0.09	0.17	0.12	0.06	0.18	0.09	0.06
K_2O	5.10	4.81	4.20	4.23	5.17	5.48	5.33	4.67	4.43	5.69	6.19	5.88	5.47	5.37	4.92	6.04
Na_2O	0.46	0.36	0.19	0.33	0.49	0.53	0.51	0.45	0.52	0.76	0.78	0.71	0.56	0.67	0.64	0.65
P_2O_5	0.10	0.10	0.23	0.13	0.08	0.09	0.09	0.07	0.07	0.07	0.07	0.07	0.03	0.09	0.07	0.07
S	0.75	0.49	0.01	0.50	1.55	0.29	0.39	0.41	0.63	0.88	0.69	0.62	1.14	0.51	0.51	1.49
CO_2	10.50	1.22	1.44	5.65	14.70	0.90	3.75	5.31	14.30	17.20	13.20	10.30	15.40	6.45	6.93	19.70
$C_{(T)}$	2.86	0.33	0.39	1.54	4.01	0.25	1.02	1.45	3.90	4.69	3.60	2.81	4.20	1.76	1.89	5.37
% Calcite	0.46	0.88	0.46	1.12	0.63	0.58	0.22	0.29	0.46	0.45	0.68	1.10	0.55	0.55	1.10	0.93
$C_{calcite}$	0.06	0.11	0.06	0.13	0.08	0.07	0.03	0.03	0.06	0.05	0.08	0.13	0.07	0.07	0.13	0.11
% Dolomite	0.46	1.83	0.46	1.83	1.94	0.34	0.46	1.71	0.46	0.69	0.68	2.04	1.02	1.03	2.15	0.56
$C_{dolomite}$	0.03	0.13	0.03	0.13	0.14	0.02	0.03	0.12	0.03	0.05	0.05	0.14	0.07	0.07	0.15	0.04
TOC	2.78	0.10	0.31	1.28	3.80	0.15	0.96	1.29	3.81	4.59	3.47	2.54	4.06	1.62	1.61	5.22
Fe_T	3.99	4.00	5.93	3.65	5.20	3.66	3.55	2.82	4.05	4.27	3.85	5.92	4.71	4.79	5.48	3.76
Fe_{HR}	2.34	2.92	4.42	2.45	3.40	1.90	1.99	1.81	2.90	2.51	1.90	2.98	2.71	1.80	3.59	1.54
Fe_U	1.65	1.08	1.52	1.20	1.80	1.77	1.56	1.01	1.15	1.76	1.95	2.94	2.00	2.99	1.88	2.23
Fe_{PY}	0.65	0.43	0.01	0.44	1.35	0.25	0.34	0.36	0.55	0.77	0.60	0.54	0.99	0.44	0.44	1.30
Al	8.53	8.72	8.78	7.38	8.11	9.67	9.36	8.03	7.46	9.04	10.05	9.64	8.45	9.45	7.69	10.07
Fe_T/Al	0.47	0.46	0.68	0.49	0.64	0.38	0.38	0.35	0.54	0.47	0.38	0.61	0.56	0.51	0.71	0.37
DOP	0.22	0.13	0.00	0.15	0.28	0.12	0.15	0.17	0.16	0.23	0.24	0.15	0.27	0.20	0.11	0.46

Supplementary Table 2 Continued

	09-JS-2A	09-JS-2B	09-JS-3A	09-JS-3B	09-JS-3C	09-JS-4A	09-JS-4B	09-JS-5A	09-JS-5B	09-JS-6A	09-JS-6B	09-JS-6C	09-JS-7A	09-JS-8	09-JS-9A	09-JS-9B
Strat (m)	3	3	6.6	6.6	6.6	9.6	9.6	10.4	10.4	11.5	11.5	11.5	12.5	12.8	16.5	16.5
Li	24543	27640	33872	53972	28083	36384	24876	42745	45510	28889	30690	36714	31109	25862	25594	51367
Be	2090	2943	3110	3230	2714	2461	2605	2861	2944	3186	3116	2879	3339	2739	2959	3650
Sc	15045	16976	16534	14769	16442	16062	18929	17429	14511	15875	13856	14731	16610	14256	16237	17829
Ti	4690851	4650080	4795560	4893664	4863704	4599939	5064653	4662005	4702006	4949885	4977817	4563167	4884724	4963767	5628640	5364282
V	104647	152850	100945	81332	102551	194633	120329	208664	319393	146660	139146	180189	256224	106832	129091	114843
Cr	71741	115842	97329	102595	101283	110098	80544	113508	121583	111349	94598	103493	111029	88357	99387	85325
Co	1803	4489	4601	5200	2706	3401	2377	2178	3179	6331	3291	4685	16957	5287	5561	8282
Ni	3294	13384	10234	14871	7913	11838	4005	10298	14212	15820	9960	13425	42366	12128	11325	14548
Cu	29784	74080	44105	47180	48053	58834	47530	63680	73716	60263	57820	62174	99482	39156	40987	7694
Zn	15657	18227	29644	32083	22785	16516	18993	18260	19177	21061	18268	21475	28013	19318	20377	29020
Ga	20715	20293	21160	18448	21193	19266	23771	20283	19244	20788	19779	20548	20900	20689	22660	25156
As	2160	8818	3186	1645	2227	10251	2377	17560	14512	6249	6807	10337	11906	7893	8041	711
Rb	149582	163835	167588	143912	165635	159955	184464	160751	160804	179916	164847	167869	164737	162873	175997	185739
Sr	39871	49155	109271	78106	41443	53688	35185	52582	53882	66846	68669	61316	64120	74968	53275	48008
Y	36087	29042	37609	28158	31711	25778	38732	26628	24497	31437	25350	27698	24131	34269	36027	46132
Zr	148653	121671	143845	124756	128764	125159	131137	143483	130039	149713	142734	128527	149571	150794	167865	148925
Nb	14349	13816	14480	14659	14604	13729	15923	14360	13643	15219	15398	14284	14646	15272	17390	16743
Mo	378	3014	1003	690	672	4002	567	4057	5329	2580	2292	3559	4875	1843	2218	283
Ag	109	323	113	81	112	280	91	272	315	245	294	214	254	366	397	46
Cd	60	52	63	68	54	57	52	61	56	68	63	60	149	60	71	71
In	71	96	92	92	78	101	89	148	152	94	95	97	118	101	93	80
Sn	2103	2565	2545	2991	2533	1769	4614	2770	3148	4128	3991	3250	3235	2433	4050	4226
Sb	329	1194	444	402	402	1356	488	1274	1507	1036	1110	1138	1257	1157	1822	244
Cs	10268	11474	10892	8371	10805	10665	12144	12073	9923	11448	10544	10972	9991	10858	12305	13359
Ba	275299	335057	292562	322039	282894	410295	297747	326245	334888	444107	360218	310025	611764	356405	354991	282100
La	52191	39758	49704	27027	47549	32383	63425	36105	35418	41548	40748	39635	31923	47534	47220	61186
Ce	114086	85422	109672	67659	105116	77741	134936	82985	84652	97046	83029	88260	69668	103290	100504	135459
Pr	13259	9352	11979	8209	11469	9401	14806	9898	9685	11464	8563	9951	7625	11216	9906	16148
Nd	45318	35081	46040	34782	43315	38448	49408	39527	38789	45630	30066	37900	28091	41438	39587	57712
Sm	7721	7084	9410	8291	8531	8534	7780	8977	8348	9109	5639	7489	5470	7685	7183	10498
Eu	1415	1224	1724	1473	1498	1312	1401	1600	1405	1426	1030	1234	886	1390	1298	1815
Gd	6415	5777	7807	6546	6673	6184	6112	7609	6833	6638	4953	5925	4756	6457	6227	8584
Tb	1039	924	1178	982	1015	899	1030	1049	971	1005	793	912	750	1036	1038	1385
Dy	6297	5527	6834	5675	5919	5163	6379	5698	5346	6107	4854	5478	4538	6280	6518	8325
Ho	1319	1149	1407	1157	1219	1052	1375	1115	1044	1288	1031	1149	954	1331	1379	1710
Er	3696	3246	3933	3314	3472	2968	3931	3091	2891	3655	3010	3276	2745	3812	3971	4791
Tm	563	502	605	521	541	462	606	477	441	564	479	510	430	587	618	725
Yb	3602	3247	3873	3363	3462	2950	3842	3069	2815	3659	3129	3299	2783	3778	3990	4591
Lu	531	480	576	503	516	436	572	453	410	539	464	486	417	562	588	681
Hf	4296	3486	4120	3689	3726	3565	3882	4083	3688	4272	4048	3724	4277	4322	4838	4326
Ta	1039	1116	1118	1187	1144	1125	1193	1173	1136	1211	1210	1168	1170	1182	1292	1245
W	1951	1978	1910	2054	2001	1842	2206	2040	2190	2076	2237	1965	2077	2113	2304	2237
Tl	632	1025	744	657	657	1375	769	1286	1564	1153	1118	1487	1909	1016	940	772
Pb	17691	100288	24018	18466	22336	109876	19971	96082	110096	80405	128801	73949	87970	126611	139606	3761
Th	12849	14688	14128	15028	14821	15082	13946	18368	14868	15256	14958	15616	14452	14286	15760	15865
U	3584	5530	3980	4313	3993	6649	3886	7946	9440	6904	5849	8332	9651	4019	4670	3318
Th/U	3.59	2.66	3.55	3.48	3.71	2.27	3.59	2.31	1.57	2.21	2.56	1.87	1.50	3.55	3.38	4.78
Y/Ho	27.35	25.27	26.73	24.33	26.02	24.50	28.17	23.87	23.46	24.41	24.59	24.10	25.30	25.75	26.12	26.98
Zr/Hf	34.60	34.90	34.91	33.81	34.56	35.10	33.78	35.14	35.26	35.04	35.26	34.51	34.97	34.89	34.70	34.43
Nb/Ta	13.80	12.38	12.95	12.35	12.76	12.21	13.35	12.24	12.01	12.57	12.72	12.23	12.52	12.93	13.46	13.45

Supplementary Table 2 Continued

	09-JS-10A	09-JS-10B	09-JS-12	09-JS-13	09-JS-14A	09-JS-14B	09-JS-15	09-JS-16A	09-JS-16B	09-JS-17A	09-JS-17B	09-JS-18	09-JS-19A	09-JS-19B	09-JS-20B	09-JS-20A
Strat (m)	24.6	24.6	26	27	28	28	35	36	36	36.4	36.4	36.4	37.5	37.5	38.6	38.6
Li	31331	37148	64881	31672	22621	35137	38489	36444	34786	28254	29634	25082	24172	59524	24096	35637
Be	2869	2770	3470	2257	1994	2999	3118	3204	3446	3079	3144	3264	2537	3830	2280	2978
Sc	16079	16939	19067	16085	13080	18557	18205	17669	17734	16399	17243	17763	14993	18830	14293	18887
Ti	5351012	5282266	4870939	4629914	4979865	5271876	5224492	5372076	5236655	5472082	5504784	5273646	5133781	5346871	5452597	5348201
V	96725	102546	108663	88590	102355	109451	102107	99713	114235	111710	112733	102420	111265	97586	100111	103605
Cr	86657	84822	80525	66838	91433	83515	93518	94977	108810	109554	107097	105301	102819	103698	108429	102693
Co	6241	6822	13161	4808	2741	5880	4628	4922	5596	3364	3821	10137	4209	16523	7446	7231
Ni	16572	10951	33071	10976	19083	11202	9498	9072	13073	10624	10177	19276	12106	25058	22541	14250
Cu	38519	26279	23211	88713	41114	21655	50949	31706	50143	45026	37849	89637	40160	57373	44808	47968
Zn	20603	25964	53466	20641	16342	27429	26873	25353	25733	18150	19572	23141	16408	28824	15293	17881
Ga	20598	22635	23072	19356	19667	23350	23856	23059	21738	20684	21885	20908	20972	21418	19719	22950
As	4883	1361	1493	16446	13134	648	2939	2380	11252	8609	7092	23514	28129	14156	19361	6581
Rb	165409	171962	159693	147198	162095	187484	184122	168977	166416	164769	172021	155200	161379	168816	157945	181265
Sr	70565	51262	30256	175282	95908	79342	107943	98999	110228	139048	109840	93470	64578	190701	131408	135853
Y	38623	36756	57800	37195	23349	29561	37698	35247	36088	37618	34158	37032	27183	40386	27245	30490
Zr	177873	147558	145165	155886	149947	135906	141475	158959	167237	173778	156068	157566	149582	165539	168609	149913
Nb	16223	16408	15314	14240	15127	16555	16534	17010	16154	16590	16939	15991	15546	16589	16006	16780
Mo	1356	343	447	1104	2069	260	914	561	2378	2190	2000	4507	2763	1588	2905	1951
Ag	346	66	67	3756	809	50	223	174	896	930	617	781	1255	212	1842	136
Cd	72	60	72	65	58	58	68	68	71	71	66	65	60	69	68	61
In	75	77	78	121	83	66	106	95	110	103	102	106	104	75	97	85
Sn	2418	2413	1083	2679	1919	4479	4097	3720	2471	4132	4449	1919	2782	1863	2996	4017
Sb	1429	274	348	7401	3952	272	895	675	1921	1421	1464	3383	4183	1919	5428	1111
Cs	11383	11525	11391	12486	10574	11471	11652	11771	11881	10637	11220	10410	10764	10617	9817	11407
Ba	296369	293193	255144	637383	367675	318831	457419	415477	412645	444812	478627	970975	463508	847177	736513	544390
La	46374	50795	59746	47968	38164	50796	51964	48441	42228	40479	41663	40568	44113	38137	34031	45369
Ce	103908	109905	136766	114294	81206	107091	113293	100118	89741	87438	86841	85500	92447	79073	70800	95249
Pr	11555	11560	17318	12456	8998	11457	12369	12160	11103	11135	10567	10380	10881	9334	8361	11255
Nd	43423	41716	67141	54180	33504	41762	46067	45101	42382	44422	39995	39213	39329	34856	30388	40633
Sm	8250	7134	16463	11940	6029	7003	7999	8055	8504	9529	7736	7936	6408	7088	5472	6783
Eu	1443	1249	2976	2142	961	1250	1325	1328	1353	1430	1233	1391	1013	1329	909	1101
Gd	6800	5850	14460	9372	4333	5336	6218	6129	6523	6955	5981	7090	4723	7028	4409	5115
Tb	1107	993	2091	1334	678	862	1030	1015	1056	1103	994	1146	793	1176	756	867
Dy	6876	6306	11559	7447	4208	5358	6444	6382	6662	6797	6143	6949	4997	7188	4798	5456
Ho	1448	1350	2217	1482	901	1147	1375	1374	1419	1448	1321	1457	1082	1533	1068	1186
Er	4179	3904	5889	4103	2647	3339	3960	3981	4099	4167	3820	4162	3166	4369	3195	3471
Tm	648	608	867	627	421	527	611	615	630	647	596	639	501	672	514	542
Yb	4201	3885	5435	4019	2790	3371	3918	4009	4095	4195	3865	4136	3271	4339	3394	3527
Lu	629	578	794	597	417	504	581	592	603	612	569	609	484	644	503	522
Hf	4955	4376	4154	4487	4251	4000	4101	4616	4854	4985	4554	4496	4311	4722	4683	4355
Ta	1266	1236	1142	1075	1199	1237	1257	1301	1268	1326	1347	1255	1234	1279	1327	1298
W	2129	2274	2183	2020	2119	2298	2427	2376	2306	2445	2470	2243	2189	2253	2282	2215
Tl	998	720	626	996	865	745	786	757	869	891	935	890	1258	738	1607	735
Pb	80708	8764	6710	462571	218059	4535	42329	30419	126031	120625	106018	169842	249156	38232	376385	38777
Th	16280	15243	14889	13984	14727	15535	15826	15818	16076	16363	16069	16504	15029	15910	16409	15926
U	4345	3141	3128	3710	3401	3299	3627	3651	4150	4581	4133	4759	4121	4863	3839	3613
Th/U	3.75	4.85	4.76	3.77	4.33	4.71	4.36	4.33	3.87	3.57	3.89	3.47	3.65	3.27	4.27	4.41
Y/Ho	26.67	27.23	26.07	25.10	25.92	25.77	27.42	25.66	25.44	25.99	25.87	25.42	25.12	26.35	25.51	25.70
Zr/Hf	35.90	33.72	34.95	34.74	35.27	33.97	34.50	34.44	34.45	34.86	34.27	35.05	34.70	35.06	36.01	34.42
Nb/Ta	12.82	13.27	13.41	13.25	12.62	13.38	13.15	13.07	12.74	12.51	12.58	12.74	12.60	12.97	12.06	12.93

Supplementary Table 2 Continued

	09-JS-2A	09-JS-2B	09-JS-3A	09-JS-3B	09-JS-3C	09-JS-4A	09-JS-4B	09-JS-5A	09-JS-5B	09-JS-6A	09-JS-6B	09-JS-6C	09-JS-7A	09-JS-8	09-JS-9A	09-JS-9B
Strat (m)	3	3	6.6	6.6	6.6	9.6	9.6	10.4	10.4	11.5	11.5	11.5	12.5	12.8	16.5	16.5
TiO_{2HCl}	0.00087	0.00450	0.00577	0.01854	0.00590	0.01094	0.00268	0.01747	0.02339	0.00825	0.01296	0.00845	0.00742	0.00425	0.00485	0.00479
Al_2O_{3HCl}	0.27823	0.41084	1.18202	2.16815	0.65165	0.31816	0.27794	0.16523	0.22977	0.39633	0.40882	0.32200	0.38648	0.36666	0.42962	1.43519
$Fe_2O_{3(T)HCl}$	3.11198	4.59518	3.20127	4.49355	4.32033	6.55322	1.86749	5.75725	5.18927	2.40347	3.13737	4.57468	4.16802	2.94287	2.20984	2.29261
MnO_{HCl}	0.00041	0.00116	0.00285	0.00571	0.00149	0.00054	0.00066	0.00044	0.00076	0.00321	0.00057	0.00103	0.01488	0.00243	0.00151	0.00442
MgO_{HCl}	0.09181	0.12061	0.31334	0.71134	0.19410	0.07682	0.07604	0.05162	0.07186	0.08205	0.04930	0.06074	0.04204	0.01958	0.03297	0.41679
CaO_{HCl}	0.17778	0.44396	0.25272	0.27774	0.21773	0.34689	0.15356	0.21875	0.26648	0.28888	0.31585	0.28967	0.21893	0.07103	0.06153	0.08815
K_2O_{HCl}	0.38599	0.43824	0.42109	0.31562	0.51947	0.66756	0.28447	0.69893	0.68335	0.35603	0.54140	0.51045	0.44914	0.36637	0.17907	0.18243
Na_2O_{HCl}	0.01297	0.02409	0.01403	0.01202	0.02558	0.05018	0.00893	0.06326	0.05048	0.01568	0.03044	0.02561	0.02690	0.02501	0.00606	0.00325
P_2O_{5HCl}	0.03126	0.05898	0.07525	0.08880	0.07231	0.10075	0.03229	0.10118	0.10319	0.05351	0.05214	0.09341	0.09337	0.04978	0.03393	0.07230
Li_{HCl}	1876	5626	10450	36377	6237	16437	1596	19624	25679	5717	8211	15933	9462	4159	2104	21085
V_{HCl}	4489	17015	10157	17510	9347	13723	4724	29816	27548	7469	10688	12160	9769	5924	6222	8171
Ni_{HCl}	467	6174	4759	9995	2280	3047	917	1309	2939	5689	2985	3774	23062	5385	2427	7477
Mo_{HCl}	168	2119	683	505	483	1945	331	2134	2599	1310	993	2066	2491	854	895	114
Cd_{HCl}	2	8	10	21	4	9	3	8	7	11	10	10	80	5	5	16
Sn_{HCl}	43	229	415	540	216	163	212	81	202	136	197	198	140	110	197	246
Sb_{HCl}	77	503	201	94	157	470	118	187	234	250	293	398	433	307	685	12
Tl_{HCl}	46	100	67	42	50	289	52	177	200	60	179	270	218	116	32	50
U_{HCl}	266	1441	800	952	656	1386	453	1898	2127	1094	1065	1808	1503	568	619	287

	09-JS-10A	09-JS-10B	09-JS-12	09-JS-13	09-JS-14A	09-JS-14B	09-JS-15	09-JS-16A	09-JS-16B	09-JS-17A	09-JS-17B	09-JS-18	09-JS-19A	09-JS-19B	09-JS-20B	09-JS-20A
Strat (m)	24.6	24.6	26	27	28	28	35	36	36	36.4	36.4	36.4	37.5	37.5	38.6	38.6
TiO_{2HCl}	0.00578	0.00669	0.00772	0.00366	0.00796	0.00872	0.00504	0.00545	0.00673	0.01074	0.00805	0.00338	0.00376	0.00304	0.00892	0.00260
Al_2O_{3HCl}	0.86728	1.66211	3.14549	0.75760	0.28151	1.59719	1.33156	1.07490	0.80359	0.63630	0.68968	0.50182	0.28509	0.92912	0.28965	0.58024
$Fe_2O_{3(T)HCl}$	3.34523	4.16837	6.31405	3.50106	4.86048	2.71359	2.84195	2.58179	4.14595	3.58226	2.71308	4.26681	3.87439	2.58010	5.13719	2.19657
MnO_{HCl}	0.00270	0.00466	0.02137	0.00562	0.00045	0.00457	0.00224	0.00218	0.00196	0.00093	0.00108	0.00173	0.00073	0.00337	0.00081	0.00119
MgO_{HCl}	0.15355	0.42672	0.97854	0.13451	0.01994	0.39199	0.22935	0.17629	0.09233	0.06470	0.08469	0.02940	0.01745	0.10737	0.01681	0.06858
CaO_{HCl}	0.08958	0.10486	0.32803	0.33396	0.37230	0.14797	0.05609	0.08211	0.08363	0.11121	0.18423	0.11793	0.08395	0.18454	0.10674	0.08114
K_2O_{HCl}	0.41914	0.38956	0.27628	0.32591	0.64607	0.34836	0.31928	0.32463	0.31286	0.51164	0.38015	0.24795	0.46199	0.21833	0.53601	0.25819
Na_2O_{HCl}	0.01612	0.01165	0.00572	0.02290	0.05466	0.00916	0.00993	0.01137	0.01452	0.02352	0.01526	0.01902	0.03449	0.01194	0.08207	0.01045
P_2O_{5HCl}	0.06023	0.07178	0.19908	0.09083	0.04619	0.06389	0.04710	0.05539	0.05634	0.04967	0.04529	0.04194	0.01606	0.05036	0.05378	0.04099
Li_{HCl}	9231	17003	39986	3834	3626	13590	13998	11031	8408	6015	6275	2878	2837	8971	3742	5906
V_{HCl}	8235	13136	18792	9219	9585	11432	8942	7075	10496	10046	8728	9507	8464	5321	7770	4867
Ni_{HCl}	3698	6614	26032	3589	1409	6472	3646	3165	4339	2030	2458	8973	2171	9457	3806	3705
Mo_{HCl}	784	174	261	750	914	108	533	354	1549	1213	1241	3357	1217	1053	1245	1181
Cd_{HCl}	5	6	15	7	3	6	5	0	0	0	0	0	0	0	1	0
Sn_{HCl}	134	407	268	145	150	472	464	300	40	49	66	21	36	133	51	101
Sb_{HCl}	680	78	88	3450	933	23	330	117	394	217	289	1017	786	461	1274	179
Tl_{HCl}	134	73	42	222	98	65	35	13	28	22	56	77	77	40	156	4
U_{HCl}	1112	275	274	1012	396	313	458	387	678	822	556	1243	653	1517	526	489